Universidade de Lisboa

Faculdade de Farmácia

Development of a tumour-selective self-immolative system

Umbelliferone probe and triazene prodrugs

João Miguel Ferreira Vaz

2020

Universidade de Lisboa

Faculdade de Farmácia

Development of a tumour-selective self-immolative system

Umbelliferone Probe and Triazene Prodrugs

João Miguel Ferreira Vaz

Monografia de Mestrado Integrado em Ciências Farmacêuticas apresentada à Universidade de Lisboa através da Faculdade de Farmácia

Orientadora: Professora Auxiliar, Maria de Jesus de Almeida Rainha Perry da Câmara Saldanha

Coorientador: Professor Catedrático, Rui Ferreira Alves Moreira

2020

Resumo

O conhecimento que temos sobre o cancro tem evoluído, desde a sua primeira definição por Hipócrates, em 400 AC. Atualmente, o cancro é compreendido a um nível molecular, o que permite o desenvolvimento de meios de diagnóstico e terapêuticas. Apesar de muito se conhecer, problemas com os atuais métodos de diagnóstico e terapêuticas ainda subsistem. Um destes problemas é a falta de seletividade dos fármacos ou sondas utilizadas, o que frequentemente leva a diagnósticos ou tratamentos ineficazes, ao aparecimento de efeitos sistémicos e ao desenvolvimento de resistência aos fármacos. Para combater estes problemas diversas estratégias têm sido desenvolvidas. Uma destas estratégias é a fotofarmacologia, a qual permite um controlo preciso e seletivo de onde e quando é libertado um fármaco ou sonda. Outra estratégia é o desenvolvimento de pró-fármacos que apenas possam ser ativados na presença de um estímulo (pró-fármacos auto-imolativos) fornecido pelas células cancerígenas ou pelo seu ambiente. Com base na literatura, o grupo 6-nitroveratrilo suscitou interesse por permitir explorar ambas as estratégias ao funcionar tanto como grupo fotoprotetor como grupo auto-imolativo. Neste trabalho, primeiro foi explorada a fotofarmacologia, ao ser sintetizado um composto que liberta um grupo fluorescente após ser exposto a luz UV de um comprimento de onda específico (funcionando como sonda). A sua síntese e purificação foram otimizadas, e o composto foi caracterizado (espectroscopia de ressonância magnética nuclear de hidrogénio e carbono, espetroscopia ultravioleta, e ponto de fusão). Foi realizado um estudo de fotoativação deste composto, sendo demonstrada a libertação do grupo fluorescente após exposição à luz UV. Em segundo lugar, sabendo que o grupo era capaz de libertar a função acoplada, foram explorados os pró-fármacos auto-imolativos. Foram sintetizados conjugados de arilmonometiltriazenos (espécies ativas de medicamentos usados no cancro) com o grupo 6-nitroveratrilo e foram feitas tentativas de otimizar a sua síntese e purificação (ao testar diferentes técnicas de purificação e misturas de eluentes). Um destes conjugados foi sintetizado com sucesso. Durante estas tentativas, ao usarmos a espetroscopia de massa para analisar os produtos da reação, obtivemos informação sobre os compostos que se formam durante a reação e sobre a possível influência do substituinte do arilmonometiltriazeno (no anel aromático) no produto da reação.

Palavras-chave: Cancro; Triazenos; Pró-fármacos; Fotofarmacologia; Sondas

Abstract

Knowledge about cancer has evolved since its first denomination by Hippocrates around 400 BC. Nowadays, cancer is understood even at the molecular level which allows for the development of therapies and diagnosis tools. Even tough so much is known, there are still problems with the current treatments and diagnosis tools. One of these problems is the lack of selectivity to the cancer cells of the used drugs or probes, which often leads to ineffective diagnosis or treatment, to the appearance of systemic effects and to the development of drug resistance. To overcome these problems, scientists have long been developing strategies. Photopharmacology is one of these strategies, which allows the precise and selective control of when and where a drug or probe is released. Another strategy is the development of prodrugs which can only be activated in the presence of a stimulus (self-immolative prodrugs) provided by the cancer cells or their environment. Searching the literature, we found that the 6-nitroveratryl group works both as a photoprotecting group and a self-immolative moiety, being suitable to explore both strategies. In this work, the photopharmacology strategy was first explored, by synthesizing a compound which releases a fluorescent moiety after being exposed to UV light of a specific wavelength (functioning as probe). Its synthesis and purification were optimized, and the compound was characterized (Hydrogen and Carbon nuclear magnetic resonance spectroscopy, UV spectroscopy, and melting point). A photoactivation study of this compound was executed and showed the release of the fluorescent moiety after the exposure of the compound to UV light of a specific wavelength. Secondly, knowing that the 6-nitroveratryl group was suitable for the release of a linked moiety, we aimed at the self-immolative prodrug strategy. Conjugates of arylmonomethyltriazenes (active species of marketed cancer drugs) with the 6-nitroveratryl group were synthesized and we attempted to optimize their synthesis and purification (by testing different eluent mixtures and purification techniques). We were able to successfully synthesize and isolate one conjugate. During these attempts, by utilizing mass spectroscopy to analyse the reaction products we were able to obtain insights about the compounds that formed during the reaction and the possible influence of the substituent of the arylmomomethyltriazene (in the aromatic ring) in the product of the reaction.

Keywords: Cancer; Triazenes; Prodrugs; Photopharmacology; Probes

Acknowledgements

First, I would like to start by thanking this faculty, which was my second home for the last five years and allowed me to grow, to have valuable opportunities, and to become a more knowledgeable person. For this, I am grateful.

Second, I would like to thank the support of both my supervisor and co-supervisor. Your roles were crucial in my development, in pursuing my goals and in my achievements. For their continuous support, patience, and guidance, I can only be thankful and present them with my utmost respect.

Third, I must also acknowledge the great contribution of my family to my success and to my perseverance throughout these years. If not for you, I would not have been able to reach such high heights. I cannot ever be thankful enough for your support. Even in distance, even with difficulties, you proved to be the best that I could have ever asked for. Thank you for the opportunity to know even more, thank you for the comprehension even in hard times, thank you for all of your patience and forgiveness, and thank you for never letting me be alone through all of these little steps that today make me proud of myself and extremely happy. I love all of you with all my heart.

Finally, my friends deserve a very special acknowledgment. As we are taught from the beginning, we can never hope to finish these five years all by ourselves. And this is the truth that I have learned along these years. I could never have reached where I am without you. You were key stones in my progress, you where there when I needed, you turned even the most difficult moments in moments that could be surpassed. All these years would not be the same without you. Your support, your insights, your ideas, your advice, and above all, your belief in me, were what made this possible. I can never thank you enough, only express my deepest gratitude and love for you. For allowing me to be where I am, and for never giving up on me, I must thank you.

Thank you Hydrogens (Vanessa Nascimento, Mariana Miranda and Mariana Bento), thank you Henrique and Margarida, thank you Filipa, Mónica, Chandani, Avinach, Gustavo, Alexandra, Inês, Joana and thanks to all that were not mentioned and were important in the course of these years.

“If you want something you've never had

You must be willing to do something you've never done.”

— Thomas Jefferson

Abbreviatures

^{13}C NMR – Carbon Nuclear Magnetic Resonance

^{1}H NMR – Hydrogen Nuclear Magnetic Resonance

6-NV – 6-nitroveratryl

ACN – Acetonitrile

ATP – Adenosine 5'-Triphosphate

$CDCl_3$ – Deuterated chloroform

CN-Aniline – 4-cyanoaniline

CN-MMT – (E)-1-(4-cyanophenyl)-3-methyltriazene

$COCH_3$-Aniline – 4-acetylaniline

$COCH_3$-MMT – (E)-1-(4-acetylphenyl)-3-methyltriazene

$COOCH_3$-Aniline – 4-methoxycarbonylaniline

$COOCH_3$-MMT – (E)-1-(4-methoxycarbonylphenyl)-3-methyltriazene

COSY - Correlation Spectroscopy

DCM – Dichloromethane

DMAP – 4-Dimethylaminopyridine

DMBNA – 4,5-dimethoxy-2-nitrobrenzyl alcohol

DMF – Dimethylformamide

DNA – Deoxyribonucleic acid

DTIC – Dacarbazine

ESI- – Negative Electrospray Ionization

ESI+ – Positive Electrospray Ionization

HAP – Hypoxia-activated Prodrug

Hex – Hexane

HMBC – Heteronuclear Multiple Bond Correlation Spectroscopy

HSQC – Heteronuclear Single Quantum Coherence Spectroscopy

Hz – Hertz

JFV-1 – 4,5-dimethoxy-2-nitrobenzyl methanesulfonate

JFV-1-Cl – 1-(chloromethyl)-4,5-dimethoxy-2-nitrobenzene

JFV-2 – (E)-1-(4-cyanophenyl)-3-(4,5-dimethoxy-2-nitrobenzyl)-3-methyltriazene

JFV-2-Ani – N-(4-cyanophenyl)-1-(4,5-dimethoxy-2-nitrobenzyl)amine

JFV-3 – (E)-1-(4-acetylphenyl)-3-(4,5-dimethoxy-2-2-nitrobenzyl)-3-methyltriazene

JFV-3-Ani – N-(4-Acetylphenyl)-1-(4,5-dimethoxy-2-nitrobenzyl)amine

JFV-4 – (E)-1-(4-methoxycarbonylphenyl)-3-(3-(4,5-dimethoxy-2-nitrobenzyl)-3-methyltriazene

JFV-4-Ani – N-(4-methoxycarbonylphenyl)-1-(4,5-dimethoxy-2-nitrobenzyl)amine

JFV-UMB – 7-((4,5-dimethoxy-2-nitrobenzyl)oxy)-2H-chromen-2-one

LC-MS – Liquid Chromatography-Mass Spectroscopy

MMT – Monomethyltriazene

MS – Mass Spectroscopy

MsCl – Methanesulfonyl chloride

NaH – Sodium hydride

NMR – Nuclear Magnetic Resonance

PBS – Phosphate-Buffered Saline

PPG – Photoremovable Protecting Group

Prep TLC – Preparative Thin Layer Chromatography

PTFE – Polytetrafluoroethylene

R-MMT – Para Substituted 1-aryl-3-methyltriazene

s – second

SIL – Self-immolative linker

S_N2 – Bimolecular nucleophilic substitution

TEA – Triethylamine

THF – Tetrahydrofuran

TLC – Thin Layer Chromatography

TMZ – Temozolomide

UHPLC - Ultra High-Performance Liquid Chromatography

UV – Ultraviolet

Index:

Figure Index:

Annex Index:

1 Introduction

1.1 Context and Previous Work

Cancer is a long-known enemy of humans. Through the times, humanity went from not knowing what was in the origin of cancer (a few centuries ago) to nowadays where cancer is understood with a huge detail at the molecular level. Although much is understood about cancer at this time, there is still much that is unknown, and several difficulties in diagnosis and treatment. To overcome these problems (from difficult diagnosis and study to treatment with severe side effects) scientists have been searching and developing strategies with promptitude (1-16).

Of these strategies, a recent area of research called photopharmacology is an interesting approach. It can be used to overcome the issues of poor drug selectivity, systemic toxicity, and drug resistance, that usually happen with cancer therapies. Photopharmacology uses light to control the action of a bioactive molecule allowing the choice of where and when that bioactive molecule is released or activated (17–22). This tool has been applied in the development of photoactivable prodrugs, releasing systems and probes with great success (18,19,31–33,23–30).

In addition to this strategy, there is an interest in the development of prodrugs or probes that can be selectively activated in the presence of an hypoxic environment (containing nitroreductases), which is a common characteristic of solid tumours and their metastases (3,34). HAPs (Hypoxia-activated prodrugs) are an interesting strategy, because they make use of the tumour characteristic hypoxia to specifically target the tumour cells and in this manner avoid off-site toxicity, achieve drug selectivity and/or specifically image the tumour area (in the case of fluorescent moieties being present). This strategy has been in development in the recent years with promising success, although no drug or probe based on this strategy is approved for the clinic, yet (3,34–40).

Both strategies present themselves as great opportunities to develop either probes or prodrugs to help in the fight against cancer. We decided to explore an interesting system (6-nitroveratryl moiety - circled in Figure 1) that can act both as a self-immolative system for a prodrug or probe in the presence of a reductive microenvironment (related to HAPs strategy) and also as a photoprotecting group (PPG) that releases a drug or

probe under a specific wavelength of light (related to photopharmacology strategy) (41–48).

In a previous work, we aimed at the synthesis and characterization of a photolabile compound (JFV-UMB, shown in Figure 1), containing a PPG (6-nitroveratryl moiety) and a fluorescent moiety (Umbelliferone), that could be used as a probe to study cancer. The synthesized compound could release its active moiety not only under a specific wavelength but also under hypoxic conditions. This particularity of the PPG leads us to continue the previous work by studying the photoactivation of the previously synthesized compound and developing more conjugates (prodrugs) of the PPG with relevant active moieties.

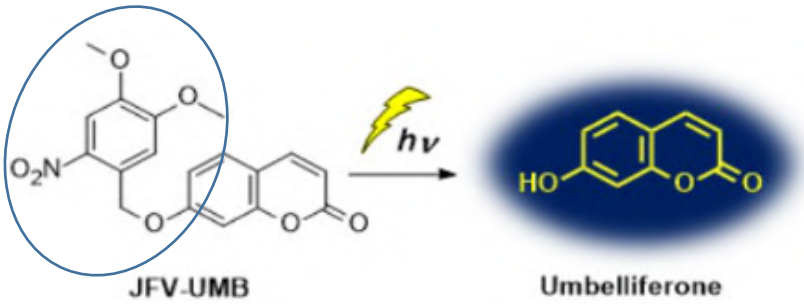

Figure 1 - JFV-UMB and its photoactivation

1.2 Cancer

The definition of cancer, since its first denomination by Hippocrates around 400 BC (49), has always been evolving to the light of breakthroughs in medicine, and in the technologies and sciences that surround it. Specially, in the last few decades this definition has changed from a tumour cell-centric perspective in which cancer is a disease of damaged genes responsible for creating rogue cells, to an immunologic perspective where cancer is defined as a failure of host immune controls on such rogue cells (50). Today, it is also recognized the great importance of the inflammatory tissue, of the microenvironment and of the immune response in promoting malignant development and progression. This has arisen, by the recent advances in understanding the mechanisms by which cancer cells suppress and evade the immune system (50). Conceptually, cancer can be defined as a growth or cell chaos where tissues and organs may become the target of invasion (13). Nowadays, cancer is viewed as an ecosystem

that is under constant evolution, gathering the resources and doing everything it cans to survive in its environment (4).

Cancer constitutes an enormous burden on society. The occurrence of cancer is increasing because of the growth and aging of the population, as well as the increasing prevalence of established risk factors such as smoking, overweight, physical inactivity, and changing reproductive patterns associated with urbanization and economic development (51). This burden is reflected on estimates from the World Health Organization (WHO) in 2015 where cancer is the first or second leading cause of dead in 91 of 172 countries. Also, according to the GLOBOCAN 2018 study, the worldwide incidence of cancer was of 18.1 million new cases and the worldwide mortality from cancer was an astonishing number of 9.6 million deaths (52).

With all this said, it can be noted that there is an increasing development of tools, equipment, and therapeutics to use in research, diagnosis, and treatment of cancer. It is a fight in progress, aiming at a better understanding, better diagnostic tools, and better treatment options for cancer.

With all the knowledge about cancer, there is an urge to develop better strategies to eliminate cancerous cells, and to effectively target these cells while sparing normal cells. This is not an easy task, because it´s known that cancers are not homogenous entities (presenting intratumor heterogeneity) and can metastasize and invade tissues, resulting in their resistance to conventional chemotherapy, radiotherapy and even to removal surgeries (1,2,4,53).

To deal with cancer, and with the therapeutic failures of conventional strategies, new strategies have been investigated and developed (2,5–11,18,54). These strategies focus mostly in increasing the specificity of the therapy to a particular cancer (based on the knowledge of its molecular characteristics) or in increasing the selectivity of the therapy to cancer cells rather than normal cells (thus avoiding side effects and increasing effectiveness).

In common, all of these recent strategies have been designed to more effectively target tumour cells aiming at the “magic bullet” concept, first coined by Paul Erlich in the 1800s (11). This concept has been the driver for the development of new strategies to deal with cancer with more specific and selective mechanisms of action than the ones of conventional chemotherapeutic agents (11).

1.3 Photopharmacology and cancer

In cancer treatments, many drugs or active compounds have a problem with selectivity because their sites of action are also expressed in sites/tissues/organs different from the desired target and this leads to inevitable side effects and to a decreased action on the desired target. Photopharmacology is one of the strategies to deal with this problem. Photopharmacology provides an external photoswitch to control off-target site activity while helping to attain selective biological activity (17,20,21). Photopharmaceutical agents are developed by incorporating photolysable moieties in compounds enabling the change of these compounds after exposure to light at a specific wavelength and subsequent biological activation as depicted in Figure 2 (17,20,21).

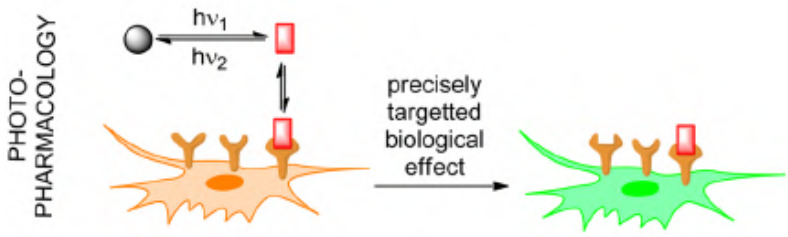

Figure 2 - Photopharmacology concept (21)

These photopharmacologic agents allow a highly selective action at the target as light can be delivered with very high spatiotemporal precision. On the other hand, there are challenges like the penetrability of light through the tissues and the possibility of photodamage to the tissues caused by UV light (17,20,21). This is a field in rapid growth, with many types of compounds developed with applications in diagnosis, research and treatment in cancer but also in other diseases and research areas (14-26).

Consequently, photopharmacology is an important tool for the improvement of the pharmacotherapeutic capabilities of many drugs for treating cancer that are discarded because of their toxicity, low selectivity and for the appearance of drug resistance (21). Figure 3 shows the utility of photopharmacology in the resolution of these problems.

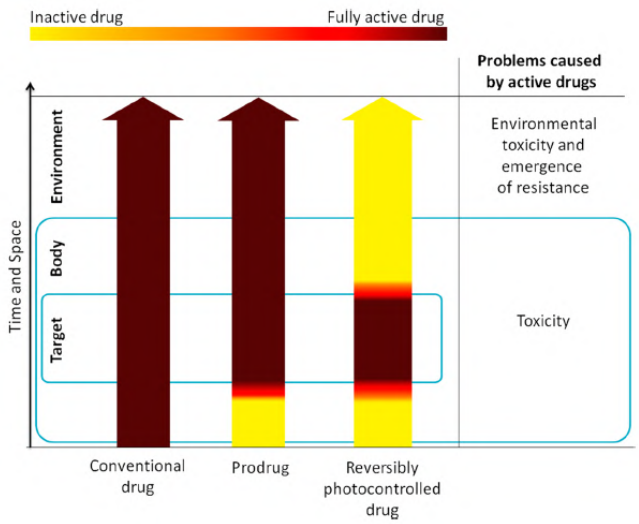

Figure 3 - Comparison between a conventional drug and two drug releasing systems in terms of problems caused by the active drug (21)

Photopharmacological treatment is especially suitable in situations where the cancer is localized. Action on exposed parts, such as the skin or eyes, is the most natural target (21,47). Photoactivation can be achieved either from outside the body, from inside the body or at the site of action (20).

1.3.1 Photocaging groups

Photocaging groups, also called photoremovable protecting groups (PPGs) are molecules that can provide spatial and temporal control over the release of various chemicals (63). Kaplan and co-workers were amongst the first to explore PPGs, achieving the photorelease of Adenosine 5'-Triphosphate (ATP). From there on, applications in synthesis and in biology started appearing (64). The latter authors, introduced the term "caged" to define a compound protected by a PPG (63). These groups can have a diverse range of applications, especially in synthesis, biochemistry, neurobiology, biomedicine, volatiles release, polymerization, and fluorescence activation (63,65).

A very interesting application is the development of chemical probes (46,66), especially to use in cancer research (i.e. to assess the overexpression of an enzyme in cells and perceive its contribution to tumorigenesis) and eventually in therapeutic applications (i.e. targeting an overexpressed enzyme in cancer cells) (42). These kinds of probes have already been proven useful in drug discovery for cancer (46,66) and research

applications (13-26) although still offering some challenges in their choice, development and application (67).

The development of prodrug systems with these groups is also of great interest, as these photoactivable systems allow a great degree of control over where and when the linked moiety is released, and that is particularly useful when we think about drugs that treat cancer but lack selectivity over normal cells. Our interest in these systems is inspired by other works, mostly focusing on drugs against cancer (18,34–45) and by the relatively recent existence of an approved drug (axitinib) that relies on photopharmacology for its specific action on cancer cells (18).

Amongst all the different photocaging groups that have been developed, nitrobenzyl, and their dimethoxy derivatives (nitroveratryl) are by far the most used because they are easily commercially available and they are often successful in achieving the desired purposes with several proofs of their functionality (63,65,69). Despite that, they have known disadvantages like low water solubility and the production of potentially toxic and strong absorbing compounds like *o*-nitrosobenzaldehyde (63). Examples of these groups are compounds 1-5 shown in Figure 4 (63).

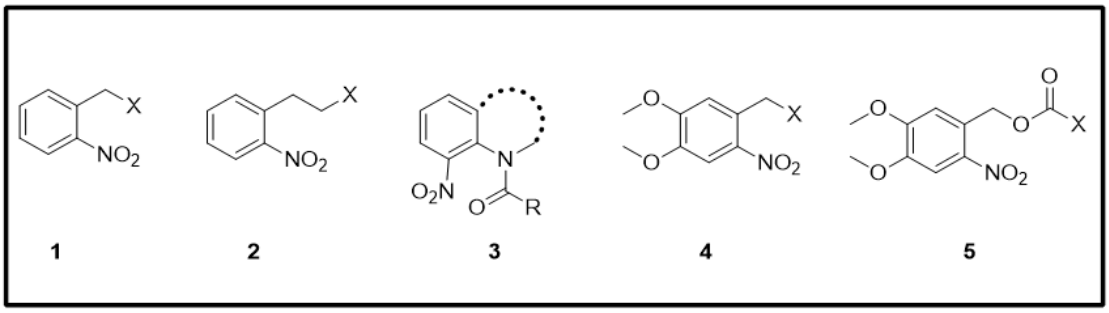

Figure 4 - Photolabile *o*-nitrobenzyl groups (63)

Several modifications on these groups were attempted to improve their properties (efficiency of release, water solubility, avoidance of the nitroso side product, etc.) either on the benzylic position or on the benzene ring. More modifications were done at the benzene ring because of the synthetic difficulties found with the benzylic position and of the low impact on absorbance that those modifications had. These modifications were helpful to tune the absorbance of the compounds and to improve their water solubility. The addition of two methoxy groups, was executed to increase the absorbance at greater wavelengths (less toxic and more penetrable) leading to compounds **4** and **5** (Figure 4) (63).

In this work, the moiety used as a photocage was compound **4**, and its photorelease mechanism can be seen in Figure 5 (70).

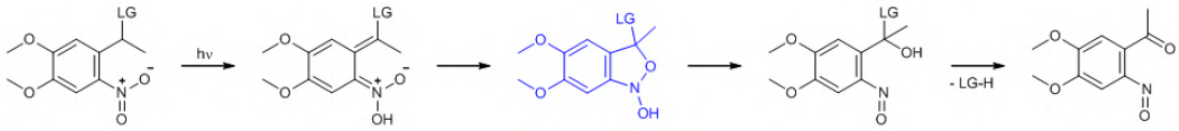

Figure 5 - Photorelease mechanism of Methyl-6-Nitroveratryl (Me-6-NV) group (70)

1.3.2 Fluorescent moieties

Fluorescence is the emission of a photon by an excited-state molecule following the absorption of light. Nowadays, fluorescence is a crucial scientific tool, allowing highly sensitive measurements and the specific visualization of fluorescent compounds in the presence of numerous non-fluorescent compounds. The use of fluorescence enables biological imaging, high-throughput screening, genome sequencing, and many other useful technologies (71).

Fluorescence can be controlled by several methods, making use of chemistry to fine-tune the structure and fluorescence properties of fluorescent moieties/compounds. Fluorescent moieties can be designed and modified to modulate its behaviour according to the desired purpose. As an example, a fluorescent moiety can be coupled with a blocking group which supresses or eliminates fluorescence (Figure 6). This fluorescence can then be retrieved by the removal of the blocking group through an enzyme-catalysed reaction, photolysis, or another covalent bond cleavage (71). These fluorescent moieties can be useful in research and development of probes and/or drugs for cancer by allowing the observation of their distribution through the body and by identifying where and when they are released (41,71). In sum, fluorescent moieties can play a role in photopharmacology, by allowing the tracking of the probe and/or drug release after a light stimulus.

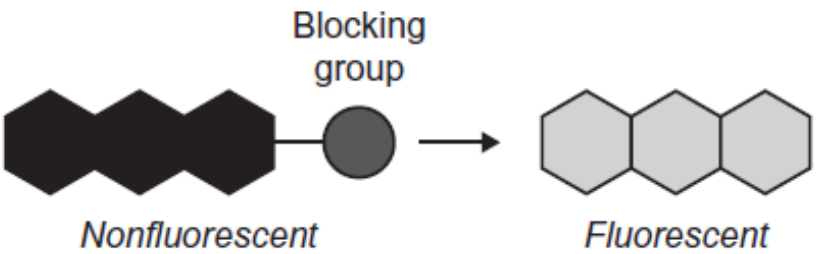

Figure 6 - Fluorescence modulation through a blocking group (71)

Coumarins are an example of these fluorescent moieties and present themselves as widely used fluorophores (chemical compounds that can re-emit light upon light excitation) (72). Their fluorescence can be modulated (lowered) through structural modifications (71). Coumarins are the largest class of 1-benzopyran derivatives, and coumarin (Figure 7), a colorless compound isolated from the tonka bean in 1820, was the initial member of this class of compounds. Since the discovery of coumarin several of its derivatives have been isolated from various natural sources, especially from higher plants (73).

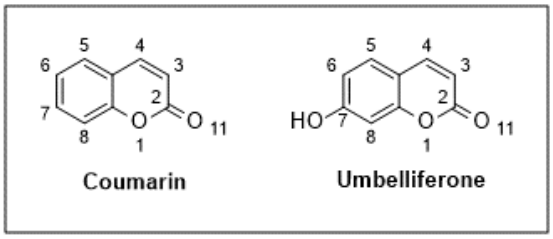

Figure 7 - Coumarin and Umbelliferone structures

Umbelliferone, which was first isolated from the family Umbelliferae, is one of the most popular compounds of the coumarin family. It is also known as 7-hydroxicoumarin and it´s the starting moiety for the synthesis of more complex coumarins (73,74). This compound has received great attention from the scientific community given its diverse bioactivities like anti-inflammatory, antinociceptive, bronchodilating, and anti-hyperglycemic effects (75).

One of its most important characteristics, is its capability to absorb UV light, being used in sun protection cosmetics (74). This characteristic, common to the coumarin family, results in the fluorescence of Umbelliferone after exposure to UV light (76–78). This fluorescence is an important property to its applicability in research and therapeutics. The observed fluorescence of Umbelliferone is of a blue or blue green colour (450-500

nm), when excited at the 320-360 nm range and depending on the pH of the solution (a more alkaline pH results in a shift to the green color). Umbelliferone fluorescence can be supressed or reduced through the addition of an alkyl or acyl substituent on the 7-hydroxy group (71).

In this work, we took advantage of the properties of umbelliferone (fluorescent moiety), photopharmacology and photocaging groups to synthesize a compound (JFV-UMB, Figure 1), that could be selectively activated either by UV light or by the presence of a reductive tumour microenvironment.

1.4 Prodrugs, self-immolative spacers and hypoxia-activated prodrugs

Prodrugs are molecules, derived from pharmacological agents, that have little or no pharmacological activity but have built-in structural lability which results in their *in vivo* conversion to the active therapeutic agent (bioconversion) (40,79,80). This bioconversion can occur either through spontaneous processes (e.g. hydrolytic degradation) or via a biocatalytic mechanism (e.g. enzyme-mediated bioconversion).

There are a lot of strategies that have been built on the prodrug foundation. From simple strategies using hydrolysable linkers (between drug and masking moiety) to more complex and recent strategies depending on very particular enzymes or other stimuli (disease or therapy related) (80).

The use of prodrugs can successfully overcome barriers to drug development and delivery, and allow for improved properties of a potential medicine (79). This strategy is highly successful and this results in a significant fraction of marketed therapeutic formulations being based on prodrugs (80).

Self-immolative spacers

Katzenellenbogen and co-workers, in 1981, were the first to describe self-immolative spacers, also called self-immolative linkers (SILs) (43,80–82). These linkers are composed of a trigger (promoiety) and a spacer moiety, and are designed to degrade spontaneously and fast, and produce by-products with an acceptable safety profile (80). They are stimuli-responsive covalent chemical structures which after a stimulus develop an intramolecular reaction that releases the desired active group (78). With these spacers, the active moiety can be released after the trigger is activated either

through chemicals, enzymes or light (83,84). Figure 8 schematizes the concept of a double prodrug, which can include this types of linkers (85).

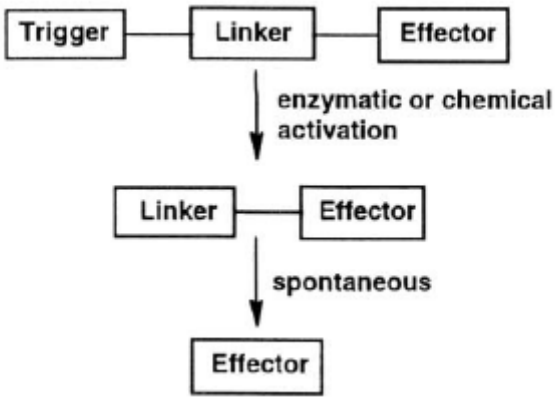

Figure 8 - Double prodrug general release mechanism (85)

SILs are useful in spatially correlating the activation location with the active group release and they have been extensively used in the design of prodrugs and in bioanalysis (82). They constitute a technology that allows the temporary installation of chemical diversity into drugs offering a good tool for prodrug design having as examples the prodrugs doxorubicin, paclitaxel and others (80).

Prodrugs containing SILs can be used to overcome the problems of lack of drug selectivity (responsible for side effects and the appearance of drug resistance in cancer therapies) (85,86). These prodrugs are composed of three units (Figure 8). First, the trigger which is essential for the prodrug activation mechanism and for tumour selectivity, so its activation must occur exclusively in the tumour area. Second, the effector which must be effectively masked in the prodrug to become a non-toxic compound. Finally, the linker which unites the effector and trigger, and which is responsible for the drug release after trigger activation. The linker is a very important part of these prodrugs because it must release the drug fast enough so no prodrug diffuses out of the tumour and also it greatly affects the prodrug properties (pharmacokinetics, organ distribution, bioavailability and enzyme recognition) (85).

SILs can have an impact on the stability of a prodrug under physiological conditions and provide the prodrug with a targeted delivery (87). It is important, in the design of self-immolative prodrugs, to consider that a good leaving group is required for the drug

release after triggering the SIL. Nevertheless, the disassembly of these self-immolative spacers can lead to the formation of toxic species as quinone methides as exemplified by the 6-NV SIL in Figure 9 (83).

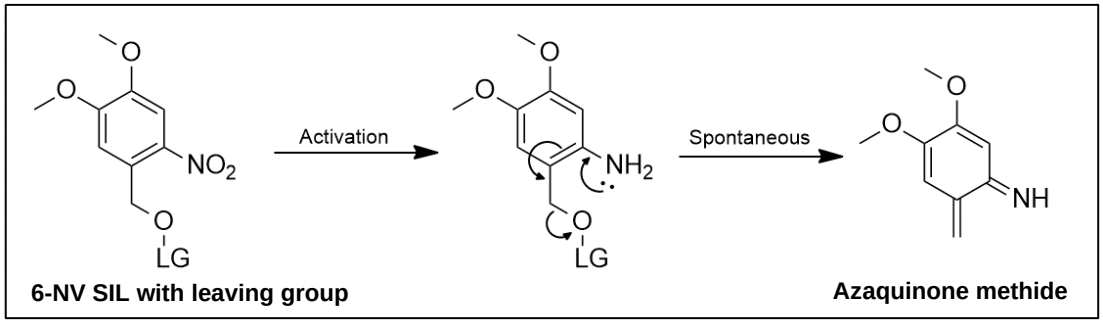

Figure 9 - Azaquinone methide formation with 6-NV as a SIL; LG - Leaving group

These linkers can be divided in two types, elimination-based linkers, or cyclization-based linkers, depending on the mechanism through which they release the active moiety. Both self-immolation processes can be induced from different functions involving heteroatoms (phenol, enol, amine, enamine, hydroxylamine, and others), which vary depending on the trigger used to target the tumour site. In both cases, the activation generates nucleophilic functional groups, conjugated with or near a leaving group, and their reaction spontaneously activates the self-immolation process, releasing the desired compound.

Elimination-based linkers work through the generation of an electronic cascade that leads to the formation of a quinone or azaquinone intermediate (see Figure 9). They are composed by an aromatic structure containing a masked/protected amino, hydroxy, or thiol group which is crucial for the electronic cascade that leads to the disassembly of the linker. When not activated, these linkers are not nucleophilic enough to trigger the electronic cascade and only after they are activated, they reveal their nucleophilicity and initiate the self-immolation process. These linkers tend to be cleaved more rapidly than cyclization-based linkers (86) and can work either through 1,2-elimination, 1,4-elimination, 1,6-elimination and 1,8-elimination processes as shown in Figure 10 and also by β-elimination (not shown) (84).

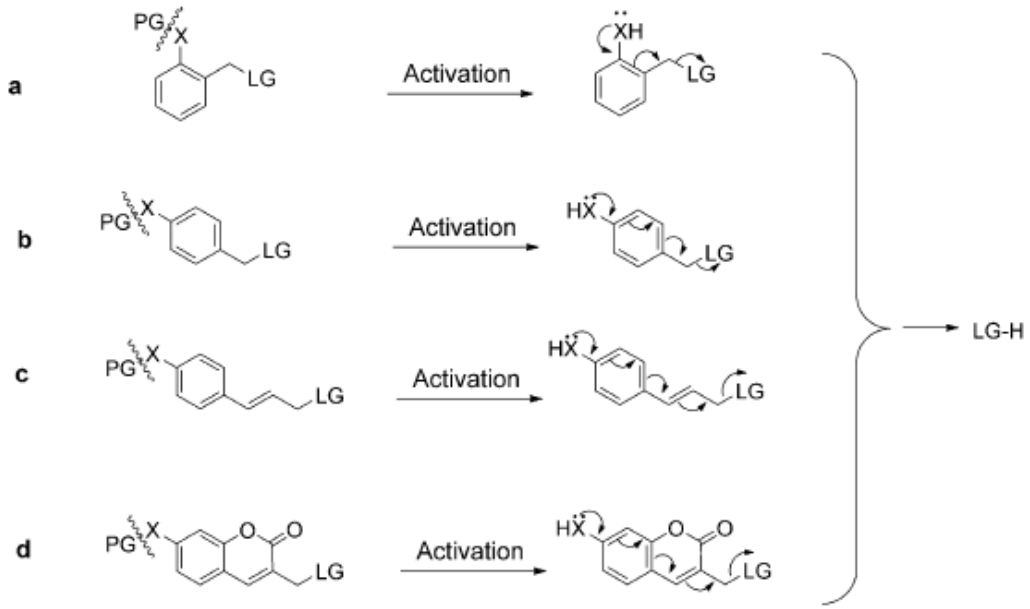

Figure 10 - Release Mechanisms of Elimination-Based Linkers; PG: Protecting group; LG: Leaving group; X = O, NH or S (80)

On the other hand, cyclization-based linkers disassembly through a cyclization process generating, for example, imidazolidinone, oxazolidinone, or 1,3-oxathiolan-2-one ring structures (which are represented in Figure 11 a)). These linkers incorporate moieties based on alkyl chains or on ortho mono- or disubstituted aromatic spacers. Once activated, their disassembly involves a nucleophilic attack on a carbonyl group or on an electrophilic aliphatic carbon atom. The associated cyclization occurs directly after activation or after a preliminary elimination step. In this case, self-immolation is driven by a positive reaction entropy and by the formation of thermodynamically stable products (5- and 6-membered rings) (84). Figure 11 depicts the diverse mechanisms of release of cyclization-based linkers.

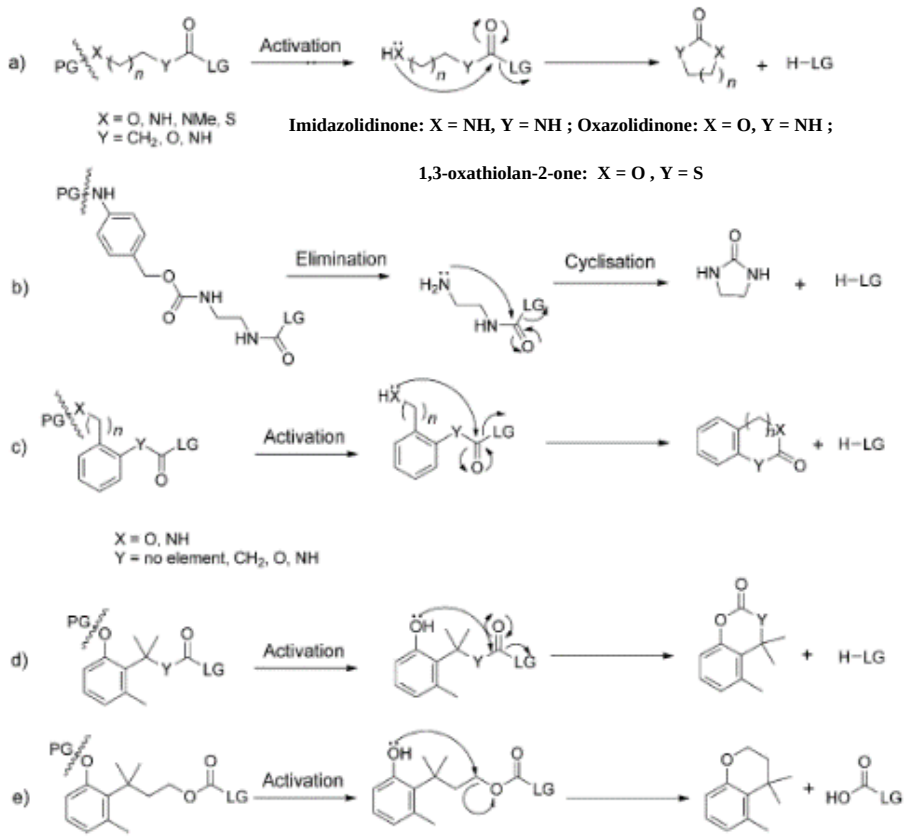

Figure 11 - Release Mechanisms of cyclization-based linkers; PG: Protecting group; LG: Leaving group ; Adapted from (80)

Hypoxia-activated Prodrugs (HAPs)

In order to treat or diagnose cancer, in special solid tumours and their metastases, one strategy under investigation is the use of the characteristic hypoxia of these tumours to guide and direct therapies to them (36,37,88,89).

Since hypoxia (deficiency in oxygen due to an inefficient vasculature of the tumour) is a relevant characteristic of the microenvironment of malignant tumours (Figure 12) it has become an important target for the research of hypoxia-directed cancer therapies. Hypoxia is attractive as a target because it is present in solid tumour cells when compared to non-tumour cells, where it is not. Besides that, hypoxic tumour cells generally are further away from blood vessels than the rest of the cancer cells which makes it difficult for the therapeutic agents to reach them (in an adequate concentration) and display their activity. This contributes to the inefficacy of radiotherapy and chemotherapy in some tumours, so targeting this environment is of great interest (Figure 12) (37,88). Targeting this environment might allow the increase

of a dose of a drug so more drug can reach its target, being selectively released and avoiding toxicity.

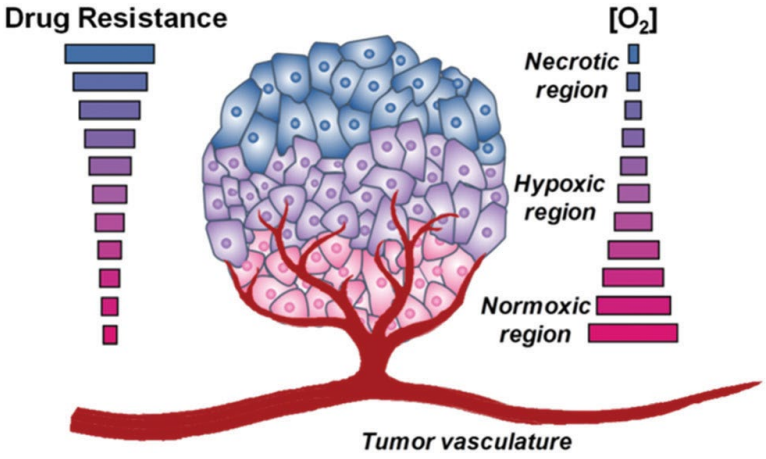

Figure 12 - Microenvironment of a solid tumour regarding its oxygen concentration and the occurrence of drug resistance (37)

In this matter, hypoxia-activated prodrugs (HAPs) are a promising approach and have been developed to specifically target hypoxic tumour cells of solid tumours, including metastases, having favourable results in clinical trials (36,37,88). Although not every one of the cells in the tumour is hypoxic (Figure 12) there is an interest in targeting these cells because at any given time, a fraction of tumour cells are in an hypoxic state, and using hypoxia-activated prodrugs in several cycles of treatment could be effective in killing a good number of tumour cells (88). Also, combining this treatment with radiotherapy or using additional treatments to increase the proportion of the hypoxic cells in a tumour, could result in an increased value of these prodrugs. A third, and attractive approach, is to use the hypoxic cells in a tumour to kill the more oxygenated cells and this requires that the released drugs are converted to more cytotoxic species. For this last approach to work, there is also the need for the drug to be stable and diffuse to the oxygenated cells, killing them on what is known as the “bystander effect” (88).

To achieve activation, hypoxia-activated prodrugs follow one of two different pathways (Figure 13). The first, and more common, is where a prodrug is converted into a transitory intermediate (prodrug one-electron adduct) that can be oxidized back to the prodrug in the presence of molecular oxygen in normal cells. The other, is when the prodrug directly competes with the molecular oxygen for the active site of a reductase

under hypoxic conditions. Both of these mechanisms generate diffusible cytotoxic species (88).

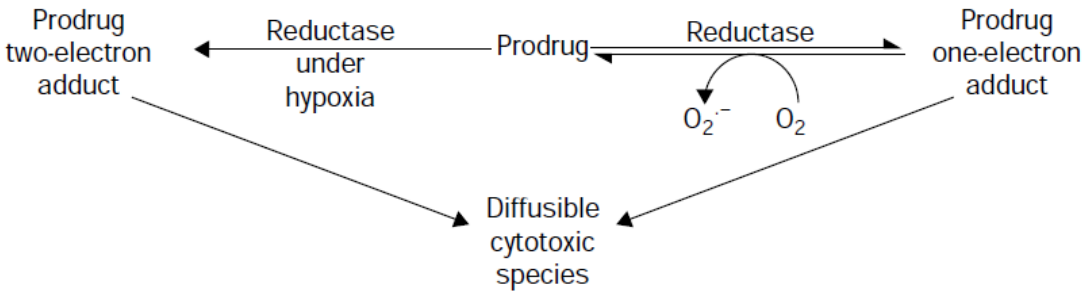

Figure 13 – Activation mechanisms of hypoxia-activated prodrugs (88)

In terms of chemical structure, we can distinguish four main types of hypoxia-activated prodrugs which are quinones, nitro-group skeletons (nitroaromatics and nitroimidazole), N-oxide analogues, and transition metal complexes (36).

Of interest to us is the nitroaromatics group which was one of the first to be explored and is widely used in the development of HAPs (36,90). This group has also been thoroughly studied in the development of probes that can image tumour hypoxia. The mechanism by which this group is activated (Figure 14) involves enzymes called nitroreductases (a family of flavin containing enzymes which effect the stepwise addition of up to six electrons) that are commonly overexpressed under hypoxic conditions and whom expression levels correlate well with tumour hypoxia (37,88).

These nitroreductases (type II nitroreductases), in human cells, have only been identified in hypoxic tumours, and hypoxic conditions are required for the progression of the reduction of the nitro group, as seen in Figure 14 (91).

Figure 14 - Nitroreductase types and reduction mechanism of nitroaromatics (91)

As HAPs, nitroaromatics have been experimented in different ways, such as being "oxygen-mimetic radiosensitizers" (stabilizing the DNA lesions caused by radiotherapy by acting as mimetics of molecular oxygen), integral components of HAPs (themselves having cytotoxicity upon the hypoxic environment) or by releasing a drug by elimination under hypoxic conditions (37).

This last approach gains our attention because it can be used to improve the delivery and reduce the side toxicity of a drug by promoting its release only within the tumour. An example of this is the 6-Me-NV group depicted in Figure 5. This group works as a self-immolative linker which upon photoactivation or activation by a reductive microenvironment releases the active drug conjugated with it.

In sum, tumour hypoxia is a very interesting therapeutic target in oncology which has progressed in the past years, allowing for a range of diverse hypoxia-based strategies to achieve a more selective and less toxic drug delivery. The fact that the activation mechanisms of these prodrugs depend on oxygen concentrations spares normal cells from cytotoxicity and directs the drug release to the desired target, benefiting the clinical perspectives for these prodrugs (36,37,88).

1.5 Triazenes as anticancer drugs

Triazenes, are a group of open chain chemical compounds characterized by having a N=N-N moiety in their structure (Figure 15). Their first synthesis was achieved in 1862, by Griess, through the incomplete diazotation of aniline. Another way to synthesize these compounds is by reacting an alkyl azide with the appropriate Grignard or alkyl lithium reagent (92–94) or by coupling a diazonium salt with an amine (95). The three adjacent nitrogen atoms are responsible for the chemical, physical and antitumor properties of triazenes (96). Generally, these compounds are associated with aromatic rings (X=Ar), in what are defined as aryltriazenes (97,98).

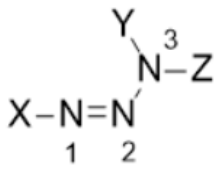

Figure 15 - General triazene structure

These compounds have been found to be useful, in a range of applications such as in the textile, paint and rubber sponge industries. They are also very useful as tools in organic synthesis because of their stability and adaptability to a number of synthetic transformations, being used, i.e., as protective groups, as intermediates in the synthesis of other chemical functions and as basis for heterocycle formation (99,100). They have also been found to show important biological activities (92,101).

Triazene´s chemistry has been extensively studied in regards of their synthesis, biological activity, mechanisms of action and stability, leading to the current understanding of these compounds, which despite being discovered more than a century ago, are still of great interest and can still lead to new compounds and potentially useful drugs (92–99,101,102).

Triazenes in cancer treatment

Of their biological activities, it is important to talk about the most studied and remarkable, its anticancer activity. Nevertheless, triazenes are also recognized for their carcinogenic, mutagenic and teratogenic activities (92,103). These activities arise from the fact that triazenes are alkylating agents, generating an highly reactive alkyldiazonium ion (Figure 16), responsible for the alkylation of DNA at the O^6 and N^7 positions of guanine, consequently leading to mutations and cell death (93,94,96).

In cancer treatment, triazenes that are of clinical interest include the agents dacarbazine (DTIC) and temozolomide (TMZ) that are used in the treatment of metastatic melanomas, soft tissue sarcoma, Hodgkin's and non-Hodgkin's lymphoma (93,96,97). Both compounds act, *in vivo*, through the formation of an active intermediate, a monomethyltriazene that itself is responsible for the cytotoxic activity of these compounds (96). Their activation and action mechanism are shown in Figure 16.

Problems associated with these compounds include necessity of metabolic activation (interindividual variability of effect), poor selectivity for cancer cells (giving rise to severe side effects) and low-water solubility (administration limitations). Although temozolomide has solved some of the problems associated with dacarbazine (dependence on hepatic activation and necessity of IV administration) by spontaneously releasing the active species at physiological pH and by allowing oral administration (having 100% bioavailability), the problem of low drug selectivity and heavy adverse effects of this medicine still remains (92,94,96,97). In consequence, there is an

increasing research and development of other triazenes to find more active compounds and overcome these problems.

To overcome these problems, diverse prodrug systems for triazenes are being investigated, either involving enzymes or other specific characteristics of the tumours that are aimed as targets (93,94,109,110,97,98,103–108).

Monomethyltriazenes

Monomethyltriazenes, provide a better alternative against dimethyltriazenes (marketed drugs) for prodrug development since they are the active moiety and are independent of metabolic activation, although having poor stability in water (94,95). The strategy of developing triazene prodrugs has been widely explored aiming at increasing specificity and reducing toxicity of these compounds (53,94). Additionally, monomethyltriazenes are adequate for prodrug synthesis, since they have an acidic hydrogen (-N**H**CH3) suitable for removal with a base which turns them into good nucleophiles that easily react with electrophiles. Ideally, this development aims at obtaining prodrugs that release the monomethyltriazene and have more suitable physicochemical properties with adequate half-lives and solubility.

In brief, triazene compounds represent a class of antineoplastic agents (alkylating agents) of primary interest in the clinic, with the possibility to expand their actual limited use, by using non-conventional strategies such as prodrugs (96).

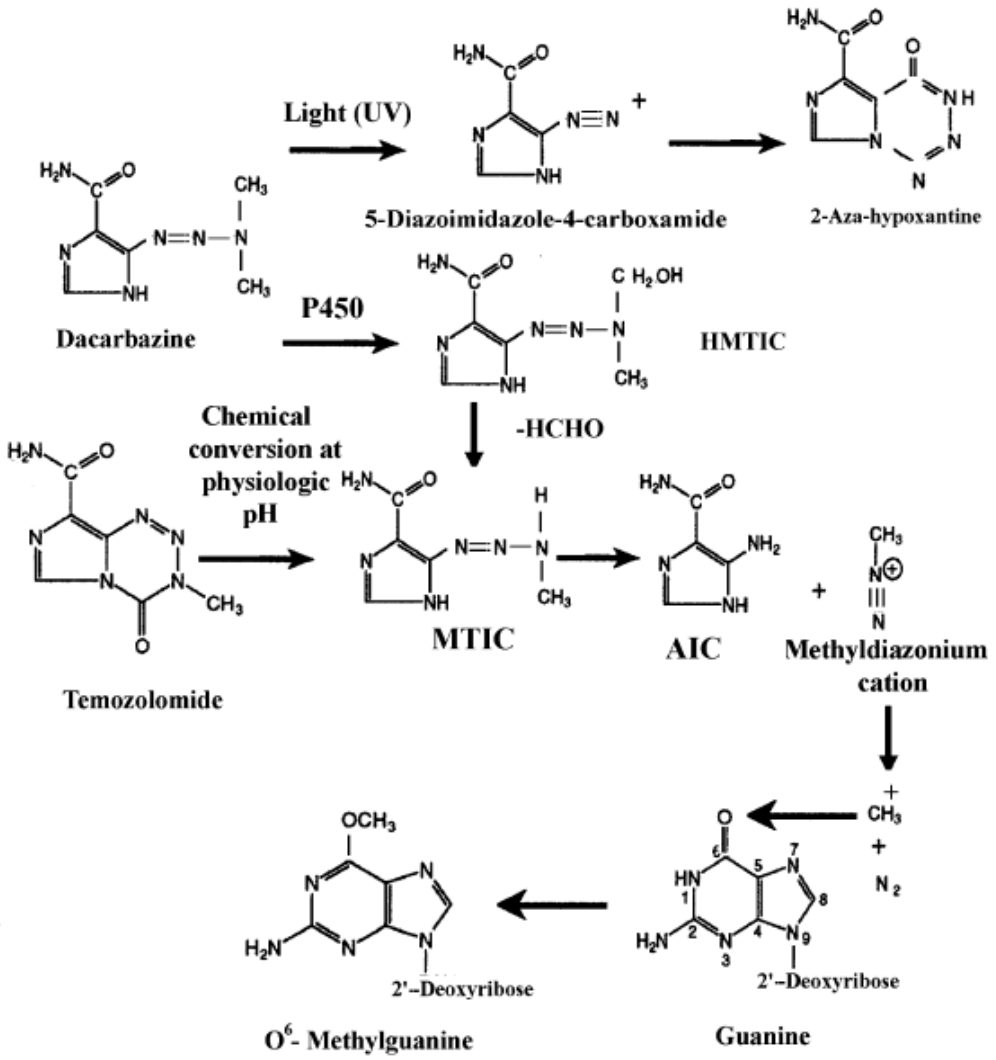

Figure 16 - Activation process for DTIC and TMZ anticancer therapeutic action (96)

2 Objectives

This work was aimed at synthesizing JFV-UMB (Figure 1), composed of a photolabile moiety (release system, the 6-nitroveratryl group) and a fluorescent moiety (umbelliferone), and identifying if it could be used as a light-dependent fluorescent probe. The main objective was to synthesize, purify and characterize this compound and to study its photoactivation after being stimulated with light of a specific wavelength for a certain amount of time. With this, we wanted to provide proof of concept for this compound as a fluorescent probe and of 6-nitroveratryl as a photolabile moiety.

After confirming the successful photoactivation of JFV-UMB, the work was aimed at developing triazene (monomethyltriazenes) prodrugs by exploring the same releasing system, this time in a self-immolative approach in which this system could release the therapeutic agent under hypoxic conditions (Figure 17). The main objective was to obtain a little library of self-immolative prodrugs that could be studied for their activity on cancer cell lines and whose release could be controlled and studied. With this, we wanted to see if it was possible to develop new anticancer triazenes to be delivered in a selective and targeted strategy, based on the hypoxic tumour microenvironment.

A future and final aim of this work, would be to connect the fluorescent probe with the triazene prodrug, obtaining not only a self-immolative prodrug, but a prodrug whose release and distribution could be followed and studied through the emission of fluorescence after drug release (functioning both as a drug and a probe).

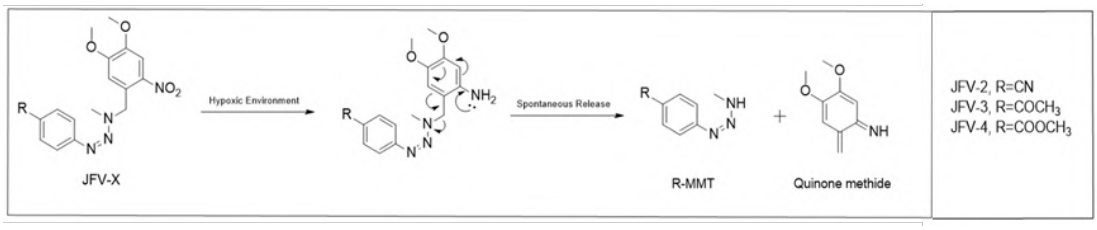

Figure 17 - Triazene prodrugs and their activation mechanism

Note

This work came amidst the SARS-CoV-2 pandemic, which severely impaired the execution of laboratorial work which was planned for March and April of 2020. This time limitation and the difficulties encountered when attempting to synthesize the

triazene conjugates led to the shortening of the presented data (no full characterization of the compounds and no *in vitro* activity studies). The work here presented follows the work developed in the curricular unit Project II where the synthesis of JFV-UMB was initiated.

3 Materials and Methods

3.1 Materials and Equipment

All reagents and solvents were purchased from commercial suppliers (Fluorochem, BDH, Aldrich Chemistry, Alfa Aesar, TCI, and Sigma-Aldrich). HPLC solvents were of analytical grade (Lichrosolv). Triazenes were synthesized by colleagues in the laboratory and should be considered as mutagenic and/or carcinogenic and appropriate care should be taken to handle them safely. All solvents were purified by standard techniques at FFUL. Reactions were monitored by thin-layer chromatography using silica-gel aluminium sheets (Merck Kieselgel 60 F254) that were visualized under UV light (CAMAG, 254nm). Column chromatography was performed using Merck silica gel 60 (230−400 mesh ASTM). Preparative thin layer chromatography (prep TLC) was carried out on glass plates coated with silica-gel (Merck Kieselgel 60 GF245). Melting points were determined using a Kofler camera Bock-Monoscop "'M'" and are uncorrected.

^{1}H and ^{13}C NMR spectra were recorded in $CDCl_3$ solutions using a Bruker Ultra-Shield 300 MHz spectrometer; chemical shifts (δ) are reported in parts per million (ppm) relative to tetramethylsilane (TMS) as internal standard and coupling constants (J) are expressed in hertz (Hz). Approximately, 3 mg of each sample were dissolved in about 0.5 mL of $CDCl_3$. Each sample was then submitted for analysis.

UV spectra were obtained with a Hitachi U-2000 Double-Beam UV/Vis Spectrophotometer. Samples' mother solutions of 0.01M were prepared (1mL). 30 μL of these mother solutions were diluted on 3 mL of ACN. These solutions' UV spectra were then recorded between 200-400nm or between 200-600nm.

Photoactivation assay was performed using a LED source (12x Nichia NCSU033B, Sahlmann Photochemical Solutions, 50% intensity, 2.7 W, 365nm). A UV lamp (CAMAG, 366nm) was used to observe the 96-well microplate after irradiation. Pictures of the photoactivation apparatus (led source + 96-well microplate) can be seen in Annex 1.

High-performance liquid chromatography (HPLC) was performed in an Elite LaChrom (VWR Hitachi) system comprised of an L-2130 pump, an L-2400 UV detector (using 320nm as the detection wavelength) and a Rheodyne® manual sample injector,

including a 20 µL sample loop. Chromatographic separation was achieved on a Lichrospher® 100 RP-18 (5µm) using a gradient solvent elution at a flow rate of 1.0 mL/min. The chromatographic elution was accomplished with a mobile phase consisting of water (A) and acetonitrile (B) in the following gradient: 0 min (10% B), 0–5 min (30% B), 5–10 min (50% B), 10–15 min (70% B), 15–20 min (90% B), 20–30 min (90% B). Total run time ranged from 20 to 30 minutes.

LC-MS was executed using a Waters Acquity™ Ultra Performance LC (Waters®, Ireland) UHPLC equipment comprised of binary pumps, a degasser, an automatic sampler, and a column oven. Chromatographic conditions are shown in Figure 18. The mass spectra were acquired using a triple quadrupole mass spectrometer, model Waters Acquity™ (Waters®, Ireland) equipped with an electrospray source operating in positive and negative mode, at different cone voltages (10 to 60V). For data acquisition and processing the MassLynx version 4.1 software was used. Approximately, 1mg of each sample was diluted in 1mL ACN. After this dilution, these samples were again diluted in ACN (1:10) and filtrated through a PTFE filter before analysis. The samples were then introduced in the UHPLC apparatus connected to the mass spectrometer, and analysed. MS (without LC) was executed with the same mass spectrometer and with the same sample preparation.

Column: Purospher® STAR RP-18 2 µm (2.1 x 50 mm)
Eluents: A: 0.1% HCOOH in water; B: Acetonitrile
Flow (mL/min): 0.3
Run time (min): 15 min
Oven temperature (°C) 35
Injection Volume (µL) 10 µL
HPLC Method:

Time (min)	A%	B%	Flow (mL/min)
0.00	90	10	0.300
1.00	90	10	0.300
6.00	5	95	0.300
10.00	5	95	0.300
10.10	90	10	0.300
15.00	90	10	0.300

Figure 18 - Chromatographic conditions for LC-MS

3.2 Methods

3.2.1 Syntheses

3.2.1.1 Synthesis of the Photolabile/Self-immolative moiety - JFV-1

DCM was dried for 30 minutes. 4,5-dimethoxy-2-nitrobenzyl alcohol (152.0 mg, 0.70 mmol), DMAP (51.6 mg, 0.42 mmol), TEA (117 µL, 0.84 mmol) and MsCl (65 µL, 0.84 mmol) were added sequentially to a round-bottom flask containing DCM (10mL). The reaction was left with magnetic stirring, under a nitrogen atmosphere and on an ice bath (at 0ºC) for 30 minutes. After this time, the reaction was left at room temperature for 40 minutes. The reaction course was followed by TLC using a Hexane:Ethyl acetate (1:1) mixture as eluent. The reaction was stopped at 70 minutes and diethyl ether (10mL) was added to the reaction mixture and left with stirring for 30 minutes.

The reaction mixture was filtered by vacuum followed by successive washes with 10% $CuSO_4$ (5mL), 5% $KHCO_3$ (5mL), Water (5mL) and Brine Reagent (5mL). The organic phase was then dried with anhydrous Na_2SO_4, filtered, collected to a round-bottom flask, and dried under vacuum. Impure product was obtained at this point.

Purification was executed by column chromatography. The column was prepared by the slurry method using a Hexane:Ethyl Acetate (7:3) mixture. The impure product was dissolved in the same mixture (2mL) and added to the column, followed by gradient elution first with a Hexane:Ethyl Acetate (7:3) (120mL) mixture and then with a Hexane:Ethyl Acetate (1:1) (110mL) mixture. JFV-1 was then collected in a round-bottom flask, the solvents were evaporated, and the compound was dried under vacuum (43.9% yield).

3.2.1.2 Synthesis of the probe - JFV-UMB

Umbelliferone (44.7 mg, 0.28 mmol) and caesium carbonate (139.8 mg, 0.41 mmol) were added to a round-bottom flask containing dried Acetone (1mL). JFV-1 (61.4 mg, 0.2 mmol) was dissolved in 1 mL of dried acetone and added to the previous solution. The reaction mixture was left overnight (18h) with stirring on a heated oil bath, under reflux (Temperature = 56ºC). During the reaction the system was protected from light with aluminium foil.

After, to precipitate JFV-UMB, 5 mL of ethyl ether were added to the reaction mixture, which was then filtered by vacuum. TLC was used to confirm the isolation of JFV-

UMB (Hexane:Ethyl Acetate 1:1 - eluent mixture). The obtained crystals were dried on a desiccator (58.3% yield). The compound´s structural properties were then obtained (Melting point, UV spectrum, and NMR spectrum).

3.2.1.3 Synthesis of the triazene prodrugs - JFV-2

JFV-1 (33.6mg, 0.115mmol) was added to a round-bottom flask containing 2mL of dried THF. This solution was put at 0ºC (with ice). The CN-MMT (18.4mg, 0.115mmol) solution was prepared with 2mL of dried THF. NaH (4.61mg, 0.173mmol - dry, 90%) was added to the CN-MMT solution yielding the activated CN-MMT salt. The activated CN-MMT was then added dropwise to the JFV-1 solution. After the addition, the ice was removed. The reaction was followed by TLC using an Ethyl Ether:Hexane 7:3 mixture and stopped at 65 minutes.

Purification of JFV-2 was executed by column chromatography (Method A). The column was prepared by the slurry method. The impure product was dissolved in an Ethyl Ether:Hexane 7:3 mixture (5mL) and added to the column, followed by regular elution with the same mixture. Fractions of interest were then collected, the solvents were evaporated, and the obtained solid was dried under vacuum. Method A failed to isolate the desired compound, so method B was employed afterwards with the obtained solid.

Purification was executed by prep TLC (Method B) using an Ethyl Ether:Hexane 7:3 mixture as eluent (120mL). The solid was dissolved in 3mL DCM and applied on the TLC plate. The TLC plate was eluted for 40-60 minutes. After the elution, the TLC plate was observed under an UV light and each signalled band was extracted from the silica using a gradient of solvents (DCM, then a DCM:Ethyl Acetate 1:1 mixture and then Ethyl Acetate). The solvents were evaporated, and the obtained solids were dried under vacuum. NMR was executed for each solid. LC-MS was also executed for the solid were JFV-2 was suspected of being present. A second prep TLC was executed with that solid using an Ethyl Ether:Hexane 1:1 mixture as eluent (120mL) and using the same prep TLC procedure.

3.2.1.4 Synthesis of the triazene prodrugs - JFV-3

JFV-1 (31.3 mg, 0.1074mmol) was added to a round-bottom flask containing 2mL of dried THF. This solution was put at 0ºC (with ice). The $COCH_3$-MMT (19mg, 0.1074 mmol) solution was prepared with 2mL of dried THF. NaH (4.33 mg, 1.612mmol - dry,

90%) was added to the $COCH_3$-MMT solution yielding the activated $COCH_3$-MMT salt. The activated $COCH_3$-MMT was then added dropwise to the JFV-1 solution. After the addition, the ice was removed. The reaction was followed by TLC using an Ethyl Ether:Hexane (7:3) mixture. The reaction was stopped at 19h and the solvent was evaporated after.

Another synthesis was executed in the same manner, using DMF as a solvent instead of THF. This reaction was stopped at 60 minutes. After the reaction, the round-bottom flask was put in a water bath (50ºC) and the DMF was removed under reduced pressure.

Purification was executed by prep TLC using a DCM:Methanol (9:0.5) mixture or an Ethyl Ether:Hexane 7:3 mixture as eluent (120mL). The compound was dissolved in 3mL DCM and applied on the TLC plate. The TLC plate was eluted for 40-60 minutes. After the elution, the TLC plate was observed under an UV light and each signalled band was extracted from the silica using a gradient of solvents (DCM, then a DCM:Ethyl Acetate 1:1 mixture and then Ethyl Acetate). The solvents were evaporated, and the obtained solids were dried under vacuum. NMR was executed for each solid. LC-MS was executed for the solid where JFV-3 was suspected of being present.

3.2.1.5 Synthesis of the triazene prodrugs - JFV-4

JFV-1 (33.9mg, 0,116mmol) was added to a round-bottom flask containing 2mL of dried THF. This solution was put at 0ºC (with ice). The $COOCH_3$-MMT (22.4mg, 0.116mmol) solution was prepared with 2mL of dried THF. NaH (4.64mg, 0.174mmol - dry, 90%) was added to the $COOCH_3$ solution yielding the activated $COOCH_3$ salt. The activated $COOCH_3$-MMT was then added dropwise to the JFV-1 solution. After the addition, the ice was removed. The reaction was followed by TLC using an Ethyl Ether:Hexane 7:3 mixture as eluent (120 mL). The reaction was stopped at 72h and the solvent was evaporated after.

Purification was executed by prep TLC using an Ethyl Ether:Hexane 7:3 mixture as eluent (120mL). The solid was dissolved in 3mL DCM and applied on the TLC plate. The TLC plate was eluted for 40-60 minutes. After the elution, the TLC plate was observed under an UV light and each signalled band was extracted from the silica using a gradient of solvents (DCM, then a DCM:Ethyl Acetate 1:1 mixture and then Ethyl Acetate). The solvents were evaporated, and the obtained solids were dried under vacuum. NMR was executed for each solid.

3.2.2 Assays

3.2.2.1 Photoactivation Assay of the probe - JFV-UMB

Umbelliferone and JFV-UMB solutions of 10^{-4}M were prepared in ACN from mother solutions of 0.01M. The Umbelliferone solution was then analysed by HPLC. The JFV-UMB solution was further diluted to 10^{-5}M in DMSO and PBS 0.01M (500µL JFV-UMB 10^{-4}M solution + 500µL DMSO + 4000µL PBS 0.01M). A blank solution was also prepared (900µL PBS 0.01M + 100µL DMSO).

200µL of the 10^{-5}M JFV-UMB solution were applied in triplicate in a 96-well microlitre plate (Figure 35) for each irradiation time. These triplicate sets of solutions were irradiated at 365 nm for, respectively, 15, 30, 45, 60 or 120 seconds. 200µL of the blank solution were applied in triplicate and irradiated along with the other solutions. 200µL of the 10^{-5}M JFV-UMB solution were also applied in triplicate and not irradiated (negative control). All solutions were observed under a UV light after irradiation. For each irradiation time and for the negative control solutions a sample was taken and analysed by HPLC. HPLC equipment and chromatographic conditions are described in point 3.1 of this report. The solutions irradiated for 15s and 120s were analysed by MS after the HPLC analysis.

4 Results and Discussion

4.1 JFV-1

4.1.1 Synthesis and Purification

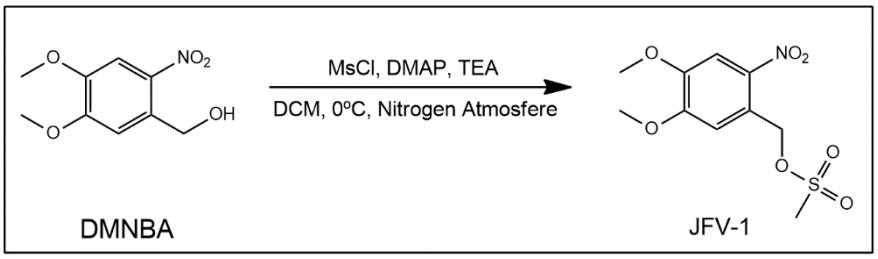

Figure 19 - Synthesis of JFV-1

JFV-1 is an intermediate product in our synthetic goals (JFV-UMB and JFV-2 to JFV-4). The need to synthesize JFV-1 comes from the nature of the reactions employed for our synthetic goals (SN2) which require a good leaving group to occur faster and with a higher yield. DMNBA has an OH group which is a bad leaving group (111), so it was necessary to convert this group to a mesylate group (by synthesizing JFV-1) which is a better leaving group (112).

JFV-1 was synthesized through the reaction shown in Figure 19. In this reaction, a rapid consumption of the DMNBA and the formation of JFV-1 were observed. After 5 minutes, the formation of a by-product (JFV-1-Cl - Figure 20) which increased through time was observed. At the end of the reaction (40 minutes), both the product and by-product were present in the reactional mixture. Since we realized by the TLC that time favours the formation of the by-product, we based the decision to stop the reaction on the TLC analysis.

JFV-1-Cl forms through a secondary reaction (S_N2) and its mechanism is shown in Figure 20 (111,112). This secondary reaction has been described (113) and is expected because it is a common reaction known from the synthesis of alkyl halides from alcohols, where first the alcohol is activated through the formation of a sulfonate group (which happens in this synthesis) which then easily is displaced by an halide (present in this synthesis after JFV-1 formation). Since in this reaction we have optimal conditions for an S_N2 reaction to occur (polar aprotic solvent and triethylamine as a base), after the desired reaction produces JFV-1, the chloride released from mesyl chloride acts as a nucleophile towards JFV-1, producing JFV-1-Cl. This reaction results

in a decrease of the yield of JFV-1 with time, and therefore it is important to control the time of the reaction to find a balance between formation of JFV-1 and its conversion to the undesired product. This control is possible, given that the reaction is quite fast to produce JFV-1, while the reaction to form the chloride occurs slowly and after the formation of JFV-1.

The reaction was stopped at 40 min, 5mL of ethyl ether were added and after 30 minutes a work-up was executed to remove water-soluble impurities like the non-consumed DMNBA and the triethylamine hydrochloride formed during the reaction. JFV-1 was then purified by column chromatography using gradient elution and the fractions containing JFV-1 and JFV-1-Cl were identified by TLC and collected. Column chromatography allowed the removal of the by-product. With this method, we were able to successfully isolate JFV-1 (43.9% yield).

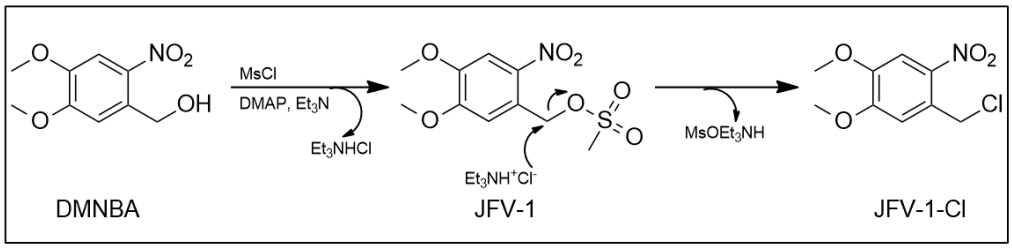

Figure 20 - Possible mechanism for by-product formation (Adapted from Ding (2011) (111)**)**

4.1.2 NMR Characterization

JFV-1 was characterized by ^{1}H NMR before (spectrum shown in Annex 2, Annex 3 and Annex 4) and after purification (spectrum shown in Annex 5 and Annex 6). The unpurified compound spectrum confirmed the presence of JFV-1 and of the by-product as already observed in the reaction TLCs. The molar quantity of by-product was superior than the one of JFV-1 since the integration values for equivalent hydrogens were bigger for JFV-1-Cl. On the purified compound spectrum, we only observed the presence of the JFV-l peaks, so we concluded that the compound was pure and suitable to proceed to the next reaction. We also collected JFV-1-Cl and obtained its ^{1}H NMR spectrum (Annex 7). On that spectrum, water and some minor impurities were observed. This was useful to have a more complete characterization of the reaction and a reference of the peaks of this impurity. A report of the chemical shifts of JFV-1 and JFV-1-Cl on the obtained spectra is shown in Figure 21 and Figure 22.

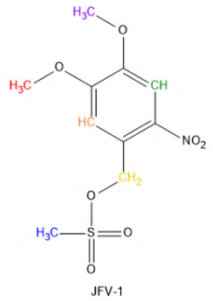

Chemical Shifts	
Purified Spectrum	**Unpurified Spectrum**
^{1}H NMR (300 MHz, $CDCl_3$) δ 7.74, 7.14, 5.64, 4.00, 3.98, 3.13.	^{1}H NMR (300 MHz, $CDCl_3$) δ 7.62, 7.03, 5.58, 3.94, 3.90, 3.08.

Figure 21 - Report of JFV-1 ^{1}H NMR shifts

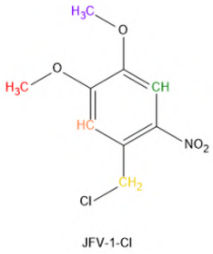

Chemical Shifts	
By-product Spectrum	**Unpurified Spectrum**
^{1}H NMR (300 MHz, $CDCl_3$) δ 7.69, 7.10, 5.01, 4.01, 3.96.	^{1}H NMR (300 MHz, $CDCl_3$) δ 7.68, 7.09, 4.94, 3.95, 3.91.

Figure 22 - Report of JFV-1-Cl ^{1}H NMR shifts

4.2 Umbelliferone-based probe

4.2.1 JFV-UMB

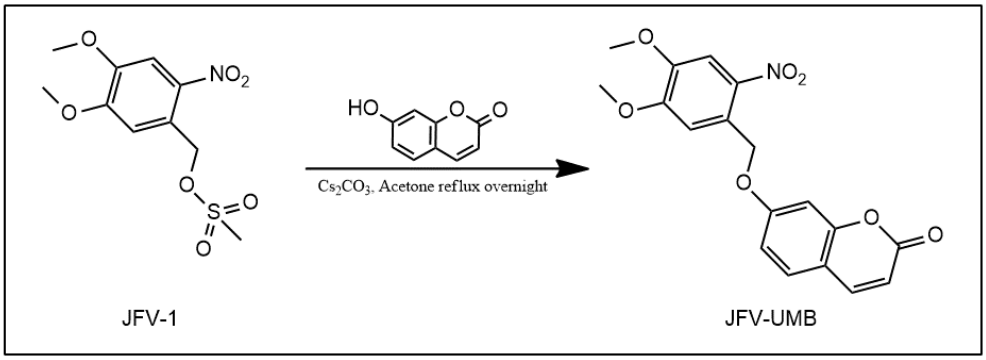

Figure 23 - Synthesis of JFV-UMB

4.2.1.1 Synthesis

We aimed at synthesizing JFV-UMB, a conjugate of Umbelliferone (fluorescent moiety) with JFV-1 (photorelease moiety), in order to obtain a non-fluorescent compound (umbelliferone fluorescence quenched by JFV-1) that could release the fluorescent moiety after being activated with a specific wavelength of light.

JFV-UMB was synthesized through the SN_2 reaction shown in Figure 23. This reaction involved the conjugation of Umbelliferone with JFV-1 and a work-up in which JFV-UMB was precipitated to separate it from Umbelliferone. The presence of JFV-UMB in the precipitate was confirmed by TLC. The yield of this reaction was of 58.3%.

Executing this synthesis, we realised the importance of using light protection during the reaction and work-up procedures (to avoid photodegradation of JFV-UMB to the starting reagents). In this matter, we chose to protect the reflux apparatus, the round-bottom flask containing the reactional mixture and the vial where the product was dried from light, using aluminium foil. Also, in the work-up, it was important to use vacuum filtration instead of simple filtration because it allows a faster separation of JFV-UMB (insoluble in ethyl ether) from the impurities present (the remaining JFV-1 and Umbelliferone) and a lower exposure time of the reactional mixture to light.

4.2.1.2 NMR Characterization

JFV-UMB was characterized by ^{1}H NMR (Annex 8). The ^{1}H NMR spectrum in chloroform showed only the peaks corresponding to JFV-UMB, free of impurities. JFV-UMB was also characterized by ^{13}C NMR (Annex 9). In the ^{13}C NMR, 17 peaks were observed, and although JFV-UMB has 18 carbons (subject to different electronical environments) this spectrum shows peaks that correspond to JFV-UMB. The peak at 56.47 ppm probably corresponds to both methoxy carbons because of the similarity of their environments explaining why only 17 peaks were observed. Figure 24 shows a report of the chemical shifts of JFV-UMB on ^{1}H-NMR and ^{13}C NMR.

JFV-UMB was further characterized using correlation spectra, including ^{1}H,^{1}H COSY (Figure 25), HSQC (Figure 26) and HMBC (Figure 27).

The COSY spectrum (Figure 25) showed a good correlation between the Hydrogen shifts (diagonal spots). Also, as expected for the pure product, a correlation between H19 and H18, between H13 and H14, and between H2 and H9 (correlation between hydrogens coupled with each other – cross peaks) was observed.

On the HSQC spectrum (Figure 26) correlation was observed between every Hydrogen and the corresponding Carbon supporting the identification of JFV-UMB (coherence of H-NMR with C-NMR).

The HMBC spectrum (Figure 27) was yet another tool to confirm the identification of JFV-UMB. On the HMBC spectrum, which suppresses correlations between carbons

and hydrogens one bond apart, most of the expected correlations between hydrogens and carbons two or three bonds apart were observed. Correlations were observed between several hydrogens and carbons, respectively: H9 – C2, H9 – C3, H9 – C4, H9 – C12, H25 – C1, H26 – C6, H19 – C15, H5 – C1, H5 – C3, H5 – C4, H5 – C6, H2 – C1, H2 – C6, H2 – C4, H2 – C9, H18 – C20, H17 – C16, H14 – C16, H14 – C12, H18 – C16.

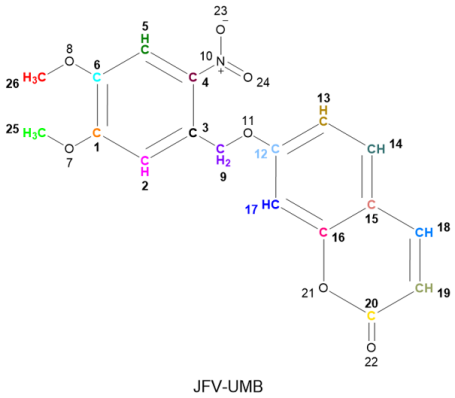

Chemical Shifts	
^{1}H NMR spectrum	^{13}C NMR spectrum
^{1}H NMR (300 MHz, $CDCl_3$) δ 7.81, 7.66, 7.44, 7.27, 6.97, 6.95, 6.30, 5.58, 4.00, 3.98.	^{13}C NMR (75 MHz, $CDCl_3$) δ 161.13, 160.85, 155.80, 154.00, 148.25, 143.15, 139.29, 129.05, 127.76, 113.81, 113.30, 112.50, 109.44, 108.28, 102.66, 67.61, 56.47.

Figure 24 - Report of JFV-UMB chemical shifts

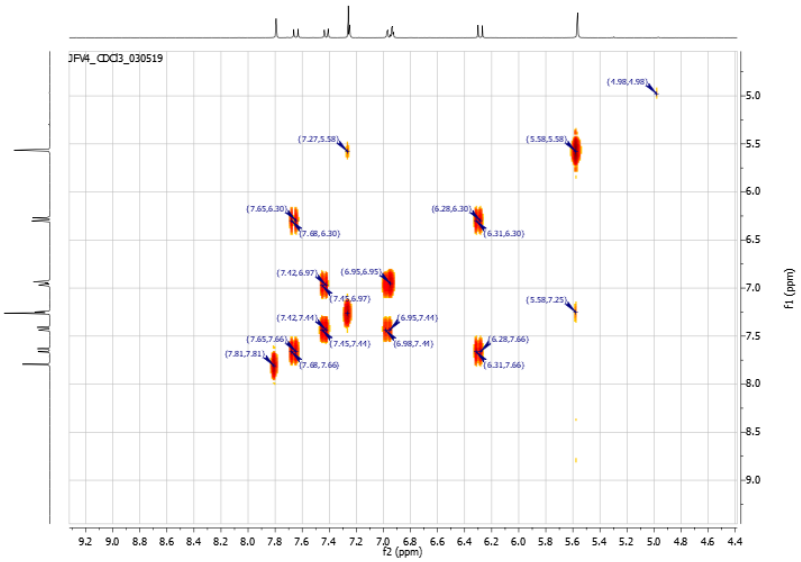

Figure 25 - JFV-UMB ^{1}H, ^{1}H COSY spectrum

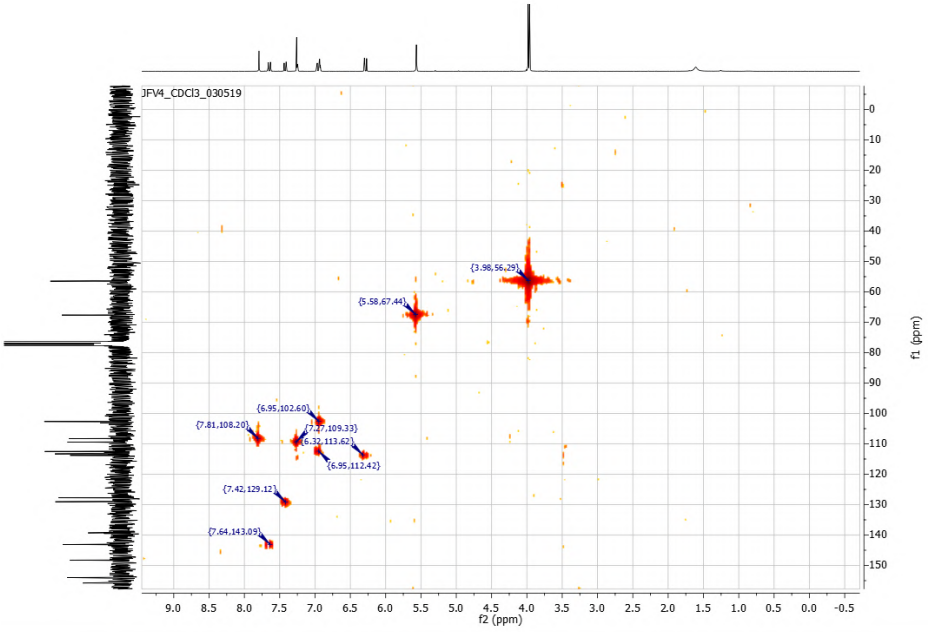

Figure 26 - JFV-UMB HSQC spectrum

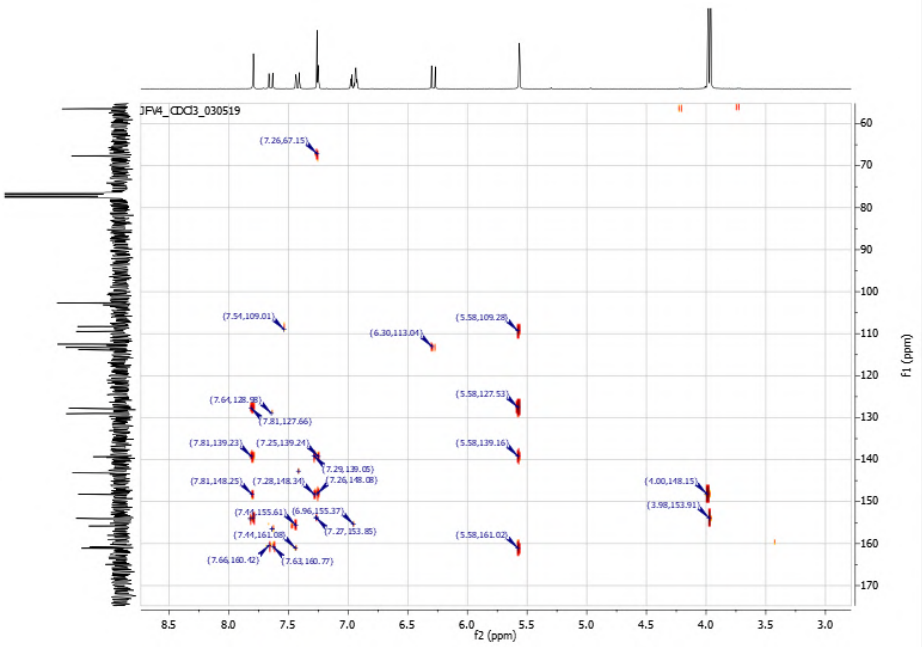

Figure 27 - JFV-UMB HMBC spectrum

4.2.1.3 Melting Point

The melting point of a substance is a characteristic of that substance in its pure state (114). Impurities lower and broaden the melting point range of pure substances, which generally have a melting point range of 0.5-2ºC (115). The determined melting point of JFV-UMB was 165-170ºC. The observed melting point range was high (5ºC) and indicates that the obtained compound contains impurities.

4.2.1.4 UV Spectrum

Given that the goal of this part of the work was the synthesis of a photoactivable compound which released a fluorescent compound after stimulation with a specific wavelength of light, we obtained the UV spectra (absorption) of both Umbelliferone and JFV-UMB. This information was useful, to study and follow the photoactivation of JFV-UMB (by detecting the appearance of Umbelliferone and disappearance of JFV-UMB through the common absorption maximum).

The obtained spectra can be seen in Figure 28 and Figure 29. For Umbelliferone, the obtained spectrum showed an absorption maximum at 319 nm which is in accord with previously reported values (77,78,116). The spectrum of JFV-UMB showed the presence of three peaks, respectively at 237, 320.5 and 399.5 nm, with the last peak having the bigger molar absorptivity.

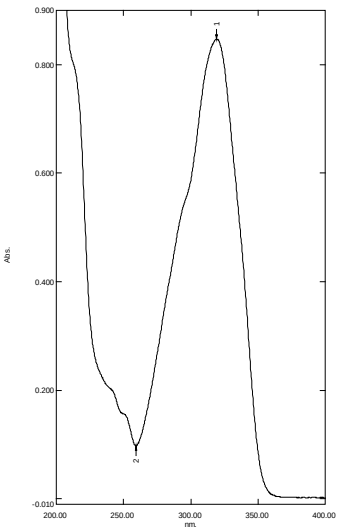

Figure 28 - Umbelliferone UV spectrum in ACN (200-400nm)

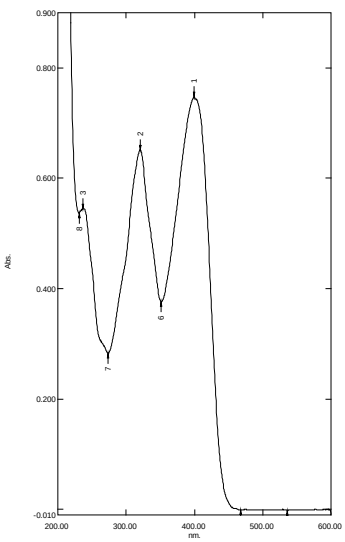

Figure 29 - JFV-UMB UV spectrum in ACN (200-600nm)

4.2.1.5 Photoactivation Assay

To provide proof of the photorelease of umbelliferone from JFV-UMB a photoactivation assay was executed. Compound solutions were irradiated in a 96-well microlitre plate for 15, 30, 45, 60 and 120 seconds and observed under a UV light for fluorescence (to confirm activation). Then, samples were taken and analysed by HPLC to verify the photoactivation of the compound. Blank (without JFV-UMB) and negative control (without irradiation) solutions were also observed under a UV light to verify the contrast between fluorescence (photoactivation of JFV-UMB) and no fluorescence (no photoactivation) before injecting the samples (with irradiated compound) in the HPLC apparatus. Irradiated solutions of JFV-UMB presented fluorescence under an UV light while negative control solutions and blank solutions weren´t fluorescent confirming that photoactivation had occurred in the irradiated solutions due to the exposure to light of a specific wavelength. A representation of the 96-well microlitre plate and solution distribution is shown in Figure 30.

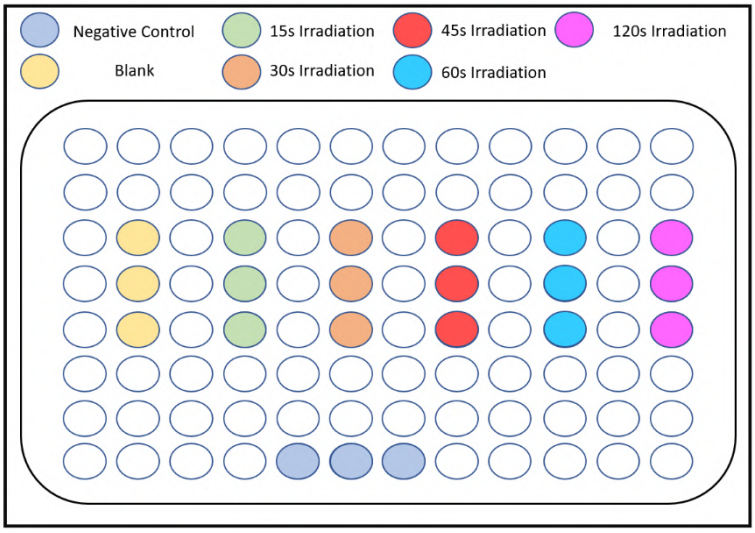

Figure 30 - 96-well microlitre plate and solution distribution for the photoactivation assay of JFV-UMB

In order to identify the umbelliferone liberation after the light irradiation of JFV-UMB, an umbelliferone standard solution was analysed by HPLC showing a retention time of 13,757 minutes (Figure 31), in accord with previously reported values (117). Non-irradiated samples (negative controls) were also analysed by HPLC, obtaining the retention time of JFV-UMB (to follow its activation) which was of 5,850 minutes (Figure 32).

Figure 33, Figure 34, Figure 35, Figure 36 and Figure 37 show the chromatograms of JFV-UMB solutions after different irradiation times. These chromatograms show JFV-UMB (peak at 6.18 minutes) being photoactivated and thus decreasing (area) with the irradiation time by releasing umbelliferone which rapidly converts to a degradation product (peak at 1.12 minutes) that is seen to increase (area) with the irradiation time. The retention time of JFV-UMB is different from the 5.850 minutes in the non-irradiated solution but this difference is justified because of the different environment (mixture of degradation products which impact the polarity of the compound in the analysed solution) to which JFV-UMB is subjected after irradiation in comparison to no irradiation. Additionally, this peak (6.18 minutes) presents an area close to the area of the JFV-UMB peak in the non-irradiated solution, which we associate with having a similar concentration (at 15s of irradiation where JFV-UMB has not degraded much yet) and thus corresponding to JFV-UMB (because both samples were prepared in the same conditions and with the same dilutions).

In order to clarify the products formed during the assay, mass spectra of the 15s and 120s irradiated solutions were obtained and are shown in Annex 10, Annex 11, Annex 12 and Annex 13. On both these spectra, the monoisotopic masses of JFV-UMB and umbelliferone weren´t observed while the masses for some umbelliferone degradation/transformation products were observed. This was in accord with what was observed on the HPLC where JFV-UMB was rapidly converted to umbelliferone degradation products. JFV-UMB wasn´t seen on the mass spectra because there was a time gap between HPLC analysis and MS analysis (one week) where the photoactivated JFV-UMB was probably converted in full to umbelliferone and umbelliferone degradation products. This was also the reason why the 15s and 120s mass spectra were very similar. The products we could observe on both spectra were hydroxylated derivatives of umbelliferone (3-Hydroxyumbelliferone and 4-hydroxyumbelliferone) which were expected in a phosphate buffer like PBS (74) and the 4-Hydroxycinnamic acid which results from the hydrolysis of the umbelliferone lactone ring. Other umbelliferone degradation products were expected (according to the literature) but not observed (118,119). Figure 38 shows the structures and monoisotopic masses of JFV-UMB, umbelliferone and the observed degradation products.

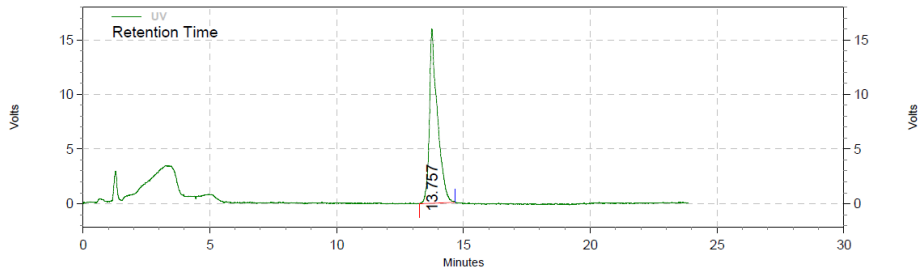

UV Results

Retention Time	Area	Area %	Height	Height %
13.757	1404234	100.00	63769	100.00

Figure 31 - Umbelliferone chromatogram (HPLC)

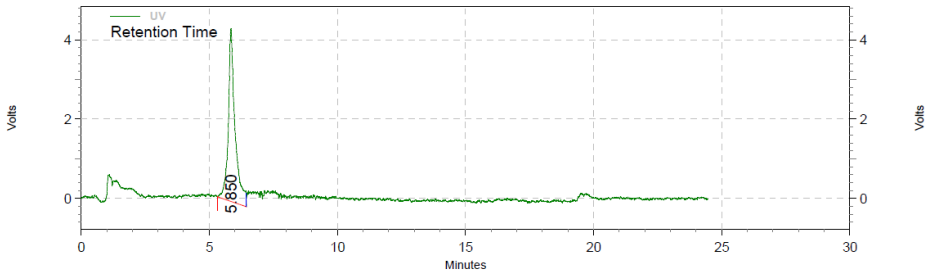

UV Results

Retention Time	Area	Area %	Height	Height %
5.850	318023	100.00	17426	100.00

Figure 32 - Non-Irradiated JFV-UMB chromatogram (HPLC)

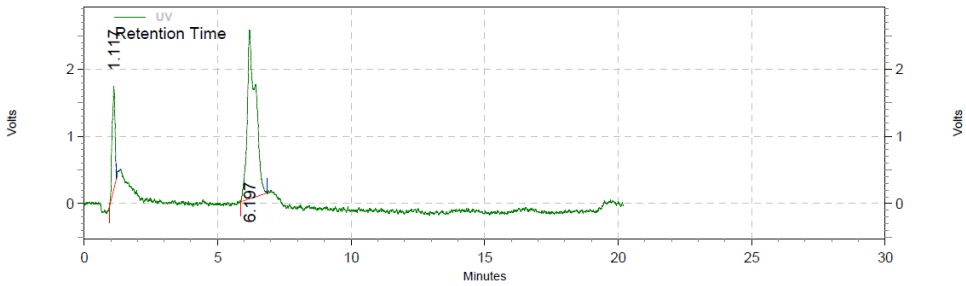

UV Results

Retention Time	Area	Area %	Height	Height %
1.117	45842	17.48	6124	37.86
6.197	216359	82.52	10052	62.14

Figure 33 - JFV-UMB Chromatogram after 15s Irradiation (HPLC)

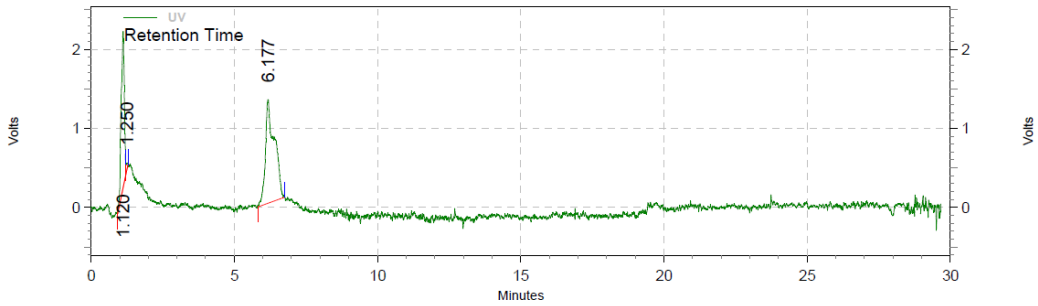

UV Results

Retention Time	Area	Area %	Height	Height %
1.120	59935	33.99	7909	58.50
1.250	1262	0.72	372	2.75
6.177	115127	65.29	5239	38.75

Figure 34 - JFV-UMB Chromatogram after 30s Irradiation (HPLC)

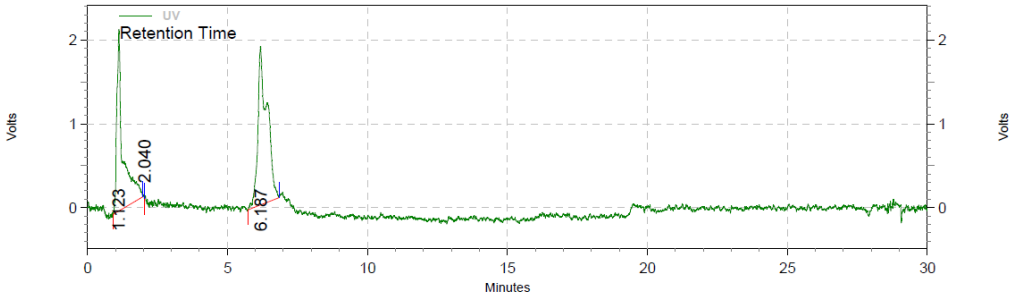

UV Results

Retention Time	Area	Area %	Height	Height %
1.123	128002	42.49	8655	53.38
2.040	1	0.00	0	0.00
6.187	173274	57.51	7559	46.62

Figure 35 - JFV-UMB Chromatogram after 45s Irradiation (HPLC)

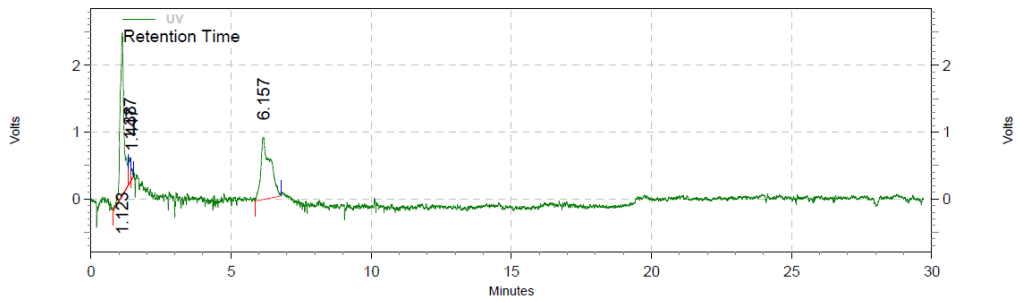

UV Results

Retention Time	Area	Area %	Height	Height %
1.123	91053	48.56	9746	61.81
1.387	7343	3.92	1565	9.93
1.447	2458	1.31	734	4.66
6.157	86666	46.22	3722	23.61

Figure 36 - JFV-UMB Chromatogram after 60s Irradiation (HPLC)

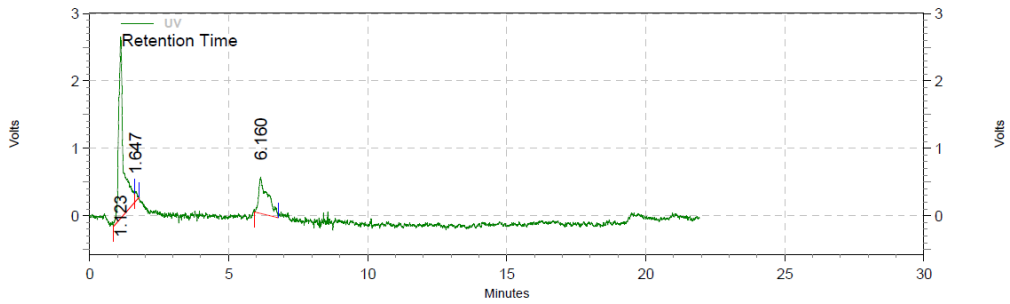

UV Results

Retention Time	Area	Area %	Height	Height %
1.123	125314	70.77	10747	79.59
1.647	3410	1.93	589	4.36
6.160	48347	27.30	2167	16.05

Figure 37 - JFV-UMB Chromatogram after 120s Irradiation (HPLC)

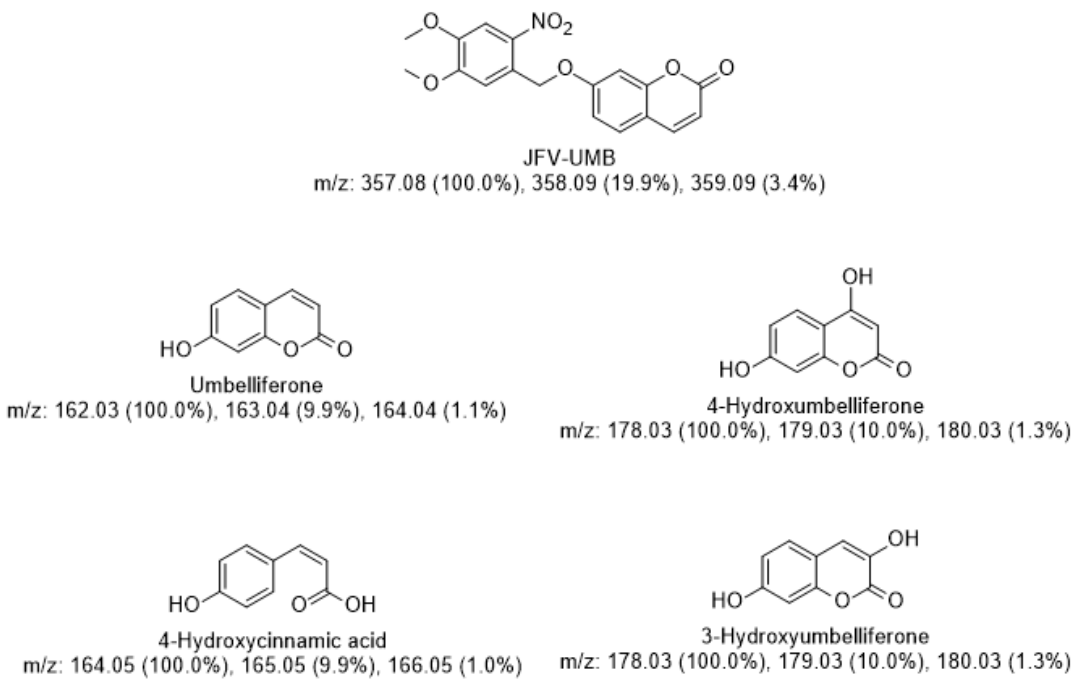

Figure 38 - JFV-UMB, Umbelliferone and Products Identified by Mass Spectroscopy on the Photoactivation Assay

4.3 Triazene Prodrugs

In the second part of our work, we aimed at synthesizing triazene prodrugs by conjugating JFV-1 with different monomethyltriazenes. With this, we intended to protect the monomethyltriazenes from their physiological instability (hydrolysis to methyldiazonium and aniline) and to achieve selective release of these cytotoxic compounds (95). The executed syntheses are schematized in Figure 39. Annex 14 and Annex 15 present a work timeline with a description of the work executed for the syntheses of the triazene prodrugs.

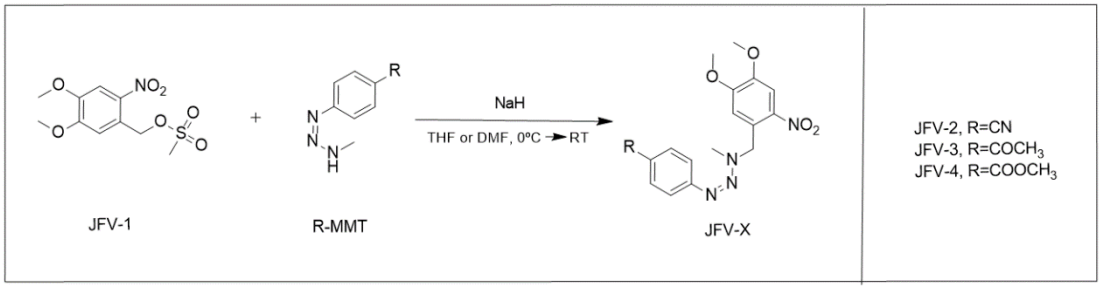

Figure 39 - Syntheses of the triazene prodrugs

4.3.1 JFV-2

We started by using CN-MMT as the triazene to conjugate with JFV-1. A flowchart of the work executed in the attempts to synthesize and isolate JFV-2 is shown in Annex 16 and includes remarks about the changes done between these attempts.

JFV-2 synthesis was attempted through the reaction shown in Figure 39. The reaction was followed by TLC. The TLCs showed that CN-MMT wasn´t fully consumed during the reaction and part of it degraded to the corresponding aniline. This degradation was expected, since triazenes are naturally unstable compounds (95). The TLCs also showed an incomplete consumption of JFV-1 and two unidentified spots (overlapping with known spots) which we suspected that could correspond to JFV-2 and a by-product. The TLCs were hard to interpret due to the overlapping of spots and to the presence of degradation products (95,120). The reaction was stopped at 65 minutes. After the reaction, column chromatography was executed but it was unsuccessful at separating the present compounds.

A second column was then attempted with an Ethyl Ether:Hexane 7:3 mixture (more polar than the previously used eluent). Once again, it was unsuccessful at separating the compounds, although two different fractions were obtained and analysed by NMR to look for JFV-2. The spectra of both fractions are shown in Annex 17 and Annex 18. The spectrum of the first fraction shows the presence of CN-Aniline and the presence of JFV-1 along with unidentified peaks that could correspond to JFV-2, CN-MMT or a possible by-product. The spectrum of the second fraction shows the presence of JFV-1 and JFV-1-Cl, which lead us to suspect the contamination of JFV-1 (starting reagent) with the by-product from its synthesis. We confirmed the contamination by obtaining the ^{1}H NMR spectrum of the JFV-1 used in this synthesis (Annex 19).

Without certainty about the presence of JFV-2 on the obtained fractions, we decided to attempt another synthesis, this time using an Ethyl Ether:Hexane 7:3 mixture for following the reaction with TLCs. During the reaction, we observed the presence of three bands. Two of them increased with time, probably corresponding to a mixture of JFV-2 and CN-Aniline. The third band decreased with time and probably corresponds to JFV-1 and/or JFV-1-Cl. Purification was attempted by column chromatography using an Ethyl Ether:Hexane 7:3 mixture. This column was unsuccessful in isolating

the desired compound. A second purification attempt was executed, this time using Prep TLC with the same eluent as the column. We chose to change the purification method due to the poor results obtained with the columns and to the expected improvement in the capability of isolating the desired compound by using Prep TLC (121). After elution, three bands were observed on the prep TLC and the compounds on each band were analysed by ^{1}H NMR.

On the lower band (spectrum not shown) we observed the presence of the contaminant (JFV-1-Cl). On the middle band (spectrum not shown) CN-Aniline and JFV-1 were present along with unidentified compounds. On the spectrum of the upper band (Annex 20) we could observe (along with unidentified compounds) the presence of CN-Aniline (degradation product) and probably the presence of a conjugate between JFV-1 and CN-Aniline (JFV-2-Ani) or of JFV-2. We could not distinguish for sure if the spectrum peaks corresponded to JFV-2 or JFV-2-Ani because we did not identify the expected N-H peak (only present in JFV-2-Ani) which is known to not appear or to be very broad (122) and we did not identify the expected N-CH_3 peak (only present in JFV-2) which should be present in a JFV-2 spectrum. Our attempt of interpretation includes both possibilities and is shown in Figure 40.

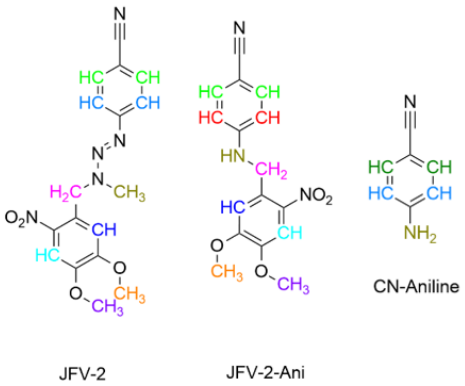

Chemical Shifts		
JFV-2	**JFV-2-Ani**	**CN-Aniline**
^{1}H NMR (300 MHz, $CDCl_3$) δ 7.55, 7.36, 7.35, 7.34, 7.33, 6.89, 4.71, 3.97, 3.96, unidentified peaks.	^{1}H NMR (300 MHz, $CDCl_3$) δ 7.55, 7.34, 7.33, 6.89, 6.53, 6.50, 4.71, 3.97, 3.96, unidentified peaks.	^{1}H NMR (300 MHz, $CDCl_3$) δ 7.36, 7.35, 6.59, 6.56, unidentified peaks.

Figure 40 - Possible report of the NMR shifts of the upper band (JFV-2 Second Synthesis)

To clarify which compounds were present in this fraction, an LC-MS analysis of the upper band was executed. Chromatograms and mass spectra can be found between Annex 21 and Annex 30. Annex 31 shows the monoisotopic masses of expected compounds. The chromatograms for ESI+ and for ESI- showed several peaks, of which

some we remark (see Figure 41). In the mass spectra, the monoisotopic mass of JFV-2 was observed confirming that the compound was successfully synthesized. The presence of CN-Aniline, of CN-MMT and of JFV-2-Ani was also observed. With this, we can conclude that the synthesis reaction was incomplete and that a secondary reaction occurred and produced JFV-2-Ani. We hypothesize that JFV-2 was present in a smaller quantity when comparing to JFV-2-Ani, based from the height of the chromatogram peaks (which can correlate with concentration), although we didn't use internal standards or calibration curves and the compounds might have different molar absorptivity constants at the used detection wavelength. Figure 41 summarizes the main finding of the LC-MS.

LC-MS		
Compound	**Retention Time**	**Monoisotopic Mass**
JFV-2	5.21 minutes ESI+	355+1
JFV-2-Ani	4.66 minutes ESI+/4.63 minutes ESI-	313+1 (ESI+), 313-1 (ESI-)
CN-Aniline	2.75 minutes ESI+ / 2.92 minutes ESI-	118+1 (ESI+), 118 (ESI-)
CN-MMT	5.05 minutes ESI-	160-1 (ESI-)

Figure 41 - Summary of LC-MS findings (JFV-2 Synthesis)

To try isolate the JFV-2 present, a second prep TLC was executed with the solid obtained from the upper band, using a new eluent (DCM). Of this prep TLC, four bands were observed and the upper three characterized by ^{1}H NMR. The spectrum of the upper band can be seen in Annex 32. On this spectrum we observed peaks that we strongly suspect that correspond to CN-MMT, although they could correspond to JFV-2 even if unlikely (based on the small peak on the MS). Figure 44 shows our interpretation of that spectrum. On the spectra of the second and third bands (not shown) we observed the presence of CN-MMT and CN-Aniline and suspected the presence of JFV-2-Ani.

With all this work executed, we can conclude that we synthesized JFV-2, although difficulties arose in its synthesis and purification. These difficulties can be explained by the intrinsic reactivity and instability of monomethyltriazenes which suffer decomposition in the reaction media, giving rise to a mixture of compounds which complicate TLC and NMR interpretation and impact the course of the reaction (97). We observed that a secondary reaction had occurred, producing JFV-2-Ani, and resulting in a low yield of JFV-2. We hypothesize (main hypothesis) that due to the high amount

of CN-Aniline formed during the reaction, the direct reaction of CN-Aniline (activated by NaH) with JFV-1 might have ocurred, producing JFV-2-Ani instead of JFV-2 (concurrent reaction seen in Figure 42). Another hypothesis is that this secondary reaction could be favoured by the known tautomerism of monomethyltriazenes (Figure 43). This tautomerism is affected by the substituent present in the aromatic ring connected to the triazene and in the case of the cyano group, which is electron withdrawing, favours the "unconjugated tautomer" (95,123–127). Based on the reaction mechanism (97), where the triazene is activated by the NaH (acts like a base by removing the amine hydrogen, raising the nucleophilicity of the triazene and favouring the S_N2 reaction), we hypothesize that with CN-MMT, the "unconjugated tautomer" could be present in a greater fraction of the total triazene, and be activated on its N-H, resulting in the synthesis of JFV-2-Ani, instead of JFV-2.

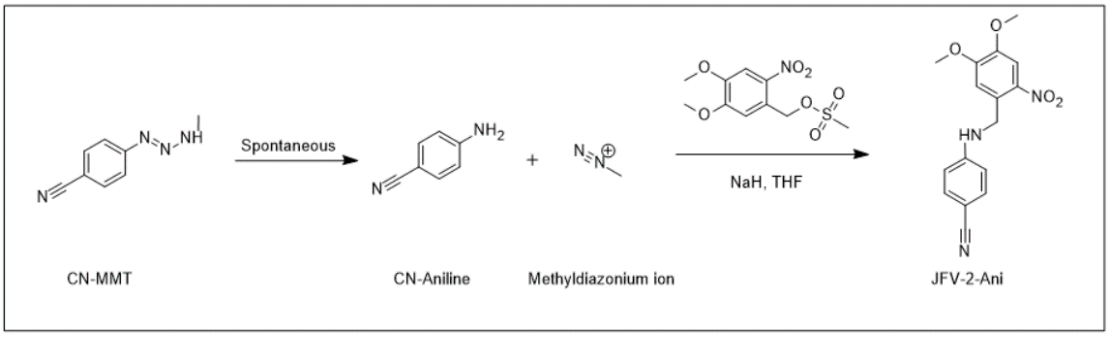

Figure 42 - Possible secondary reaction in the synthesis of JFV-2

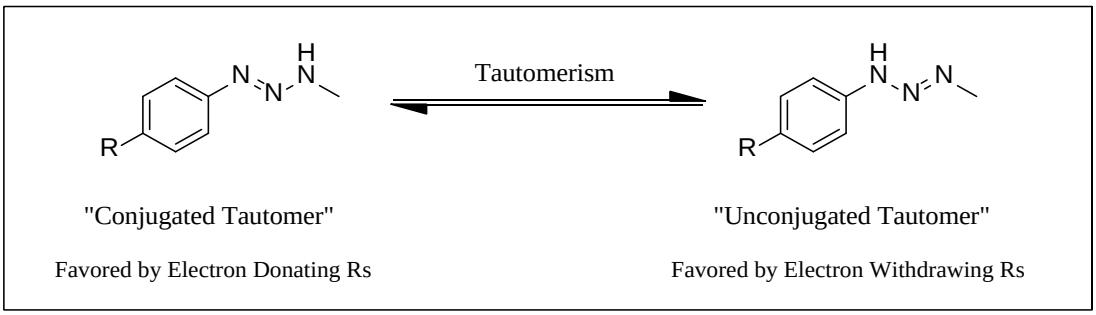

Figure 43 - Tautomerism of monomethyltriazenes

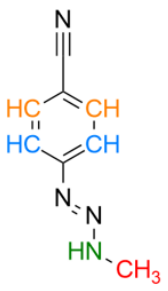

CN-MMT

Chemical Shifts
^{1}H NMR (300 MHz, $CDCl_3$) δ 7.66, 7.64, 7.45, 7.44, 3.85, unidentified peak.

Figure 44 - Report of the NMR shifts of the upper band (JFV-2 Second Synthesis Third Purification Attempt)

4.3.2 JFV-3

After the poor yield obtained with JFV-2 and its unsuccessful isolation we decided to try the reaction again using another monomethyltriazene ($COCH_3$-MMT). The reason behind our choice of MMT lies on the difficulties in analysing the ^{1}H NMR when using CN-MMT as a reagent because in the spectrum it only presents aromatic hydrogens (excluding N-CH_3 and N-H which were hard to identify) which can be confused with the hydrogens from JFV-1, JFV-1-Cl, DMNBA and other present compounds. Using $COCH_3$-MMT, we expected to observe the $COCH_3$ peak on the NMR, allowing us to determine the presence of the MMT or of the desired compound (JFV-3). Another reason for the change in substituent is the tautomerism of MMTs (Figure 43), which we suspected to favour the secondary reaction that occurred when we used CN-MMT, so we wanted to see if with the acetyl group it would be different (differences in electron withdrawing properties). The greater instability of triazenes with electron donating groups (128) refrained us from using triazenes with those groups.

A flowchart of the work executed in the attempts to synthesize and isolate JFV-3 is shown in Annex 33 and includes remarks about the changes done between these attempts.

JFV-3 synthesis was attempted through the reaction shown in Figure 39. The reaction was followed by TLC using an Ethyl Ether:Hexane 7:3 mixture. The TLCs showed the consumption of JFV-1 and $COCH_3$-MMT (not fully consumed) and the appearance of some $COCH_3$-Aniline with time. Additionally, a spot which could correspond to JFV-

3 appeared from 30 minutes on, increasing intensity with time. The reaction was left overnight this time to try to fully react JFV-1 with the $COCH_3$-MMT.

Before proceeding to the purification, a more polar eluent mixture (DCM:Methanol - 9:0.5) was tested in separating the compounds by TLC. With this eluent mixture we observed the separation of $COCH_3$-MMT and $COCH_3$-Aniline from JFV-1 and possibly JFV-3.

In the prep TLC, using the tested mixture as eluent, three bands were obtained, and their compounds were isolated and analysed by ^{1}H NMR. Their spectra can be seen in Annex 34, Annex 35 and Annex 36. On the spectrum of the upper band the presence of JFV-3 was observed, thus confirming that it had been successfully synthesized. On the spectrum of the middle band we can observe the presence of $COCH_3$-MMT, and $COCH_3$-Aniline as expected from the reaction. On the spectrum of the lower band we can observe the presence of $COCH_3$-Aniline and JFV-1-Cl therefore confirming the contamination of JFV-1 by JFV-1-Cl once again. JFV-1 was not observed in any band leading us to suspect that it was fully consumed during the reaction.

^{13}C NMR was obtained of the upper band was obtained (Annex 37). The ^{13}C NMR spectrum revealed that JFV-3 was present, although the carbonyl peak did not appear where expected (around 190 ppm). Interpretation of the NMR spectra for the three bands is shown in Figure 45.

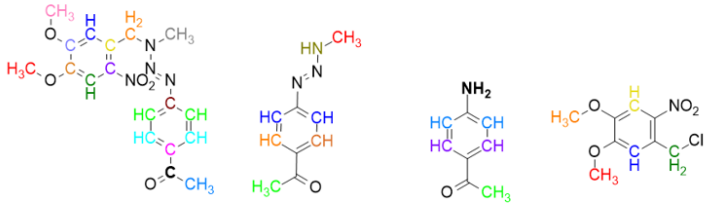

Chemical Shifts (bands from the prep TLC)					
Upper Band		Middle Band		Lower Band	
JFV-3		$COCH_3$-MMT	$COCH_3$-Aniline	$COCH_3$-Aniline	JFV-1-Cl
^{1}H NMR	^{13}C NMR	^{1}H NMR	^{1}H NMR	^{1}H NMR	^{1}H NMR
^{1}H NMR (300 MHz, $CDCl_3$) δ **7.71, 7.43, 7.12, 6.80, 5.03, 3.96, 3.92, 3.89, 2.52.**	^{13}C NMR (75 MHz, $CDCl_3$) δ **154.16, 152.70, 148.55, 148.23, 140.78, 140.52, 127.85, 124.84, 110.24, 107.69, 107.61, 60.09, 59.12, 56.41, 29.68.**	^{1}H NMR (300 MHz, $CDCl_3$) δ **7.96, 7.93, 7.45, 7.43, 3.96, 3.94, 3.92, 3.88, 2.54, peak not observed.**	^{1}H NMR (300 MHz, $CDCl_3$) δ **7.75, 7.72, 6.59, 6.56, 2.43, peak not observed.**	^{1}H NMR (300 MHz, $CDCl_3$) δ **7.75, 7.72, 6.59, 6.56, 2.43, peak not observed.**	^{1}H NMR (300 MHz, $CDCl_3$) δ **7.64, 7.12, 4.90, 3.94, 3.89.**

Figure 45 - Report of NMR shifts of the bands from the prep TLC (JFV-3 Synthesis Attempt 1)

To ascertain if JFV-3 was present on the upper band, we analysed it by LC-MS. The chromatogram and mass spectra are shown between Annex 38 and Annex 41. Annex 42 shows the monoisotopic masses of expected compounds (know contaminants, reagents, expected products or degradation products). On these spectra we could observe the presence of JFV-3, the presence of JFV-3-Ani and the presence of 4,5-dimethoxy-2-nitrosobenzaldehyde. JFV-3 was found to be present in the in the highest peak of the chromatogram (5.08min), confirming that this synthesis was successful. JFV-3-Ani was present in a smaller peak (4.74min). These observations could favour the theory formulated in the synthesis of JFV-2 (relevance of the aromatic substituent in the tautomerism of the MMT and on the reaction that occurs between the MMT and JFV-1), although we cannot correlate the peaks´ height with its concentration on the sample (no internal standards or calibration curves and differences in molar absorptivity constants). The reaction was also left overnight in opposition to JFV-2 synthesis which might have allowed more $COCH_3$-MMT to react with JFV-1 and produce more JFV-3. 4,5-dimethoxy-2-nitrosobenzaldehyde (mechanism of formation depicted in Figure 5) was also present and this shows that JFV-3 and/or JFV-3-Ani degraded when exposed to light (probably in the HPLC UV detector or when in storage), although $COCH_3$-Ani

or $COCH_3$-MMT (which would have been released when JFV-3 was exposed to light) were not observed on the mass spectra (might have degraded to smaller fragments that were not identified). Figure 46 summarizes the LC-MS findings.

LC-MS		
Compound	**Retention Time**	**Monoisotopic Mass**
JFV-3	5.08 minutes on ESI+	372+1 (ESI+)
JFV-3-Ani	4.74 minutes on ESI+	330+1 (ESI+)
4,5-dimethoxy-2-nitrosobenzaldehyde	4.39 minutes on ESI+	195+1 (ESI+)

Figure 46 - Summary of LC-MS findings (JFV-3 Synthesis)

Since JFV-3 was obtained in a small quantity and was not pure, a new attempt at its synthesis (Attempt 2) was executed as before. The reaction was followed by TLC and the same was observed as in the first attempt. This time, purification was attempted with column chromatography, using a DCM:Methanol (9:05) mixture as eluent to see if this method could be viable for purification. The column was unsuccessful at separating the different compounds in the reactional mixture except for the last TLC spot (suspected DMNBA - possible contaminant from JFV-1 synthesis or formed during this reaction) which was discarded. To purify the remaining mixture, we returned to the previously successful method and so a prep TLC was executed with the same eluent as the column. Three bands were obtained, isolated, and characterized by NMR. The spectra for the upper and middle band can be seen in Annex 43 and Annex 44. On the first spectrum the presence of JFV-3 can be observed along with unidentified peaks, confirming the successful synthesis of the compound and that it was still contaminated. On the spectrum of the middle band the presence of $COCH_3$-MMT, $COCH_3$-Aniline and JFV-3-Ani can be seen (Interpretation for JFV-3-Ani peaks in Figure 47). On the spectrum of the lower band, as in the previous attempt, the presence of JFV-1-Cl and $COCH_3$-Aniline was observed. These results show that JFV-1 is contaminated with JFV-1-Cl, that $COCH_3$-MMT degraded to the aniline during the reaction and that a secondary reaction still occurs and produces JFV-3-Ani.

To deepen the understanding of the products present or formed during the reaction, the lower band was analysed by MS. Mass spectra can be seen between Annex 45 and Annex 47. Annex 42 shows the monoisotopic masses of expected compounds. On the MS we observed the presence of $COCH_3$-Aniline confirming what was seen on the ^1H NMR spectrum, $COCH_3$-MMT in a very small peak only seen in the zoomed spectra

and 4,5-dimethoxybenzaldehyde resulting from the degradation of JFV-3 or JFV-3-Ani. JFV-1-Cl (present on the NMR) was not observed, probably due to degradation to smaller fragments during the analysis.

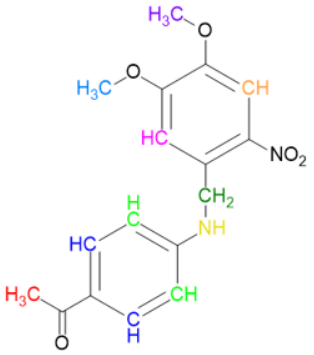

JFV-3-Ani

Chemical Shifts
^{1}H NMR (300 MHz, $CDCl_3$) δ 7.96, 7.93, 7.67, 6.94, 6.54, 6.51, 4.74, 3.96, 3.94, 3.92, 3.91, 2.44, not identified peak.

Figure 47 - Report of NMR shifts (of JFV-3-Ani) of the middle band of the prep TLC (JFV-3 Synthesis Attempt 2)

Based on the NMR results, to isolate JFV-3, another prep TLC was executed with the upper band of the previous prep TLC. The used eluent was DCM and four bands which we could not identify clearly (correspondence between band and compound) were observed on the prep TLC, isolated, and characterized by NMR. Their spectra can be seen between Annex 48 and Annex 51. On the spectrum of the first band 4,5-dimethoxy-2-nitrosobenzaldehyde was observed (Interpretation in Figure 48). On the spectra of the second and third bands no known or suspected compounds were identified although the peaks of the aromatic ring of JFV-1 and of its methoxy groups were present. On the spectrum of the fourth band we observed the presence of JFV-3 confirming its successful isolation.

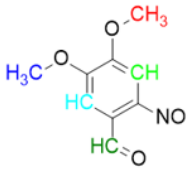

4,5-dimethoxy-2-nitrosobenzaldehyde

Chemical Shifts
^{1}H NMR (300 MHz, $CDCl_3$) δ **10.47, 7.64, 7.44, 4.05, 4.04.**

Figure 48 - Report of NMR shifts of the first band of the second prep TLC (JFV-3 Synthesis Attempt 2)

Although we successfully isolated JFV-3, we only obtained a small amount (about 5mg) of the compound (low yield of the synthesis and purification procedures). To try to improve the yield, now knowing how to isolate the compound, another synthesis was attempted using DMF as the reaction solvent (more suited to a S_N2 reaction) and stopping the reaction after 60 minutes (to avoid excessive degradation of $COCH_3$-MMT and by-product formation). DMF is a polar aprotic solvent, with an higher dielectric constant and dipole moment than THF (129–133). By choosing DMF as the reaction solvent, we aimed at increasing the strength of the nucleophile and promoting a faster reaction with a higher yield. With a faster reaction expected, we chose to stop the reaction at 60 minutes, to avoid undesired reactions. The reaction was followed by TLC (Ethyl Ether:Hexane 7:3 mixture) where we could observe the appearance of JFV-3 (suspected), and the appearance of spots in the Aniline/Triazene zone and disappearance in the JFV-1 zone. After the reaction, a prep TLC was executed using an Ethyl Ether:Hexane (7:3) mixture as eluent. Two bands were obtained and isolated, but the faculty was closed due to the Covid-19 outbreak, so the NMR spectra were not obtained.

We can conclude that we successfully synthesized JFV-3, with a low yield, and bypassed the problem seen in the synthesis of JFV-2 (secondary reaction) by choosing a MMT with a different substituent (possibly impacting the tautomerism of the triazene) and by improving the reaction conditions (time of the reaction) and the purification

method (prep TLC instead of column chromatography, and choice of a different eluent mixture).

4.3.3 JFV-4

With the success in the synthesis of JFV-3 we decided to attempt the synthesis of another conjugate using $COOCH_3$-MMT as the triazene and THF as solvent.

A flowchart of the work executed in the attempt to synthesize and isolate JFV-4 is shown in Annex 52 and includes remarks about this attempt.

JFV-4 synthesis was attempted through the reaction shown in Figure 39. The reaction was followed by TLC using an Ethyl Ether:Hexane 7:3 mixture as eluent. The TLCs showed the presence of the MMT (not fully consumed) and the corresponding aniline (degradation product) during the reaction. They also showed that JFV-1 was not totally consumed. A spot where JFV-4 was suspected to be appeared at 30 minutes and increased from there on. The reaction was left over 72h to fully consume the reagents.

After the reaction, a preparative TLC was executed (Ethyl Ether:Hexane 7:3 mixture), presenting three bands after elution. Each band was isolated and analysed by NMR. The ^{1}H NMR spectra for the three bands are shown in Annex 53, Annex 54 and Annex 55. The spectrum of the upper band (Interpretation in Figure 49) shows the presence of $COOCH_3$-Aniline (MMT degradation product), the spectrum of the middle band shows the presence of JFV-1-Cl and the spectrum of the third band doesn't show any compounds. With this, we concluded that the synthesis was unsuccessful, probably due to the excessive reaction time, which allowed for the full degradation of any formed product into $COOCH_3$-MMT and of the MMT into $COOCH_3$-Aniline. Once again, JFV-1-Cl was observed indicating the contamination of JFV-1.

In sum, we were able to synthesize and isolate one triazene prodrug (JFV-3) and learned, during the syntheses attempts, the importance of the duration of the reaction in the formation of degradation and secondary products and the importance of the eluent, either on the TLCs or on the prep TLCs, in the isolation of the desired compound from the complex mixture that arises from the reaction. Additionally, we were able to learn about the occurrence of a secondary reaction and hypothesize that it could happen because the degradation of the MMT to aniline, or because of the known tautomerism of triazenes.

In future attempts, to try to improve the yields of these syntheses (JFV-2, JFV-3, and JFV-4), we should test the reactions using DMF as a solvent, allowing for a faster and more complete S_N2 reaction and expectably higher yields. Additionally, when writing this report, we came across the fact that triazenes can also be used as photolabile moieties, being responsive and sensitive to light (63). Having known the instability of triazenes (and therefore of the desired products) to light (63,128,134,135), we could, in future attempts, make use of aluminium foil to protect the reactional mixture and the compound during purification and storage, to avoid degradation and excessive complexity which in the current syntheses attempts led to difficulty in isolation of the desired product.

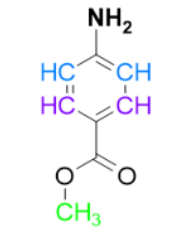

$COOCH_3$-Aniline

Chemical Shifts
^{1}H NMR (300 MHz, $CDCl_3$) δ 7.78, 7.76, 6.57, 6.54, 3.77, **peak not observed.**

Figure 49 - Report of NMR shifts of the upper band of the prep TLC (JF4-Synthesis)

5 Conclusions

Cancer is a thoroughly known enemy of humanity. Although many diagnosis tools and treatment options exist, they still don't suffice. Both diagnosis tools and treatment options still lack specificity and often associate with severe side effects and the appearance of drug resistance. Lately, strategies to overcome these problems have been investigated. Photopharmacology and the design of self-immolative prodrugs are amongst these strategies and gained our attention.

In this work, we have synthesized a compound (JFV-UMB), consisting of a release moiety and a fluorescent moiety, that could function as a chemical probe and be selectively activated (emitting fluorescence) in the presence of tumour cells (reductive microenvironment activation). After optimizing the synthesis and purification of this compound (obtaining a good yield) we characterized it (melting point, UV spectrum, ^{1}H NMR, ^{13}C NMR and correlation spectra). Then, we provided proof of concept for the release of the fluorescent moiety from the compound by using UV light of a specific wavelength to irradiate the compound (photoactivation assay). After the proof of concept, we synthesized conjugates of monomethyltriazenes (active species of marketed cancer drugs) that could function as self-immolative prodrugs, releasing the active species under a hypoxic environment (present in tumours). Difficulties arose in these syntheses, regarding the identification of the products that formed during the reaction, the isolation of the desired compound and the occurrence of a secondary undesired reaction. By experimenting different eluent mixtures and different purification techniques (column chromatography and prep TLC) and by using MS to analyse the compounds formed during the reaction we were able to overcome these problems. We successfully synthesized and isolated one of these compounds (JFV-3) with a low yield, having in this process hypothesized about the influence of the degradation of the monomethyltriazene or about the influence of its substituent (in the aromatic ring) in the product of the reaction. Due to the COVID-19 outbreak we were unable to pursue the experiments we originally planned and to fully finish the characterization of these compounds to assess their usefulness.

In the future, our aim lies in finishing this work by analysing the pending spectra, optimizing the reaction conditions and by further developing a compound which combines the probe moiety and the active moiety, and then studying the obtained

compound´s cytotoxicity and the release of the fluorescent and active moieties from the compound in ***in vitro*** studies.

References

1. Bedard PL, Hansen AR, Ratain MJ, Siu LL. Tumour heterogeneity in the clinic. Nature. 2013;501(7467):355–64.

2. Panchal RG. Novel therapeutic strategies to selectively kill cancer cells. Biochem Pharmacol. 1998;55(3):247–52.

3. Martin M, Wei H, Lu T. Targeting microenvironment in cancer therapeutics. Oncotarget. 2016;7(32):52575–83.

4. Tabassum DP, Polyak K. Tumorigenesis: It takes a village. Nat Rev Cancer [Internet]. 2015;15(8):473–83. Available from: http://dx.doi.org/10.1038/nrc3971

5. Ali ES, Md. Sharker S, Torequl Islam M, Khan IN, Shaw S, Rahman MA, et al. Targeting cancer cells with nanotherapeutics and nanodiagnostics: Current status and future perspectives. Semin Cancer Biol. 2020;(January):2–7.

6. Velcheti V, Schalper K. Basic Overview of Current Immunotherapy Approaches in Cancer. Am Soc Clin Oncol Educ B [Internet]. 2016 May;(36):298–308. Available from: http://ascopubs.org/doi/10.1200/EDBK_156572

7. Tsimberidou AM. Targeted therapy in cancer. Cancer Chemother Pharmacol. 2015;76(6):1113–32.

8. Chari RVJ. Targeted cancer therapy: Conferring specificity to cytotoxic drugs. Acc Chem Res. 2008;41(1):98–107.

9. Du W, Elemento O. Cancer systems biology: Embracing complexity to develop better anticancer therapeutic strategies. Oncogene. 2015;34(25):3215–25.

10. Dalby KN, Tekedereli I, Lopez-Berestein G, Ozpolat B. Targeting the prodeath and prosurvival functions of autophagy as novel therapeutic strategies in cancer. Autophagy. 2010;6(3):322–9.

11. Imai K, Takaoka A. Comparing antibody and small-molecule therapies for cancer. Nat Rev Cancer. 2006;6(9):714–27.

12. Duncan M, Moschopoulou E, Herrington E, Deane J, Roylance R, Jones L, et al. Review of systematic reviews of non-pharmacological interventions to improve

quality of life in cancer survivors. BMJ Open. 2017;7(11):1.

13. Erren TC, Groß JV, Koch MS, Erren M, Meyer-Rochow VB. What do we know 40 years after nixon declared the “War on Cancer”? on the origin, prevention and treatment of cancer. J Cancer Educ. 2012;27(4):597–600.

14. LACINA L, ČOMA M, DVOŘÁNKOVÁ B, KODET O, MELEGOVÁ N, GÁL P, et al. Evolution of Cancer Progression in the Context of Darwinism. Anticancer Res. 2018;39(1):1–16.

15. Hanahan D, Weinberg RA. Hallmarks of cancer: the next generation. Cell [Internet]. 2011;144(5):646–74. Available from: http://www.ncbi.nlm.nih.gov/pubmed/21376230

16. Leong SP, Aktipis A, Maley C. Cancer initiation and progression within the cancer microenvironment. Clin Exp Metastasis [Internet]. 2018;35(5–6):361–7. Available from: http://dx.doi.org/10.1007/s10585-018-9921-y

17. Sarma P, Medhi B. Photopharmacology. Indian J Pharmacol [Internet]. 2017 [cited 2019 Jul 2];49(3):221–2. Available from: http://www.ncbi.nlm.nih.gov/pubmed/29033480

18. Schmidt D, Rodat T, Heintze L, Weber J, Horbert R, Girreser U, et al. Axitinib: A Photoswitchable Approved Tyrosine Kinase Inhibitor. ChemMedChem. 2018;13(22):2415–26.

19. Van Rixel VHS, Busemann A, Göttle AJ, Bonnet S. Preparation, stability, and photoreactivity of thiolato ruthenium polypyridyl complexes: Can cysteine derivatives protect ruthenium-based anticancer complexes? J Inorg Biochem [Internet]. 2015;150:174–81. Available from: http://dx.doi.org/10.1016/j.jinorgbio.2015.05.010

20. Lerch MM, Hansen MJ, van Dam GM, Szymanski W, Feringa BL. Emerging Targets in Photopharmacology. Angew Chemie - Int Ed. 2016;55(37):10978–99.

21. Velema WA, Szymanski W, Feringa BL. Photopharmacology: Beyond proof of principle. J Am Chem Soc. 2014;136(6):2178–91.

22. Pfaff P, Samarasinghe KTG, Crews CM, Carreira EM. [ASAP] Reversible Spatiotemporal Control of Induced Protein Degradation by Bistable PhotoPROTACs. ACS Cent Sci [Internet]. Available from:

http://dx.doi.org/10.1021/acscentsci.9b00713?utm_source=researcher_app&utm_medium=referral&utm_campaign=RESR_MRKT_Researcher_inbound

23. Lv W, Li Y, Li F, Lan X, Zhang Y, Du L, et al. Upconversion-like Photolysis of BODIPY-Based Prodrugs via a One-Photon Process. J Am Chem Soc. 2019;141(44):17482–6.

24. Škalamera D, Matković M, Uzelac L, Kralj M, Mlinarić-Majerski K, Bohne C, et al. Photodeamination to quinone methides in cucurbit[n] urils: Potential application in drug delivery. Org Biomol Chem. 2018;16(46):8908–12.

25. Dion J, Minoshima F, Saito S, Kiyoi K, Hasehira K, Tateno H. Photoactivable Elimination of Tumorigenic Human Induced Pluripotent Stem Cells by Using a Lectin–Doxorubicin Prodrug Conjugate. ChemBioChem. 2019;20(12):1606–11.

26. Evans MA, Huang PJ, Iwamoto Y, Ibsen KN, Chan EM, Hitomi Y, et al. Macrophage-mediated delivery of light activated nitric oxide prodrugs with spatial, temporal and concentration control. Chem Sci. 2018;9(15):3729–41.

27. Giles NM, Kumari S, Gang BP, Yuen CWW, Billaud EMF, Giles GI. The Molecular Design of S-Nitrosothiols as Photodynamic Agents for Controlled Nitric Oxide Release. Chem Biol Drug Des. 2012;80(3):471–8.

28. Li LS, Babendure JL, Sinha SC, Olefsky JM, Lerner RA. Synthesis and evaluation of photolabile insulin prodrugs. Bioorganic Med Chem Lett. 2005;15(17):3917–20.

29. Imberti C, Zhang P, Huang H, Sadler PJ. New Designs for Phototherapeutic Transition Metal Complexes. Angew Chemie - Int Ed. 2020;59(1):61–73.

30. Thiel Z, Rivera-Fuentes P. Single-Molecule Imaging of Active Mitochondrial Nitroreductases Using a Photo-Crosslinking Fluorescent Sensor. Angew Chemie - Int Ed. 2019;58(33):11474–8.

31. Wei Y, Yan Y, Pei D, Gong B. A photoactivated prodrug. Bioorganic Med Chem Lett. 1998;8(18):2419–22.

32. Zhang Z, Hatta H, Ito T, Nishimoto SI. Synthesis and photochemical properties of photoactivated antitumor prodrugs releasing 5-fluorouracil. Org Biomol Chem. 2005;3(4):592–6.

33. Zhao J, Liu N, Sun S, Gou S, Wang X, Wang Z, et al. Light-activated ruthenium (II)-bicalutamide prodrugs for prostate cancer. J Inorg Biochem [Internet]. 2019;196(March):1–9. Available from: https://doi.org/10.1016/j.jinorgbio.2019.03.024

34. Koch CJ, Evans SM. Optimizing hypoxia detection and treatment strategies. Semin Nucl Med [Internet]. 2015;45(2):163–76. Available from: http://dx.doi.org/10.1053/j.semnuclmed.2014.10.004

35. Wan QQ, Gao XH, He XY, Chen SM, Song YC, Gong QY, et al. A cresyl violet-based fluorescent off-on probe for the detection and imaging of hypoxia and nitroreductase in living organisms. Chem - An Asian J. 2014;9(8):2058–62.

36. Liang J. Hypoxia-activated prodrugs and redox-responsive nanocarriers. 2018;

37. Sharma A, Arambula JF, Koo S, Kumar R, Singh H, Sessler JL, et al. Hypoxia-targeted drug delivery. 2019;48(3):771–813.

38. Zhou F, Feng B, Yu H, Wang D, Wang T, Ma Y, et al. Tumor Microenvironment-Activatable Prodrug Vesicles for Nanoenabled Cancer Chemoimmunotherapy Combining Immunogenic Cell Death Induction and CD47 Blockade. 2019;31(14):1–11.

39. Zhang X, Li X, You Q, Zhang X. Prodrug strategy for cancer cell-specific targeting: A recent overview. 2017;139:542–63. Available from: http://dx.doi.org/10.1016/j.ejmech.2017.08.010

40. Abet V, Filace F, Recio J, Alvarez-Builla J, Burgos C. Prodrug approach: An overview of recent cases. 2017;127:810–27. Available from: http://dx.doi.org/10.1016/j.ejmech.2016.10.061

41. Zhao Y, Zheng Q, Dakin K, Xu K, Martinez ML, Li WH. New Caged Coumarin Fluorophores with Extraordinary Uncaging Cross Sections Suitable for Biological Imaging ApplicatZhao, Y., Zheng, Q., Dakin, K., Xu, K., Martinez, M. L., & Li, W. H. (2004). New Caged Coumarin Fluorophores with Extraordinary Uncaging Cro. J Am Chem Soc. 2004;126(5):4653–63.

42. Sedgwick AC, Hayden A, Hill B, Bull SD, Elmes RBP, James TD. A simple umbelliferone based fluorescent probe for the detection of nitroreductase. Front Chem Sci Eng. 2018;12(2):311–4.

43. Dillon KM, Powell CR, Matson JB. Self-Immolative Prodrugs: Effective Tools for the Controlled Release of Sulfur Signaling Species. 2019;30(5):525–31.

44. Zang C, Wang H, Li T, Zhang Y, Li J, Shang M, et al. A light-responsive, self-immolative linker for controlled drug delivery: Via peptide- and protein-drug conjugates. 2019;10(39):8973–80.

45. Li Z, Li X, Gao X, Zhang Y, Shi W, Ma H. Nitroreductase detection and hypoxic tumor cell imaging by a designed sensitive and selective fluorescent probe, 7-[(5-Nitrofuran-2-yl)methoxy]-3 H -phenoxazin-3-one. Anal Chem. 2013;85(8):3926–32.

46. Grimm JB, Heckman LM, Lavis LD. The chemistry of small-molecule fluorogenic probes [Internet]. 1st ed. Vol. 113, Progress in Molecular Biology and Translational Science. Elsevier Inc.; 2013. 1–34 p. Available from: http://dx.doi.org/10.1016/B978-0-12-386932-6.00001-6

47. Horbert R, Pinchuk B, Davies P, Alessi D, Peifer C. Photoactivatable Prodrugs of Antimelanoma Agent Vemurafenib. ACS Chem Biol. 2015;10(9):2099–107.

48. Shamay Y, Adar L, Ashkenasy G, David A. Light induced drug delivery into cancer cells. Biomaterials. 2011;32(5):1377–86.

49. Shin SH, Bode AM, Dong Z. Precision medicine: the foundation of future cancer therapeutics. npj Precis Oncol [Internet]. 2017 Dec 24 [cited 2019 Jul 2];1(1):1–2. Available from: http://www.nature.com/articles/s41698-017-0016-z

50. Cancer Essentials - Immunotherapy [Internet]. [cited 2019 Jul 2]. Available from: https://www.elsevier.com/connect/cancer-essentials-immunotherapy

51. Torre LA, Bray F, Siegel RL, Ferlay J, Lortet-Tieulent J, Jemal A. Global cancer statistics, 2012. CA Cancer J Clin [Internet]. 2015;65(2):87–108. Available from: http://www.ncbi.nlm.nih.gov/pubmed/25651787

52. Bray F, Ferlay J, Soerjomataram I, Siegel RL, Torre LA, Jemal A. Global cancer statistics 2018: GLOBOCAN estimates of incidence and mortality worldwide for 36 cancers in 185 countries. CA Cancer J Clin [Internet]. 2018;68(6):394–424. Available from: http://www.ncbi.nlm.nih.gov/pubmed/30207593

53. Holohan C, Van Schaeybroeck S, Longley DB, Johnston PG. Cancer drug resistance: an evolving paradigm. Nat Rev Cancer [Internet]. 2013 Oct

24;13(10):714–26. Available from: http://www.nature.com/articles/nrc3599

54. Drake CG. Basic overview of current immunotherapy approaches in urologic malignancy. Urol Oncol Semin Orig Investig [Internet]. 2006 Sep;24(5):413–8. Available from: https://linkinghub.elsevier.com/retrieve/pii/S1078143905002061

55. Du L, Li M, Zheng S, Wang B. Rational design of a fluorescent hydrogen peroxide probe based on the umbelliferone fluorophore. Tetrahedron Lett. 2008;49(19):3045–8.

56. Fomina N, Sankaranarayanan J, Almutairi A. Photochemical mechanisms of light-triggered release from nanocarriers. Adv Drug Deliv Rev. 2012;64(11):1005–20.

57. Ryu KA, Stutts L, Tom JK, Mancini RJ, Esser-Kahn AP. Stimulation of innate immune cells by light-activated TLR7/8 agonists. J Am Chem Soc. 2014;136(31):10823–5.

58. Lee KS, Kim HJ, Kim GH, Shin I, Hong JI. Fluorescent chemodosimeter for selective detection of cyanide in water. Org Lett. 2008;10(1):49–51.

59. Yuan Z, Xu M, Wu T, Zhang X, Shen Y, Ernest U, et al. Design and synthesis of NQO1 responsive fluorescence probe and its application in bio-imaging for cancer diagnosis. Talanta [Internet]. 2019;198(February):323–9. Available from: https://doi.org/10.1016/j.talanta.2019.02.009

60. Liu J, Yin Z. A novel NIR-emissive probe with large Stokes shift for hypochlorite detection and imaging in living cells. Talanta [Internet]. 2019;196(December 2018):352–6. Available from: https://doi.org/10.1016/j.talanta.2018.12.086

61. Elamri I, Heumüller M, Herzig LM, Stirnal E, Wachtveitl J, Schuman EM, et al. A New Photocaged Puromycin for an Efficient Labeling of Newly Translated Proteins in Living Neurons. ChemBioChem. 2018;19(23):2458–64.

62. Weis S, Shafiq Z, Gropeanu RA, Del Campo A. Ethyl substituted coumarin-4-yl derivatives as photoremovable protecting groups for amino acids with improved stability for SPPS. J Photochem Photobiol A Chem [Internet]. 2012;241:52–7. Available from: http://dx.doi.org/10.1016/j.jphotochem.2012.05.014

63. Kla P, Bochet CG, Givens R, Rubina M, Popik V, Kostikov A, et al. Photoremovable protecting groups in chemistry and biology: reaction mechanisms and efficacy. Chem Rev [Internet]. 2013;113(1):119–91. Available from: http://www.ncbi.nlm.nih.gov/pubmed/23256727

64. Kaplan JH, Forbush B, Hoffman JF. Rapid photolytic release of adenosine 5'-triphosphate from a protected.pdf. 1978;17(10):1929–35.

65. Pelliccioli AP, Wirz J. Photoremovable protecting groups: Reaction mechanisms and applications. Photochem Photobiol Sci. 2002;1(7):441–58.

66. Garbaccio RM, Parmee ER. The Impact of Chemical Probes in Drug Discovery: A Pharmaceutical Industry Perspective. Cell Chem Biol [Internet]. 2016;23(1):10–7. Available from: http://dx.doi.org/10.1016/j.chembiol.2015.11.011

67. Blagg J, Workman P. Choose and Use Your Chemical Probe Wisely to Explore Cancer Biology. Cancer Cell [Internet]. 2017;32(1):9–25. Available from: http://dx.doi.org/10.1016/j.ccell.2017.06.005

68. Selvarasu S, Ow DSW, Lee SY, Lee MM, Oh SKW, Karimi IA, et al. Characterizing escherichia coli DH5α growth and metabolism in a complex medium using genome-scale flux analysis. Biotechnol Bioeng. 2009;102(3):923–34.

69. Givens RS, Rubina M, Wirz J. Applications of p-hydroxyphenacyl (pHP) and coumarin-4-ylmethyl photoremovable protecting groups. Photochem Photobiol Sci [Internet]. 2012 Feb 16 [cited 2020 Oct 27];11(3):472. Available from: http://xlink.rsc.org/?DOI=c2pp05399c

70. Horbert R, Pinchuk B, Davies P, Alessi D, Peifer C, Figures S. Supplementary Information for Paper Photoactivatable prodrugs of anti-melanoma agent vemurafenib Content 1 . Supplementary Figures 2 . Supplementary Tables 3 . Methods , Chemical synthesis and Compound Characterization 4 . Supplementary References. :1–39.

71. Grimm JB, Heckman LM, Lavis LD. The chemistry of small-molecule fluorogenic probes. Vol. 113, Progress in Molecular Biology and Translational Science. Elsevier Inc.; 2013. 1–34 p.

72. Stockert JC, Blazquez-Castro A. Fluorescence Microscopy in Life Sciences [Internet]. BENTHAM SCIENCE PUBLISHERS; 2017. 61–95 p. Available from: http://www.eurekaselect.com/158339/volume/1

73. Sarker SD, Nahar L. Progress in the Chemistry of Organic Natural Products 107 [Internet]. Vol. 107. 2018. 241–243 p. Available from: http://link.springer.com/10.1007/978-3-319-93506-5

74. Dawidowicz AL, Bernacik K, Typek R. Umbelliferone instability during an analysis involving its extraction process. Monatshefte fur Chemie [Internet]. 2018;149(8):1327–40. Available from: https://doi.org/10.1007/s00706-018-2188-9

75. Kabeya LM, Fuzissaki CN, Taleb-Contini SH, Ana AM, Naal Z, Santos EOL, et al. 7-Hydroxycoumarin modulates the oxidative metabolism, degranulation and microbial killing of human neutrophils. Chem Biol Interact [Internet]. 2013;206(1):63–75. Available from: http://dx.doi.org/10.1016/j.cbi.2013.08.010

76. Goodwin RH, Pollock BM. Ultraviolet absorption spectra of coumarin derivatives. Arch Biochem Biophys. 1954;49(1):1–6.

77. Fink DW, Koehler WR. pH Effects on Fluorescence of Umbelliferone. Anal Chem. 1970;42(9):990–3.

78. Hrdlovic P, Donovalova J, Stankovicova H, Gaplovsky A. Influence of polarity of solvents on the spectral properties of bichromophoric coumarins. Molecules. 2010;15(12):8915–32.

79. Rautio J, Meanwell NA, Di L, Hageman MJ. The expanding role of prodrugs in contemporary drug design and development. Nat Rev Drug Discov. 2018;17(8):559–87.

80. Walther R, Rautio J, Zelikin AN. Prodrugs in medicinal chemistry and enzyme prodrug therapies. Adv Drug Deliv Rev [Internet]. 2017;118:65–77. Available from: http://dx.doi.org/10.1016/j.addr.2017.06.013

81. Carl PL, Chakravarty PK, Katzenellenbogen JA. A Novel Connector Linkage Applicable in Prodrug Design. J Med Chem. 1981;24(5):479–80.

82. Alouane A, Labruère R, Silvestre KJ, Le Saux T, Schmidt F, Jullien L. Disassembly kinetics of quinone-methide-based self-immolative spacers that

contain aromatic nitrogen heterocycles. Chem - An Asian J. 2014;9(5):1334–40.

83. Zang C, Wang H, Li T, Zhang Y, Li J, Shang M, et al. A light-responsive, self-immolative linker for controlled drug delivery: Via peptide- and protein-drug conjugates. Chem Sci [Internet]. 2019;10(39):8973–80. Available from: http://dx.doi.org/10.1039/C9SC03016F

84. Alouane A, Labruère R, Le Saux T, Schmidt F, Jullien L. Self-immolative spacers: Kinetic aspects, structure-property relationships, and applications. Angew Chemie - Int Ed. 2015;54(26):7492–509.

85. Papot S, Tranoy I, Tillequin F, Florent JC, Gesson JP. Design of selectively activated anticancer prodrugs: Elimination and cyclization strategies. Curr Med Chem - Anti-Cancer Agents. 2002;2(2):155–85.

86. Kratz F, Müller IA, Ryppa C, Warnecke A. Prodrug strategies in anticancer chemotherapy. ChemMedChem. 2008;3(1):20–53.

87. Yan J, Lee S, Zhang A, Yoon J. Self-immolative colorimetric, fluorescent and chemiluminescent chemosensors. Chem Soc Rev. 2018;47(18):6900–16.

88. Denny WA. The role of hypoxia-activated prodrugs. 2000;25–9.

89. Jaworski J. Luminescent Probe Based Techniques for Hypoxia Imaging. J Nanomedicine Res. 2017 Nov 20;6(3):1–14.

90. Sharma A, Arambula JF, Koo S, Kumar R, Singh H, Sessler JL, et al. Hypoxia-targeted drug delivery. Chem Soc Rev. 2019;48(3):771–813.

91. Chevalier A, Zhang Y, Khdour OM, Kaye JB, Hecht SM. Mitochondrial Nitroreductase Activity Enables Selective Imaging and Therapeutic Targeting. J Am Chem Soc [Internet]. 2016 Sep 21;138(37):12009–12. Available from: https://pubs.acs.org/doi/10.1021/jacs.6b06229

92. Rosa E, Carvalho E, Cheng SC, Fernandes L, Iley J, Moreira R, et al. Triazenos Antitumorais: Mecanismo De Accao Biologica E Desenvolvimento De Pro-Farmacos. Rev Port Farm. 1992;42(3):7–14.

93. Patel DB. The synthetic study of novel aryltriazene derivatives and their biological evaluation [Internet]. Veer Narmad South Gujarat University; 2015. Available from: http://hdl.handle.net/10603/77020

94. Francisco AP, Mendes E, Santos AR, Perry MJ. Anticancer Triazenes: from Bioprecursors to Hybrid Molecules. Curr Pharm Des [Internet]. 2019 Aug 16;25(14):1623–42. Available from: http://www.eurekaselect.com/172637/article

95. Connors TA, Cartei G. TRIAZENES : Chemical, Biological, and Clinical Aspects. 1990. 1–119 p.

96. Marchesi F, Turriziani M, Tortorelli G, Avvisati G, Torino F, De Vecchis L. Triazene compounds: Mechanism of action and related DNA repair systems. Pharmacol Res. 2007;56(4):275–87.

97. Sousa A, Santos F, Gaspar MM, Calado S, Pereira JD, Mendes E, et al. The selective cytotoxicity of new triazene compounds to human melanoma cells. Bioorganic Med Chem. 2017;25(15):3900–10.

98. Monteiro AS, Almeida J, Cabral G, Severino P, Videira PA, Sousa A, et al. Synthesis and evaluation of N-acylamino acids derivatives of triazenes. Activation by tyrosinase in human melanoma cell lines. Eur J Med Chem. 2013;70:1–9.

99. Kimball DB, Haley MM. Triazenes: A versatile tool in organic synthesis. Angew Chemie - Int Ed. 2002;41(18):3338–51.

100. Mendes E, Perry MJ, Francisco AP. The synthetic utility of triazenes in heterocycle synthesis. In: Heterocyclic Targets in Advanced Organic Synthesis. 2011. p. 125–44.

101. Schmid FA, Hutchison DJ. Chemotherapeutic, Carcinogenic, and Cell-regulatory Effects of Triazenes. Cancer Res. 1974;34(7):1671–5.

102. Nifontov VI, Bel'skaya NP, Shtokareva EA. The reactivity and mechanism of action of triazenes (review). Pharm Chem J [Internet]. 1994 Oct;28(10):687–706. Available from: http://link.springer.com/10.1007/BF02219299

103. Braga C, Vaz AR, Oliveira MC, Matilde Marques M, Moreira R, Brites D, et al. Targeting gliomas with triazene-based hybrids: Structure-activity relationship, mechanistic study and stability. Eur J Med Chem. 2019;172:16–25.

104. Jawaid S, Khan T, Osborn H, Williams N. Tyrosinase Activated Melanoma Prodrugs. Anticancer Agents Med Chem. 2012;9(7):717–27.

105. Pinheiro R, Braga C, Santos G, Bronze MR, Perry MJ, Moreira R, et al. Targeting Gliomas: Can a New Alkylating Hybrid Compound Make a Difference? ACS Chem Neurosci. 2017;8(1):50–9.

106. Hansen MN, Farjami E, Kristiansen M, Clima L, Pedersen SU, Daasbjerg K, et al. Synthesis and application of a triazene?ferrocene modifier for immobilization and characterization of oligonucleotides at electrodes. J Org Chem. 2010;75(8):2474–81.

107. Capucha V, Mendes E, Francisco AP, Perry MJ. Development of triazene prodrugs for ADEPT strategy: New insights into drug delivery system based on carboxypeptidase G2 activation. Bioorganic Med Chem Lett. 2012;22(22):6903–8.

108. Perry M de J, Carvalho E, Rosa E, Iley J. Towards an efficient prodrug of the alkylating metabolite monomethyltriazene: Synthesis and stability of N-acylamino acid derivatives of triazenes. Eur J Med Chem. 2009;44(3):1049–56.

109. Lei Q, Zhang S, Liu M, Li J, Zhang X, Long Y. Synthesis and biological evaluation of glycosides containing triazene-chalcones. Mol Divers. 2017;21(4):957–66.

110. Arrowsmith J, Jennings SA, Clark AS, Stevens MFG. Antitumor imidazotetrazines. 41.1 Conjugation of the antitumor agents mitozolomide and temozolomide to peptides and lexitropsins bearing DNA major and minor groove-binding structural motifs. J Med Chem. 2002;45(25):5458–70.

111. Ding R, He Y, Wang X, Xu J, Chen Y, Feng M, et al. Treatment of alcohols with tosyl chloride does not always lead to the formation of tosylates. Molecules. 2011;16(7):5665–73.

112. Jia H, Li Q, Bayaguud A, She S, Huang Y, Chen K, et al. Tosylation of alcohols: An effective strategy for the functional group transformation of organic derivatives of polyoxometalates. Sci Rep. 2017;7(1):2–10.

113. Netscher T, Bohrer P. Towards highly activating leaving groups: Studies on the preparation of some halogenated alkyl sulfonates. Molecules. 2002;7(8):601–17.

114. Prahlada Rao S, Sunkada S. Making sense of boiling points and melting points. Resonance [Internet]. 2007 Jun 7;12(6):43–57. Available from:

http://link.springer.com/10.1007/s12045-007-0059-5

115. Klepper RR. Melting Point Determination : Purity and Identity of Crystalline. 2009;1–8.

116. Abu-Eittah RH, El-Tawil BAH. The electronic absorption spectra of some coumarins. A molecular orbital treatment. Can J Chem [Internet]. 1985 Jun;63(6):1173–9. Available from: http://www.nrcresearchpress.com/doi/10.1139/v85-200

117. Chu LL, Pandey RP, Lim HN, Jung HJ, Thuan NH, Kim T-S, et al. Synthesis of umbelliferone derivatives in Escherichia coli and their biological activities. J Biol Eng [Internet]. 2017 Dec 5;11(1):1–15. Available from: http://jbioleng.biomedcentral.com/articles/10.1186/s13036-017-0056-5

118. Mazimba O. Umbelliferone: Sources, chemistry and bioactivities review. Bull Fac Pharmacy, Cairo Univ [Internet]. 2017 Dec;55(2):223–32. Available from: https://linkinghub.elsevier.com/retrieve/pii/S1110093117300297

119. Cissé L, Tine A, Kaboré L, Saba A. Mass Spectrometry Study of Coumarins: Correlation Between Charges of Atoms and Fragmentation Processes. Spectrosc Lett [Internet]. 2009 Feb 24;42(2):95–9. Available from: https://www.tandfonline.com/doi/full/10.1080/00387010802428666

120. Hesek D, Lee M, Noll BC, Usher JF, Mobashery S. Complications from dual roles of sodium hydride as a base and as a reducing agent. J Org Chem. 2009;74(6):2567–70.

121. Regional N. [8] Preparative Thin-Layer Chromatography. (12):60–4.

122. Foris A. On NH NMR Chemical Shifts, Part I. 2017;(April 2016):1–4.

123. Vaughan K. The effect of electron-withdrawing substituents on the tautomerism between 1-aryl-3-methyltriazenes and 3-aryl-1-methyltriazenes. J Chem Soc Perkin Trans 2. 1977;IIIc(1):17–20.

124. Wilman DE V. The Chemistry of Antitumour Agents. The Chemistry of Antitumour Agents. 1990. 159–183 p.

125. Vaughan K, Liu MTH. Kinetics and mechanism of unimolecular decomposition of 3-methyl-1- p -tolyltriazene . Can J Chem. 1981;59(6):923–6.

126. Vaughan K, Stevens MFG. Monoalkyltriazenes. Chem Soc Rev [Internet]. 1978;7(3):377. Available from: http://xlink.rsc.org/?DOI=cs9780700377

127. Donald B, Scotia N, Vaughan K, Scotia N. 13C and 1H Nuclear Magnetic Resonance Study of Solvent Effects on Tautomerism in 1-Aryl-3methyltriazenes. 1981;1161–5.

128. Kolar GF, Preussmann R. Validity of a Linear Hammett Plot for the Stability of Some Carcinogenic 1-Aryl-3,3-dimethyltriazenes in an Aqueous System. Zeitschrift fur Naturforsch - Sect B J Chem Sci. 1971;26(9):950–3.

129. Heravi MM, Ghavidel M, Mohammadkhani L. Beyond a solvent: Triple roles of dimethylformamide in organic chemistry. RSC Adv. 2018;8(49):27832–62.

130. Nucleophile - Chemistry LibreTexts [Internet]. [cited 2020 Jul 31]. Available from: https://chem.libretexts.org/Bookshelves/Organic_Chemistry/Supplemental_Modules_(Organic_Chemistry)/Reactions/Substitution_Reactions/SN2/Nucleophile

131. Polar Protic? Polar Aprotic? Nonpolar? All About Solvents [Internet]. [cited 2020 Aug 1]. Available from: https://www.masterorganicchemistry.com/2012/04/27/polar-protic-polar-aprotic-nonpolar-all-about-solvents/

132. Pock V. Book Review, Encyclopedia of Reagents for Organic Synthesis. Synthesis (Stuttg). 1996;1996(03):419–22.

133. Parker AJ. Rates of Bimolecular Substitution Reactions in Protic and Dipolar Aprotic Solvents. Adv Phys Org Chem. 1967;5(C):173–235.

134. Kazem-Rostami M. Factors influencing the thermal stability of azo and bisazo compounds. J Therm Anal Calorim [Internet]. 2020;140(2):613–23. Available from: https://doi.org/10.1007/s10973-019-08884-4

135. Schotten C, Leprevost SK, Yong LM, Hughes CE, Harris KDM, Browne DL. Comparison of the Thermal Stabilities of Diazonium Salts and Their Corresponding Triazenes. Org Process Res Dev. 2020;A-F.

Annexes

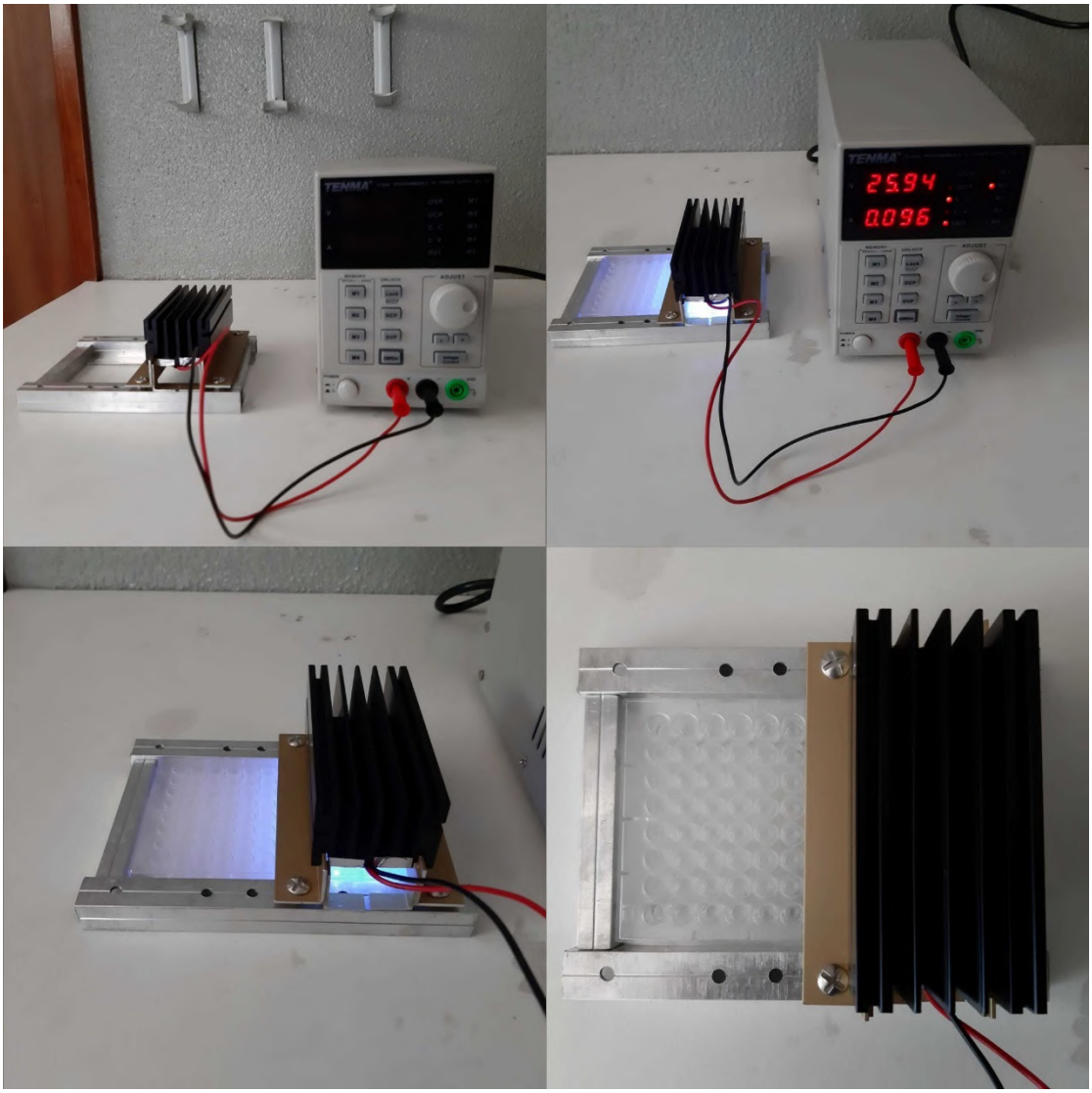

Annex 1 - Photoactivation apparatus (Photoactivation assay)

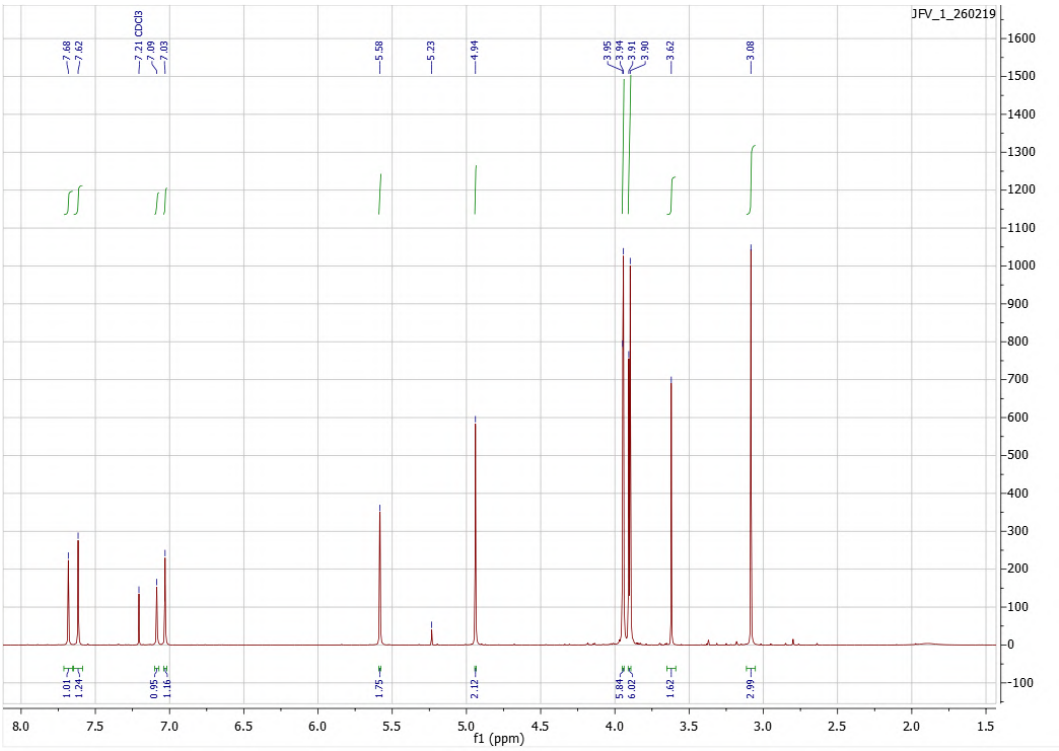

Annex 2 - JFV-1 ^{1}H NMR spectrum in $CDCl_3$ (unpurified)

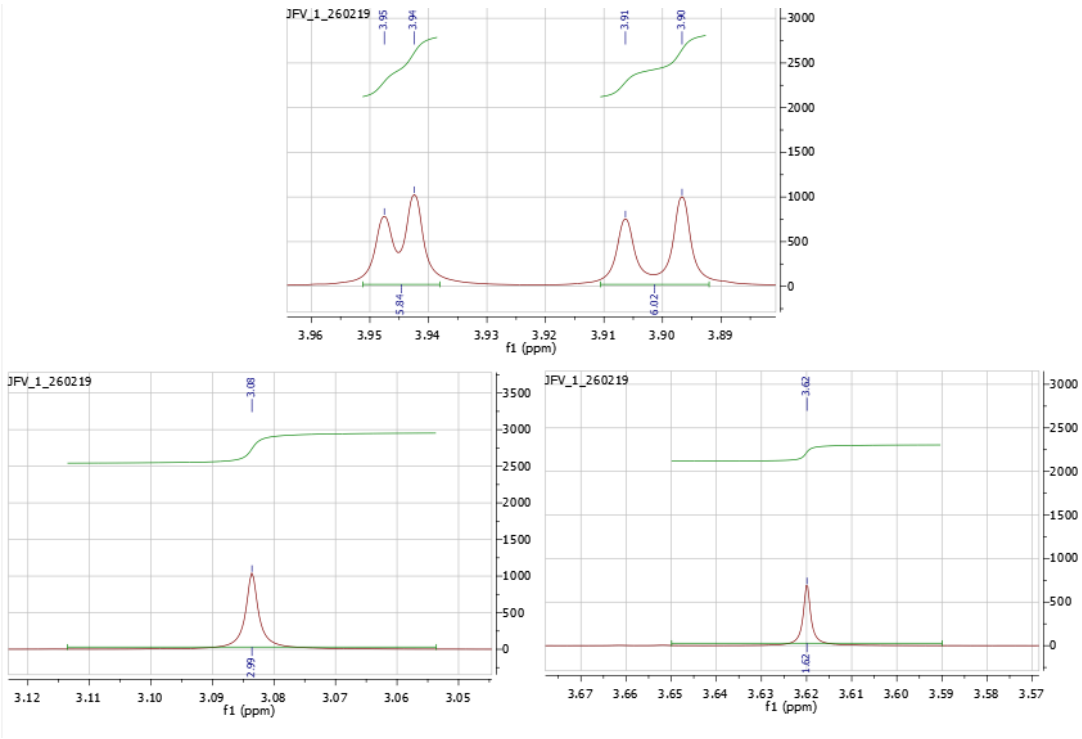

Annex 3 - JFV-1 Close-up ^{1}H NMR spectrum in $CDCl_3$ (unpurified) between 3-4 ppm

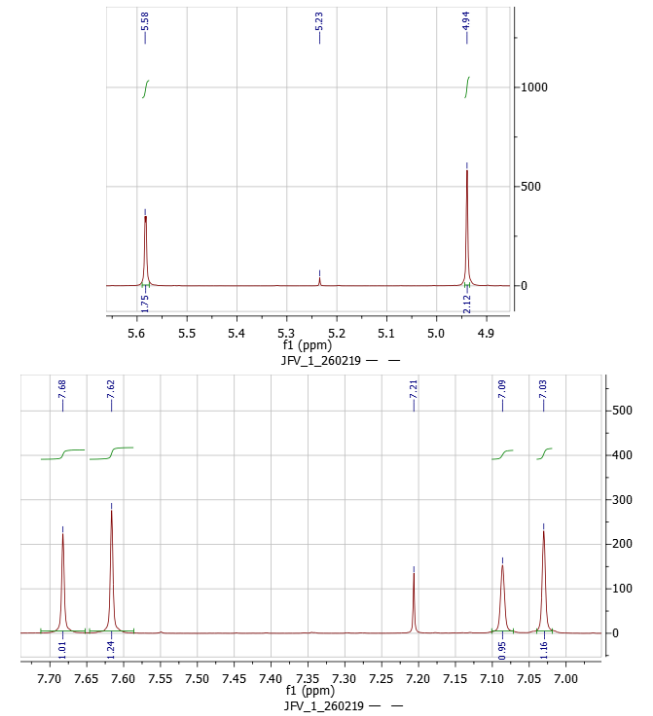

Annex 4 - JFV-1 ^{1}H NMR Close-up spectrum in $CDCl_3$ (unpurified) between 4.9-7.7 ppm

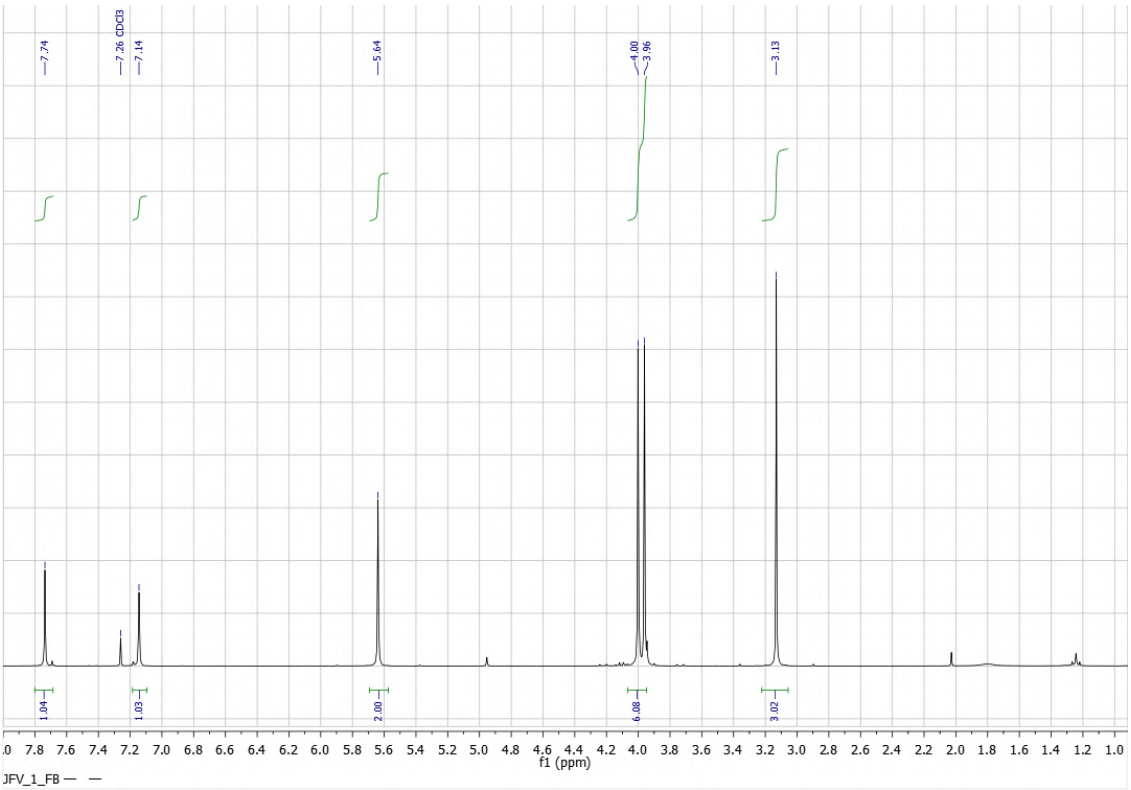

Annex 5 - JFV-1 ^{1}H NMR spectrum in $CDCl_3$ (purified)

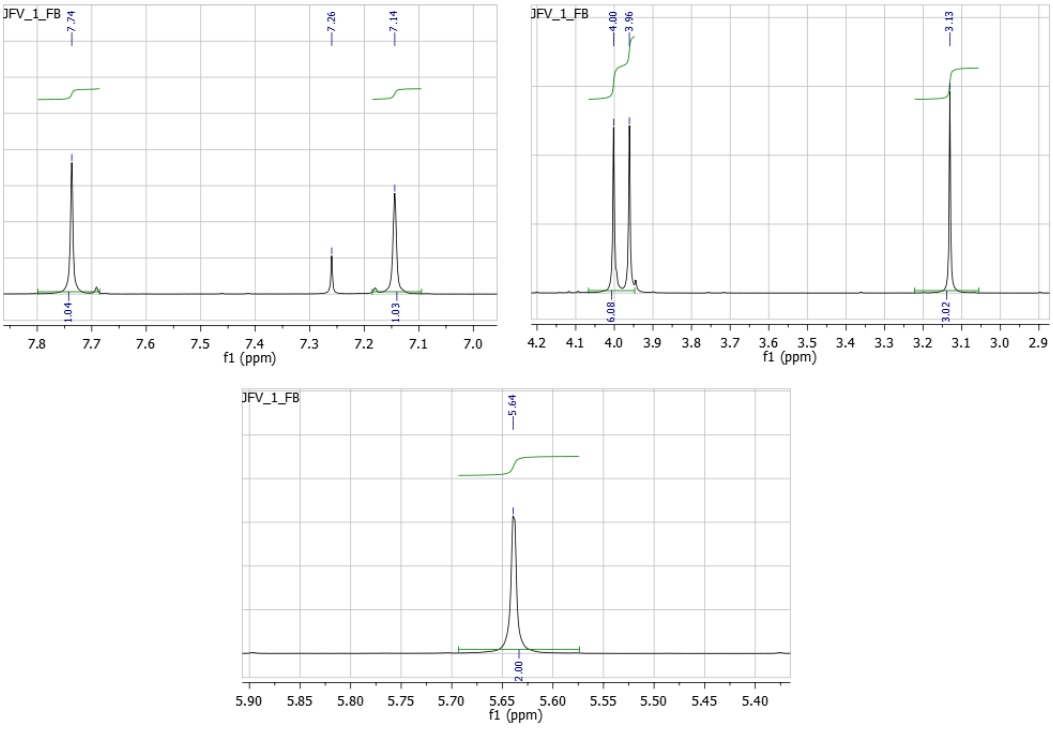

Annex 6 - JFV-1 Close-up ^{1}H NMR spectrum in $CDCl_3$ (purified)

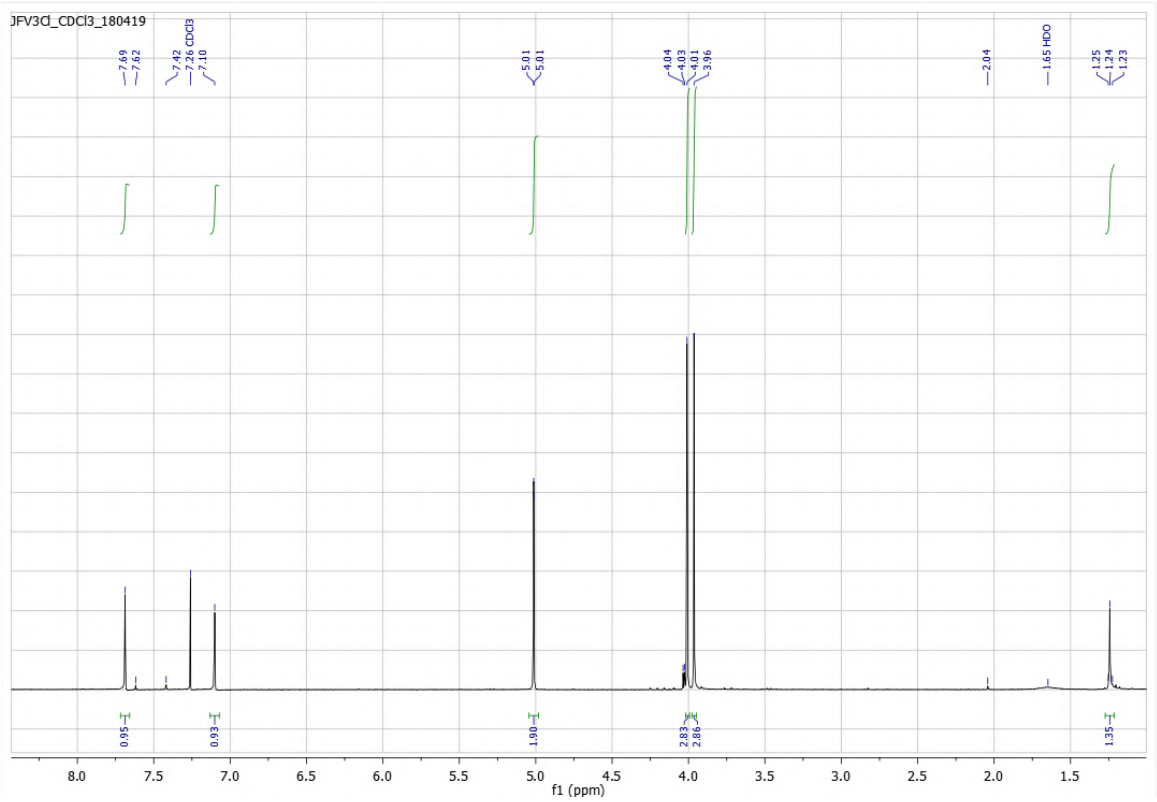

Annex 7 - JFV-1-Cl ^{1}H NMR spectrum in $CDCl_3$

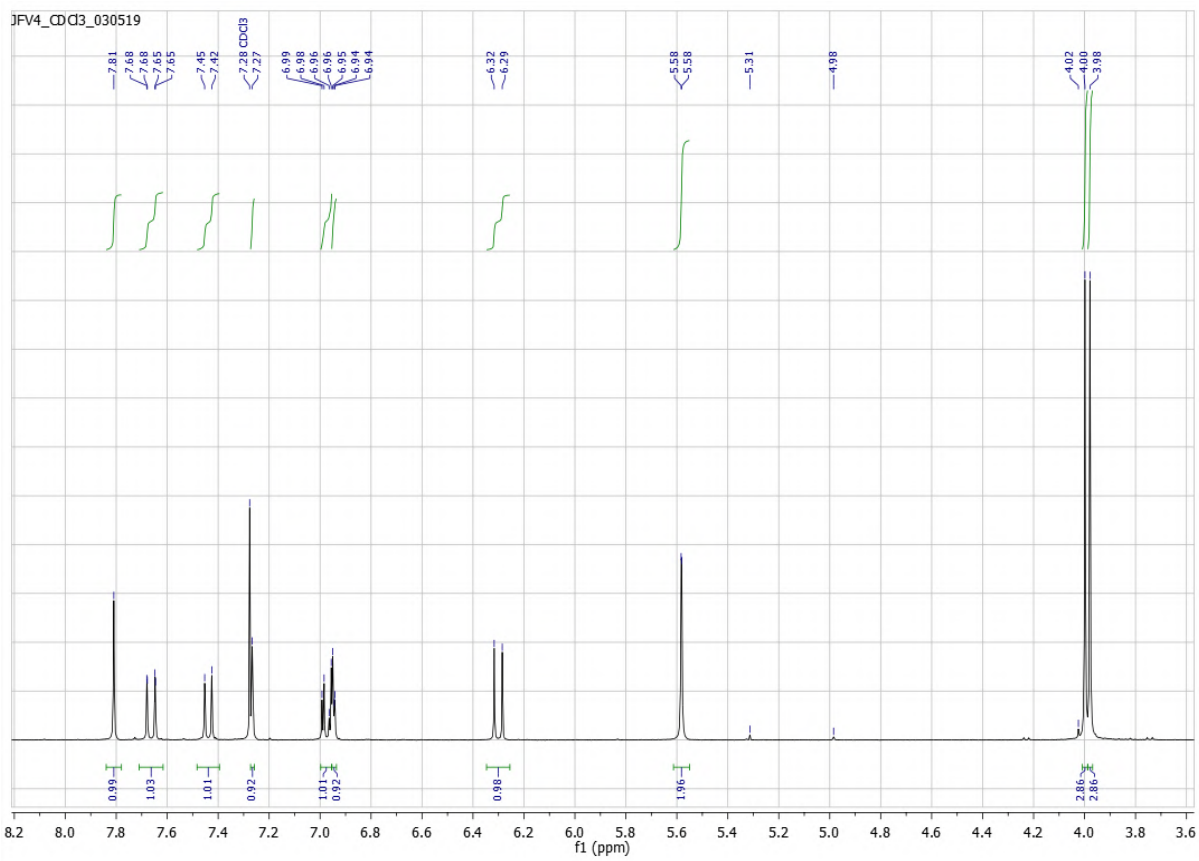

Annex 8 - JFV-UMB ^{1}H NMR spectrum in $CDCl_3$

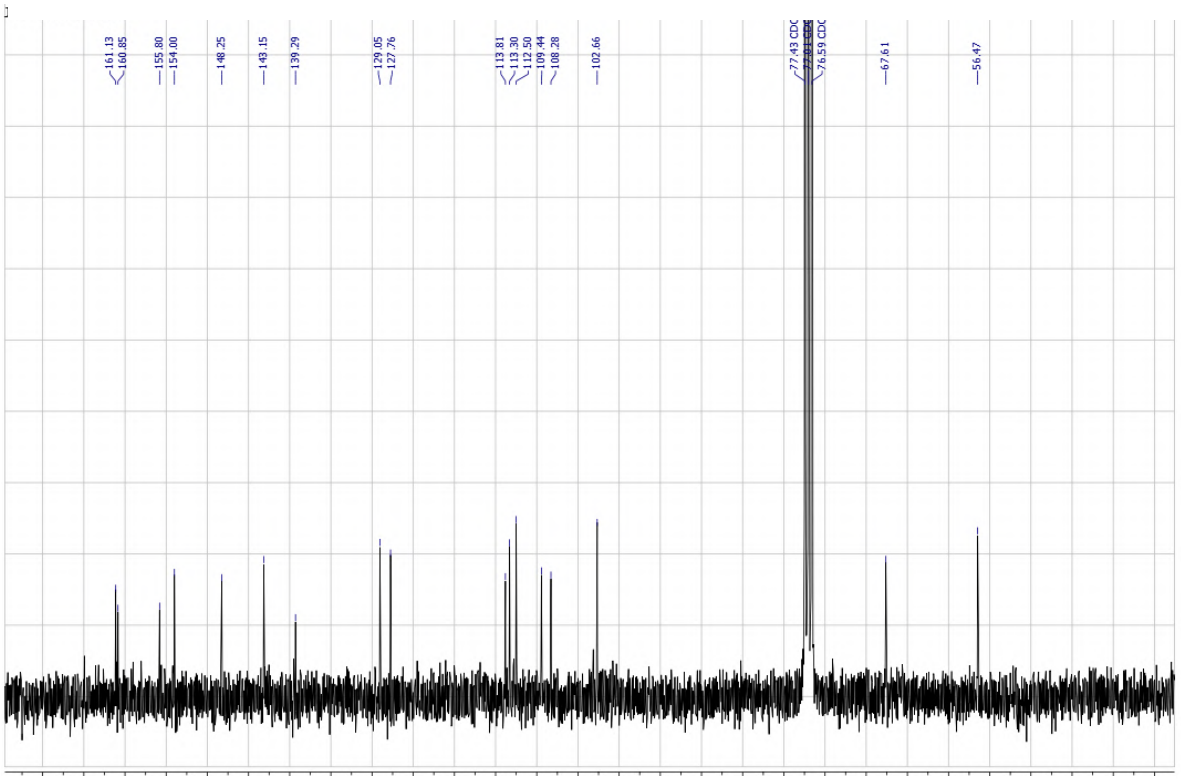

Annex 9 - JFV-UMB ^{13}C NMR spectrum in $CDCl_3$

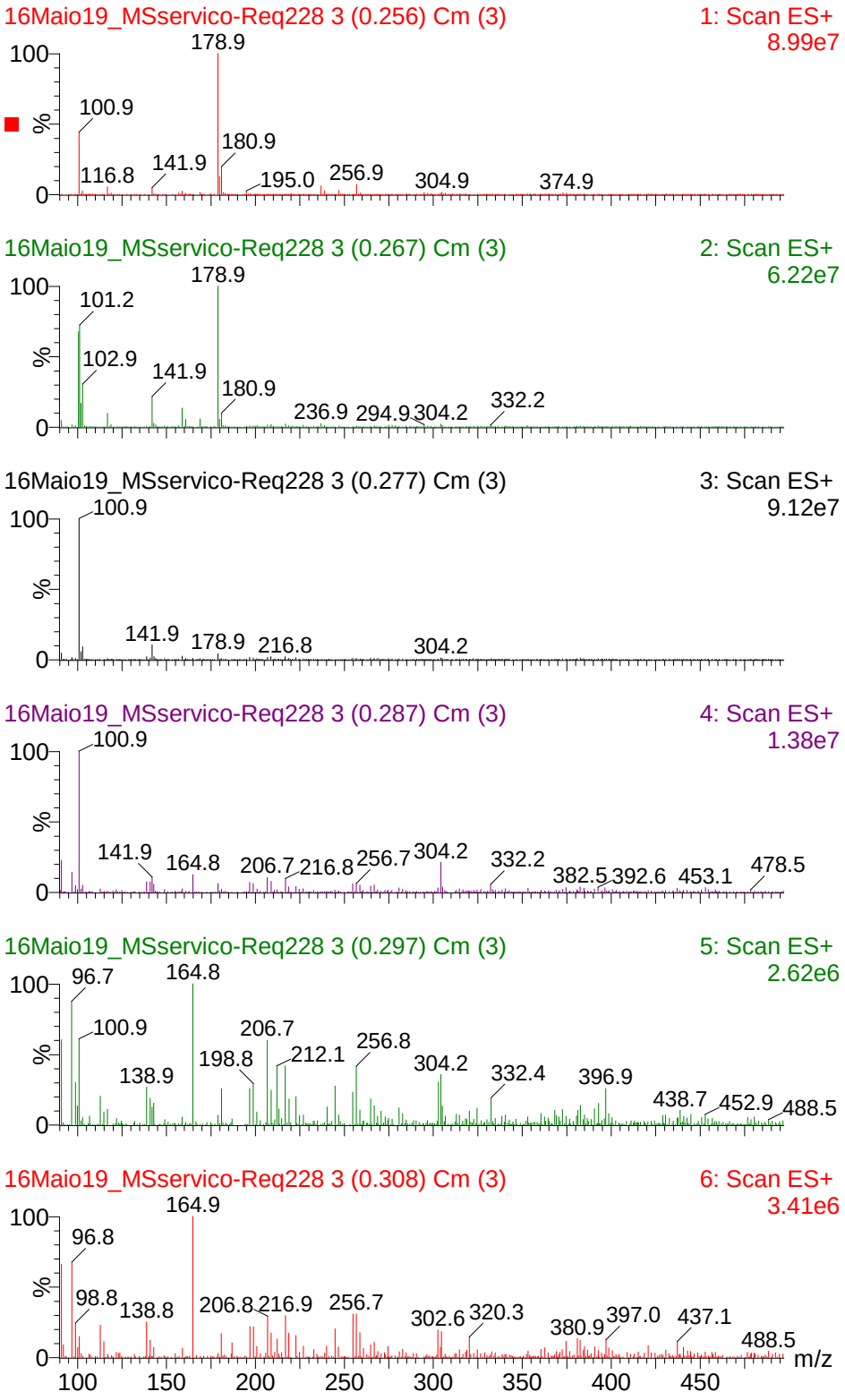

Annex 10 - Mass spectrum of JFV-UMB after 15s irradiation (ESI+)

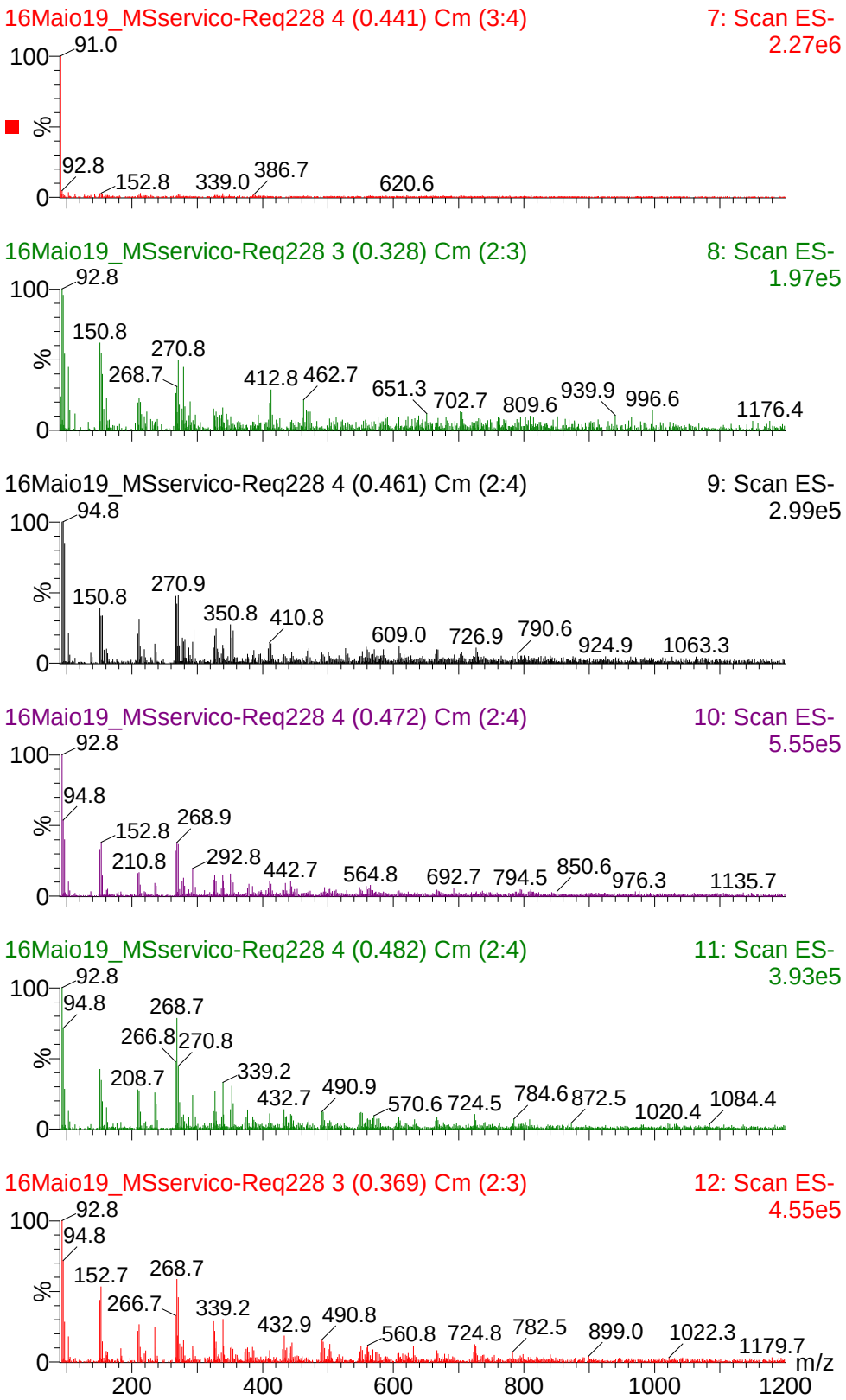

Annex 11 - Mass spectrum of JFV-UMB after 15s irradiation (ESI-)

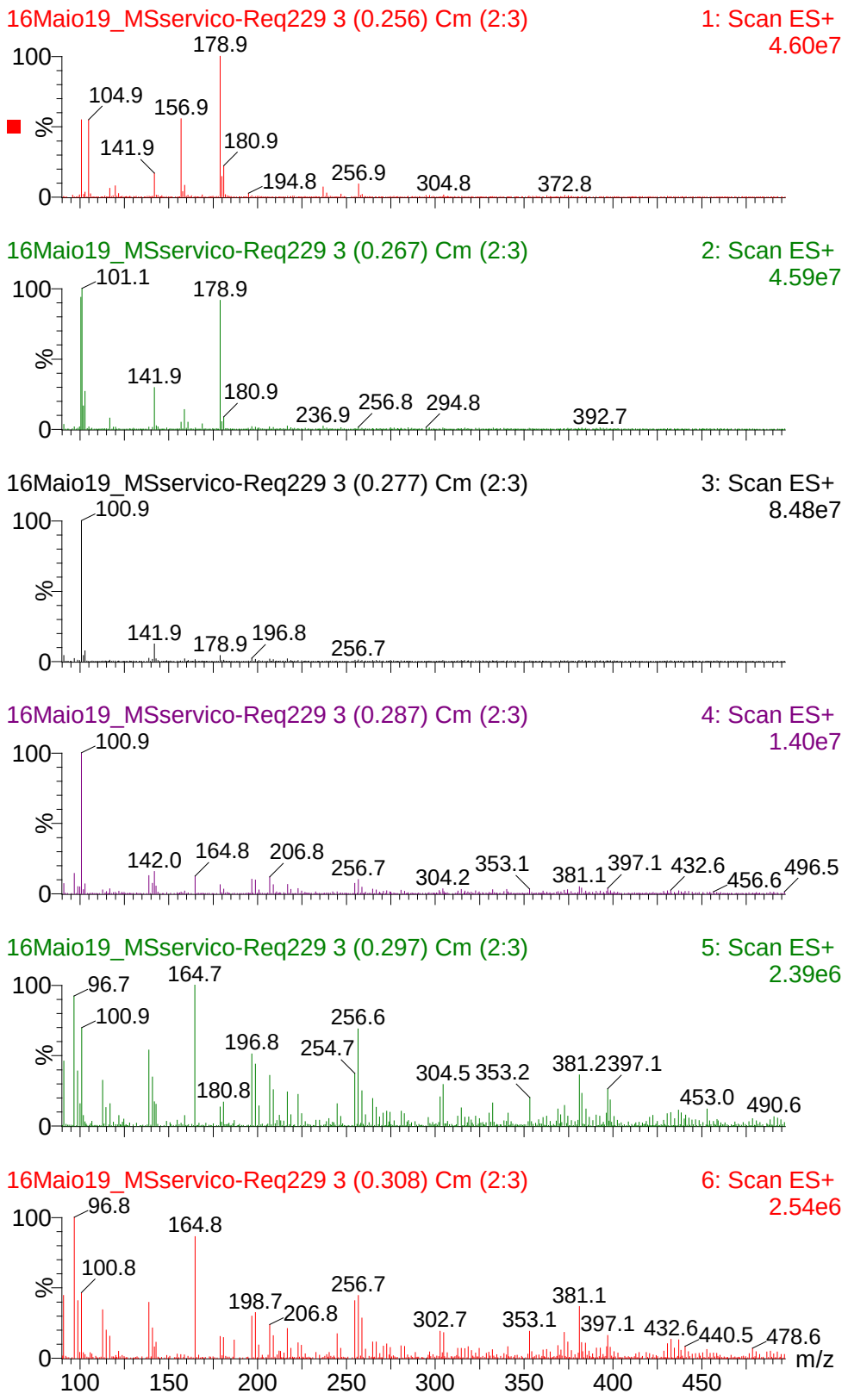

Annex 12 - Mass spectrum of JFV-UMB after 120s irradiation (ESI+)

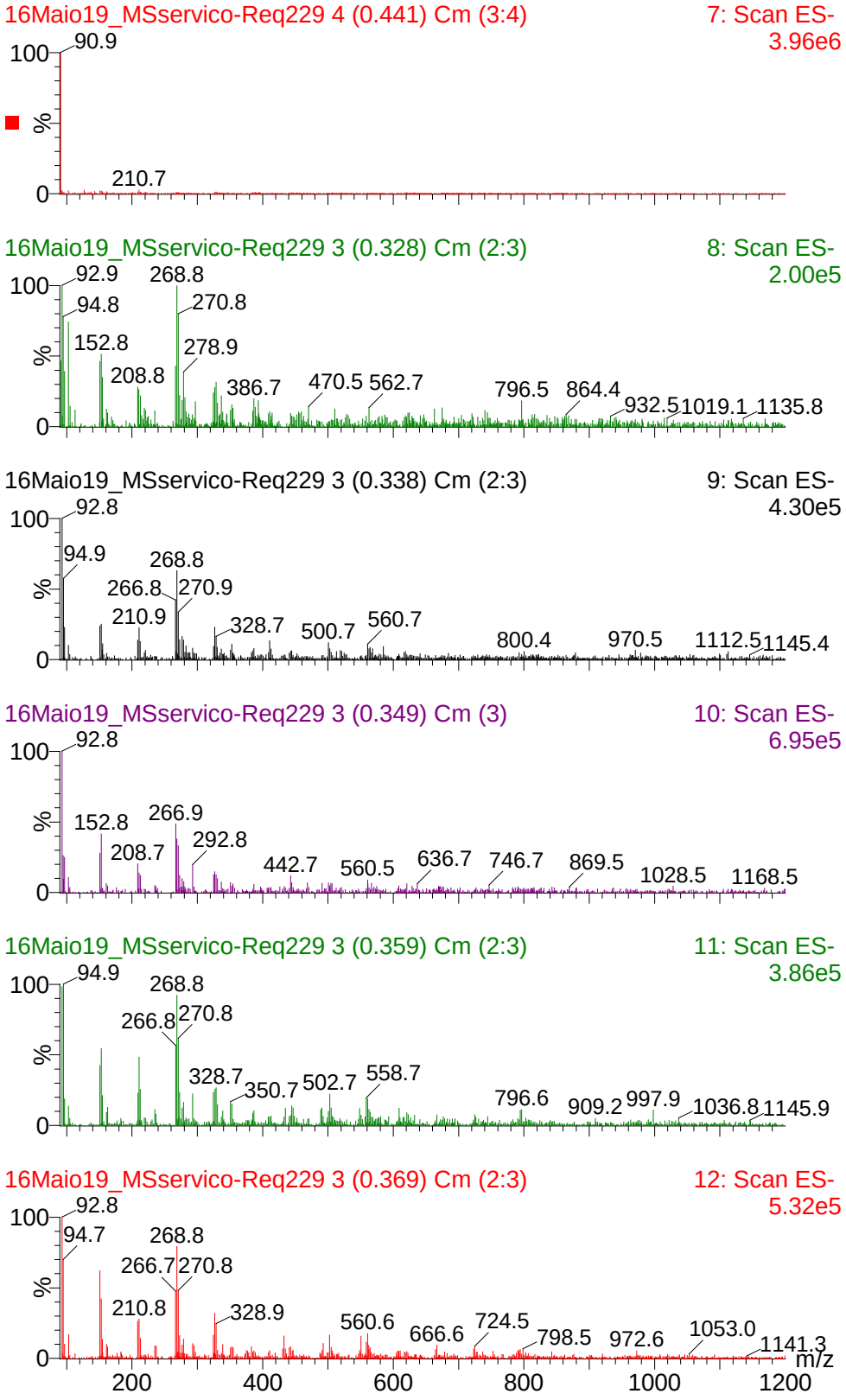

Annex 13 - Mass spectrum of JFV-UMB after 120s irradiation (ESI-)

Annex 14 - Work Timeline for the Triazene Prodrugs (Part One)

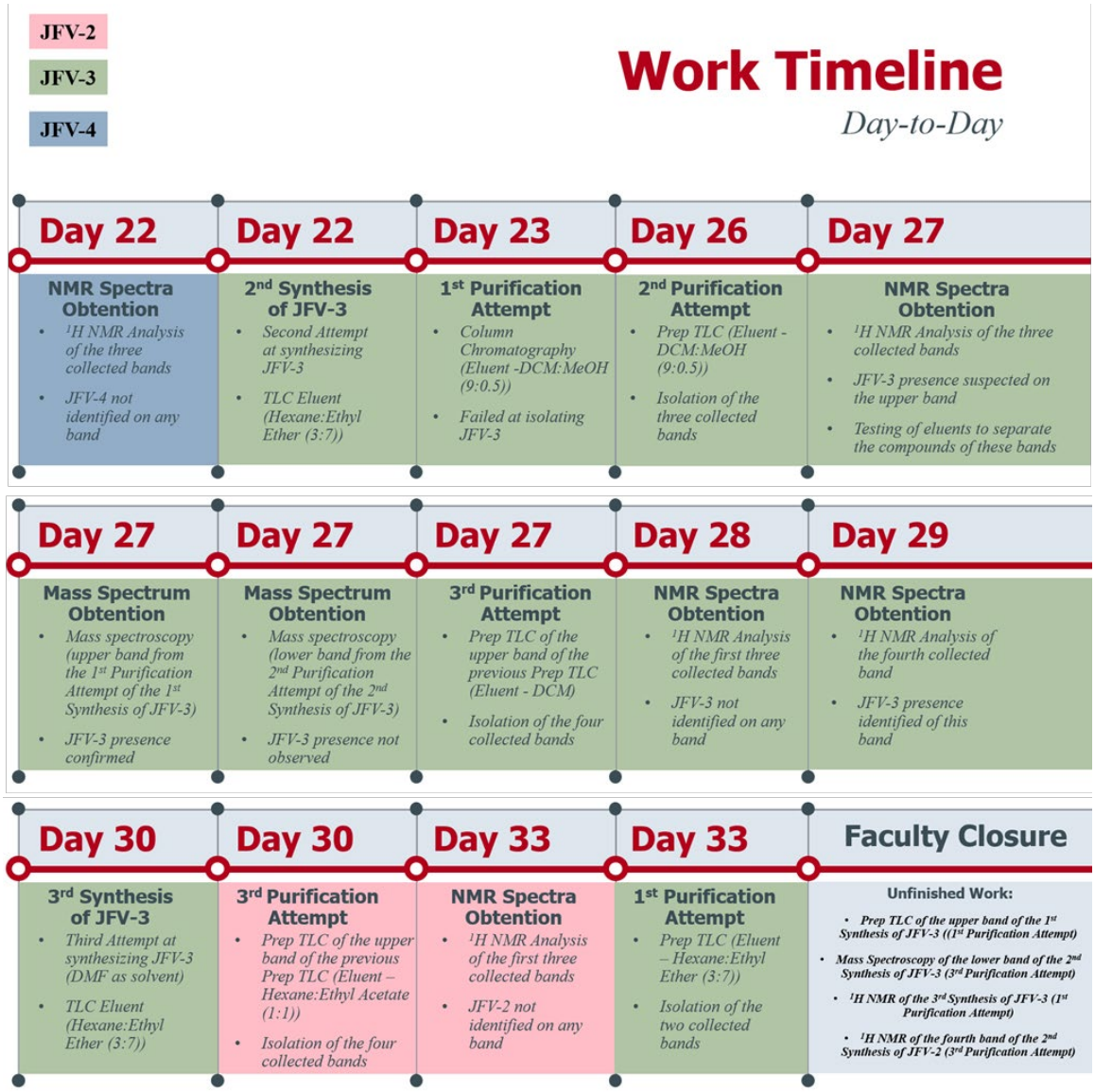

Annex 15 - Work Timeline for the Triazene Prodrugs (Part Two)

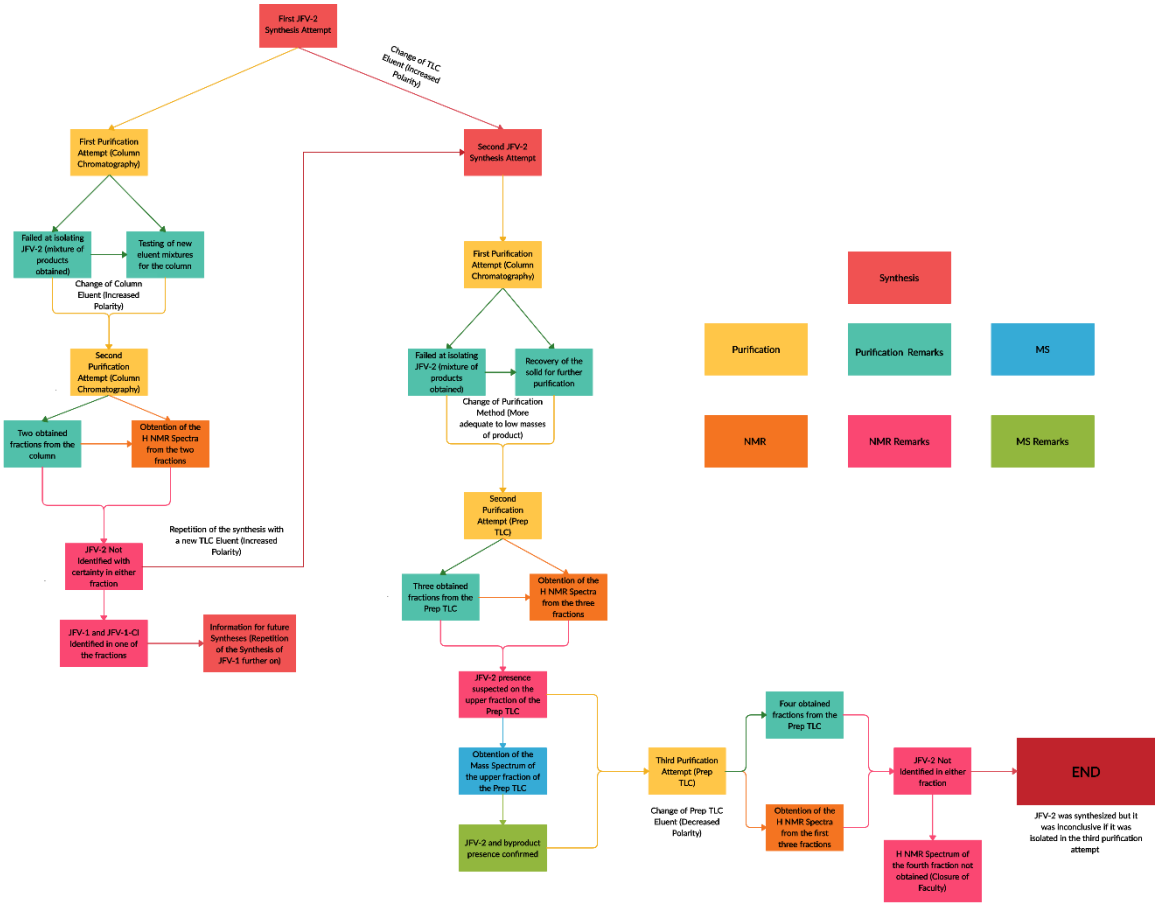

Annex 16 - Flowchart of the work executed for synthesizing JFV-2

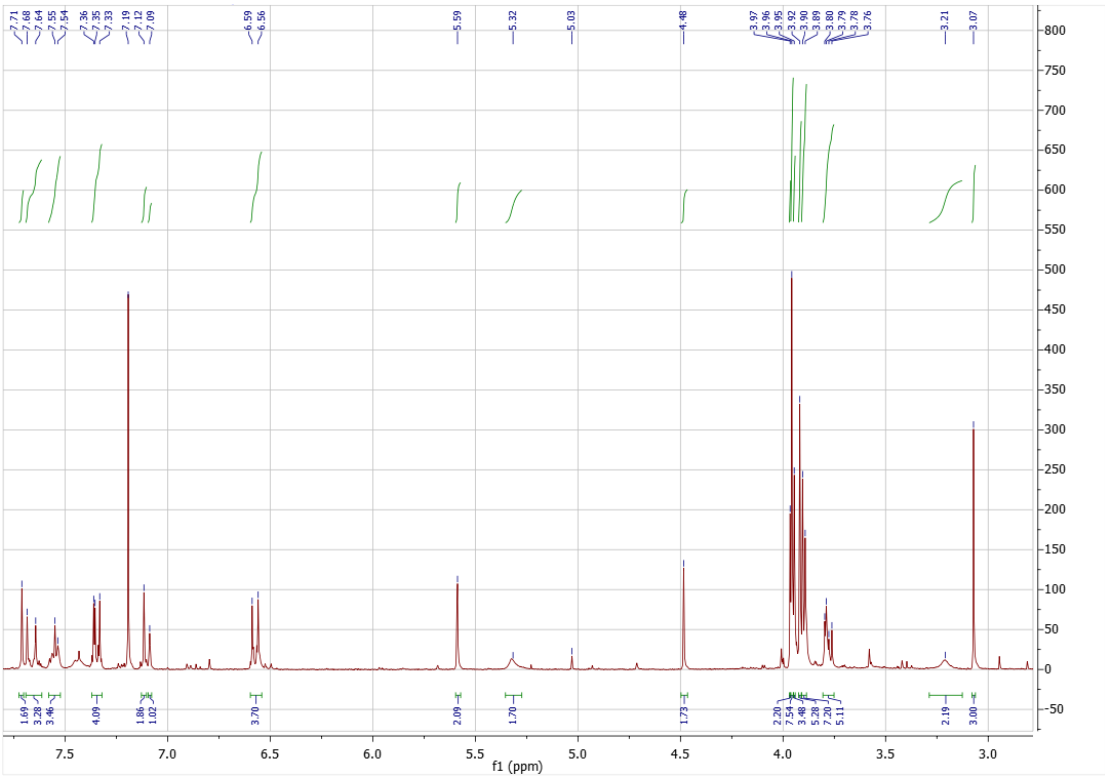

Annex 17 - ^{1}H NMR spectrum of Fraction 1 (JFV-2 Synthesis Attempt 1)

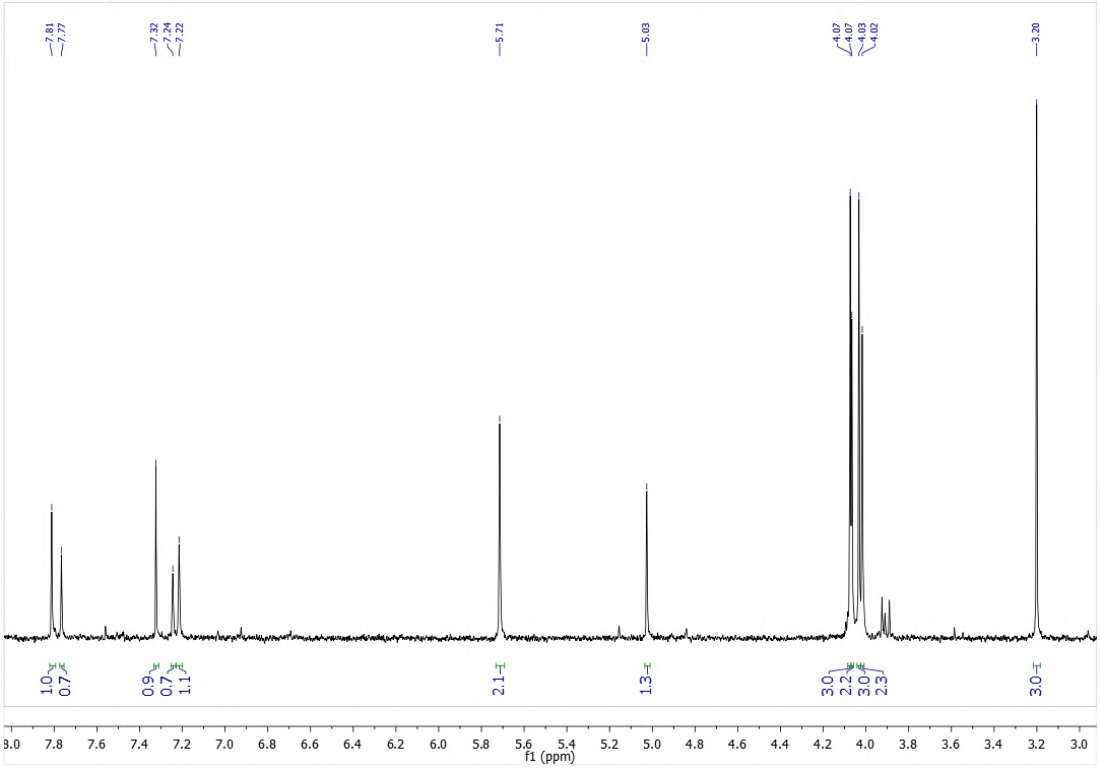

Annex 18 - ^{1}H NMR spectrum of Fraction 2 (JFV-2 Synthesis Attempt 1)

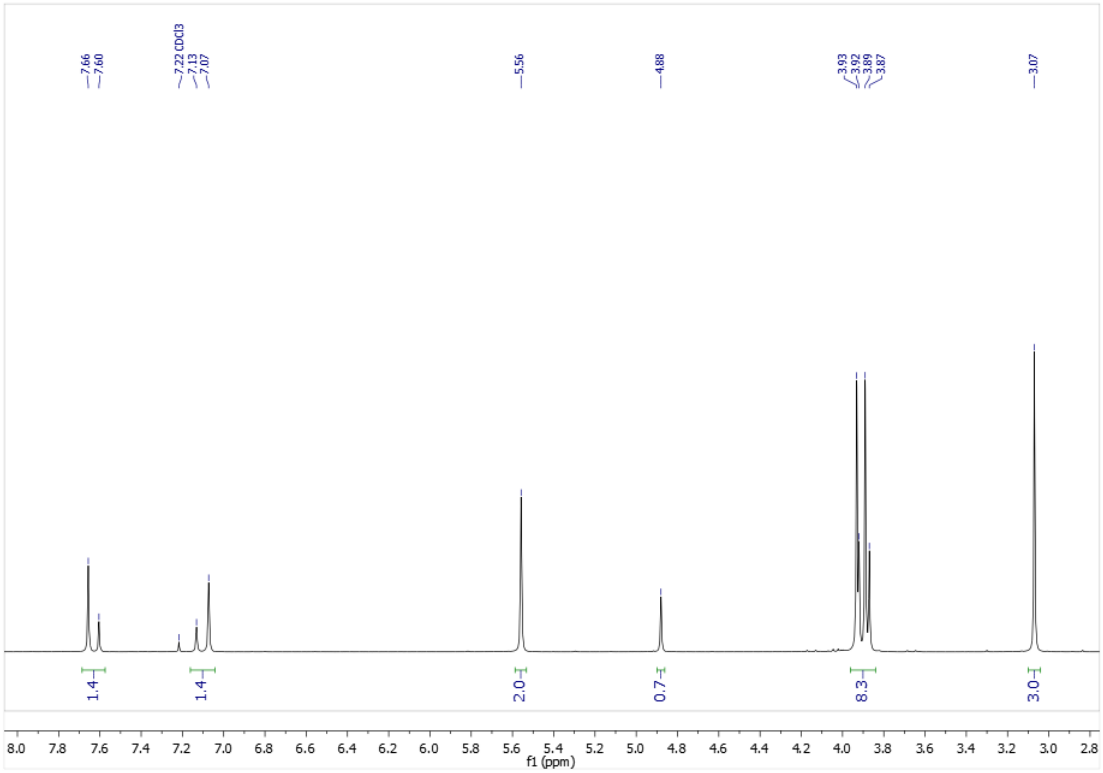

Annex 19 - ^{1}H NMR spectrum of the JFV-1 used in the first JFV-2 synthesis

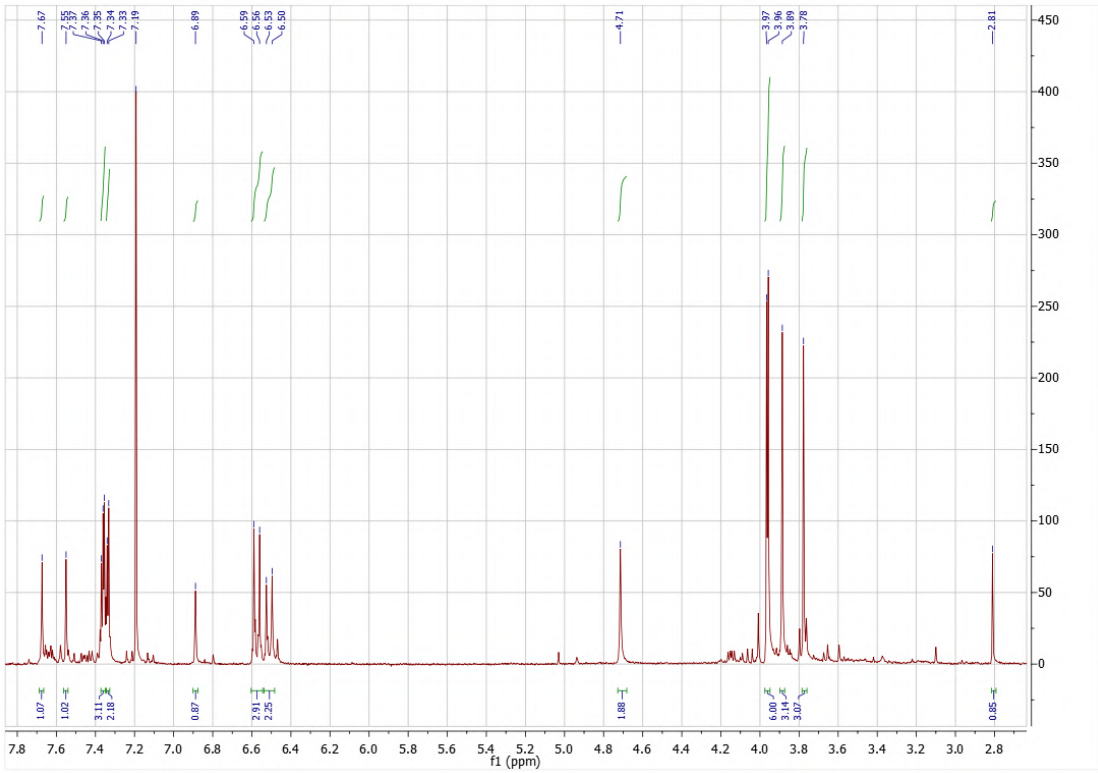

Annex 20 - ^{1}H NMR spectrum of the upper band of the prep TLC (JFV-2 Synthesis Attempt 2)

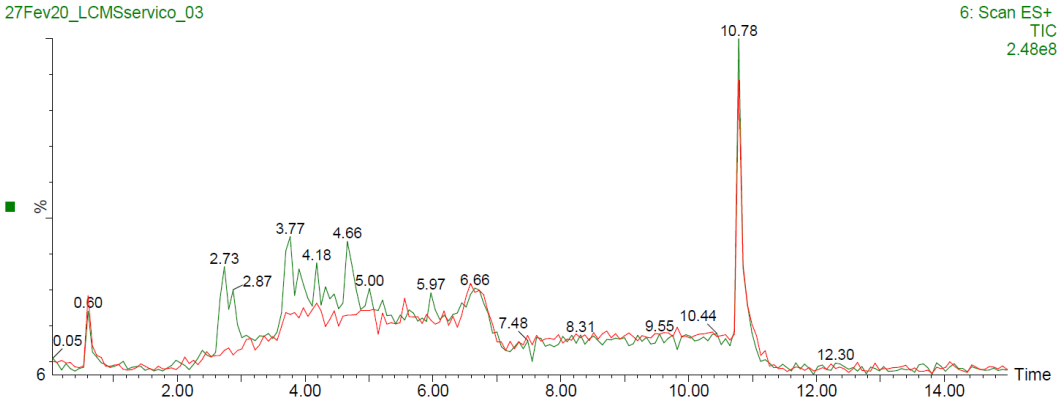

Annex 21 - Chromatogram of the upper band of the prep TLC (JFV-2 Synthesis) - ESI+

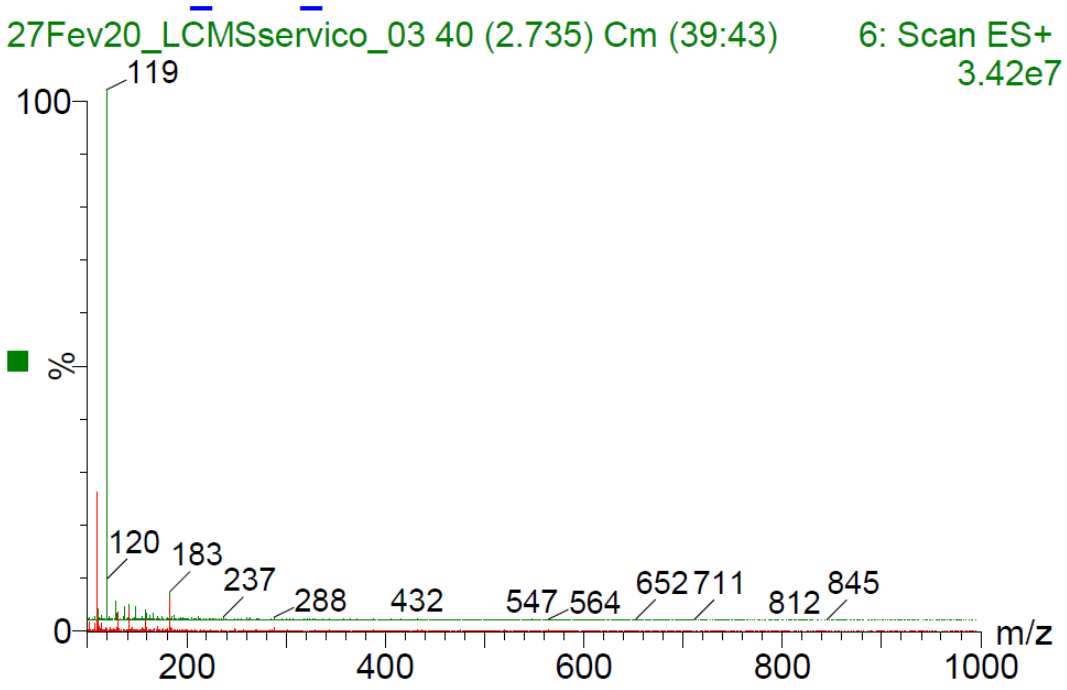

Annex 22 - ESI+ Mass spectrum of the upper band of the prep TLC (JFV-2 Synthesis) - 2.75 min

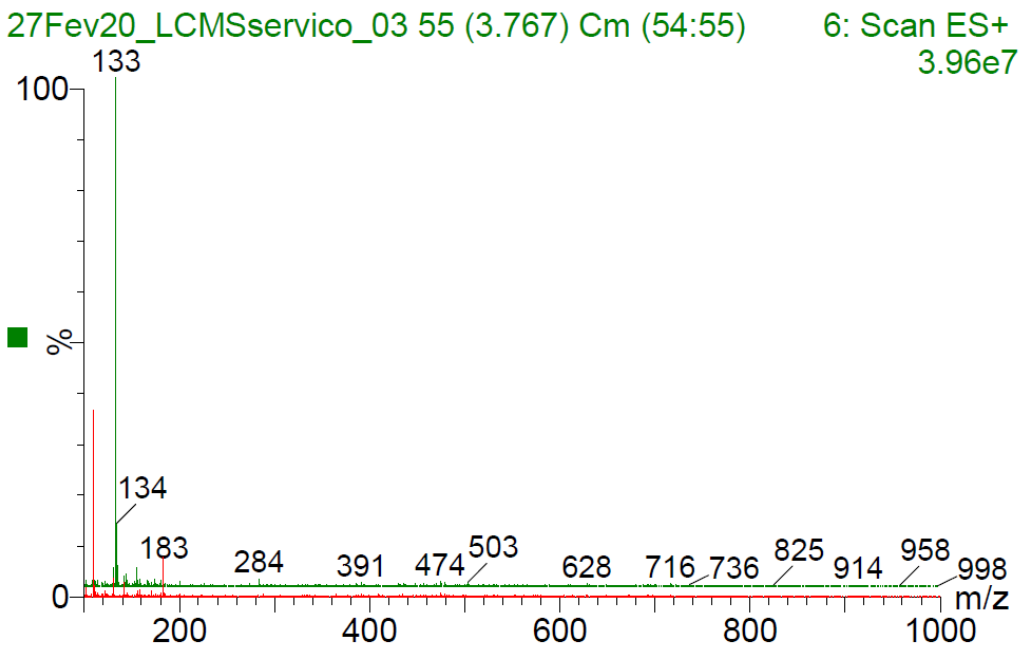

Annex 23 - ESI+ Mass spectrum of the upper band of the prep TLC (JFV-2 Synthesis) - 3.77 min

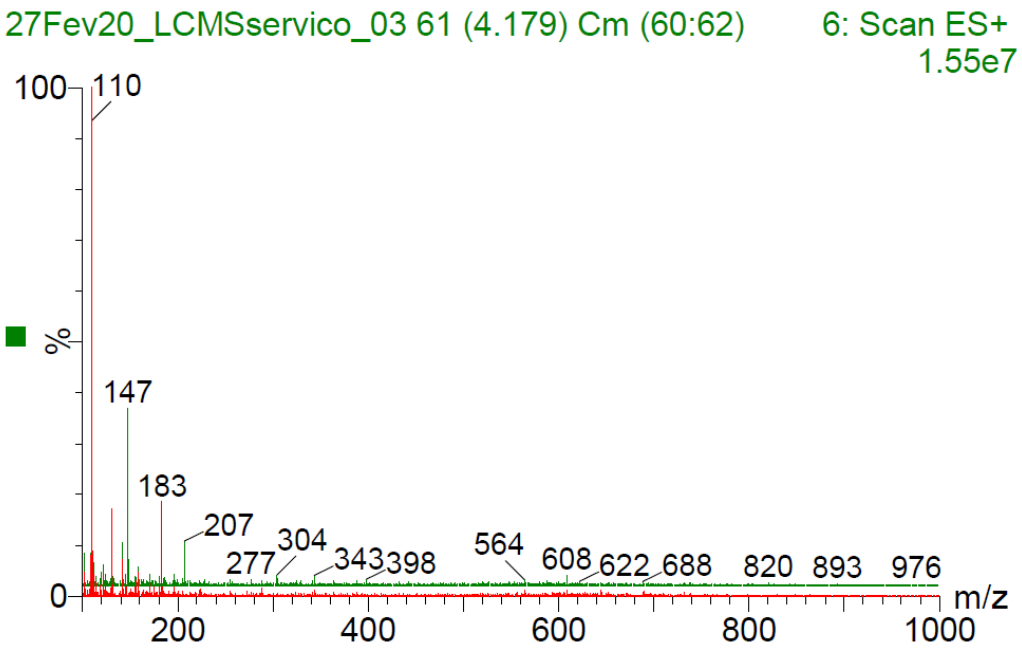

Annex 24 - ESI+ Mass spectrum of the upper band of the prep TLC (JFV-2 Synthesis) - 4.18 min

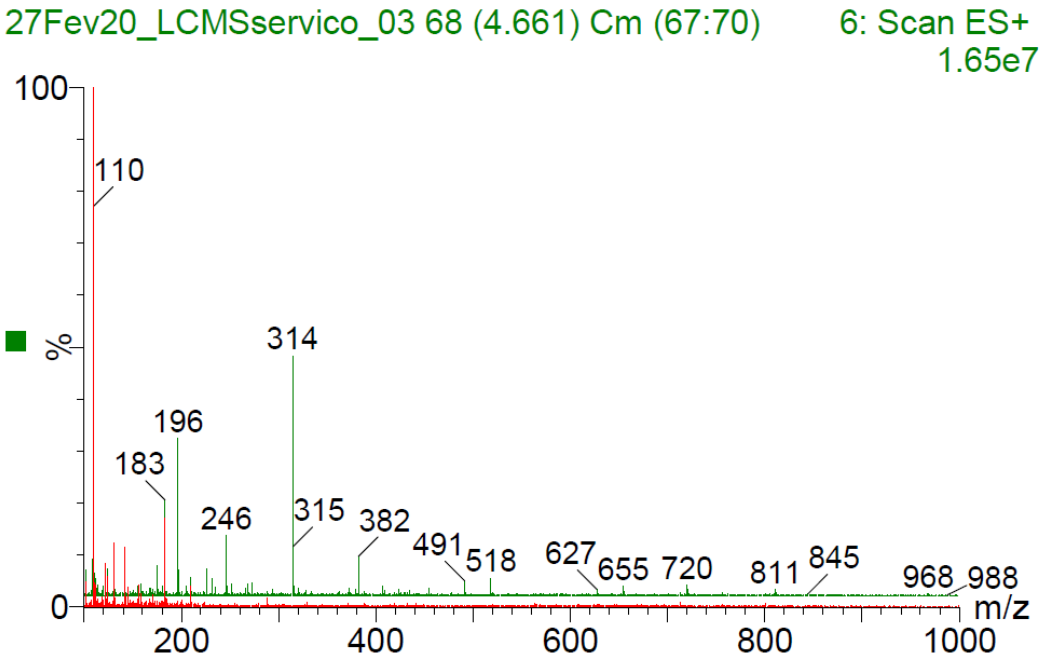

Annex 25 - ESI+ Mass spectrum of the upper band of the prep TLC (JFV-2 Synthesis) - 4.66 min

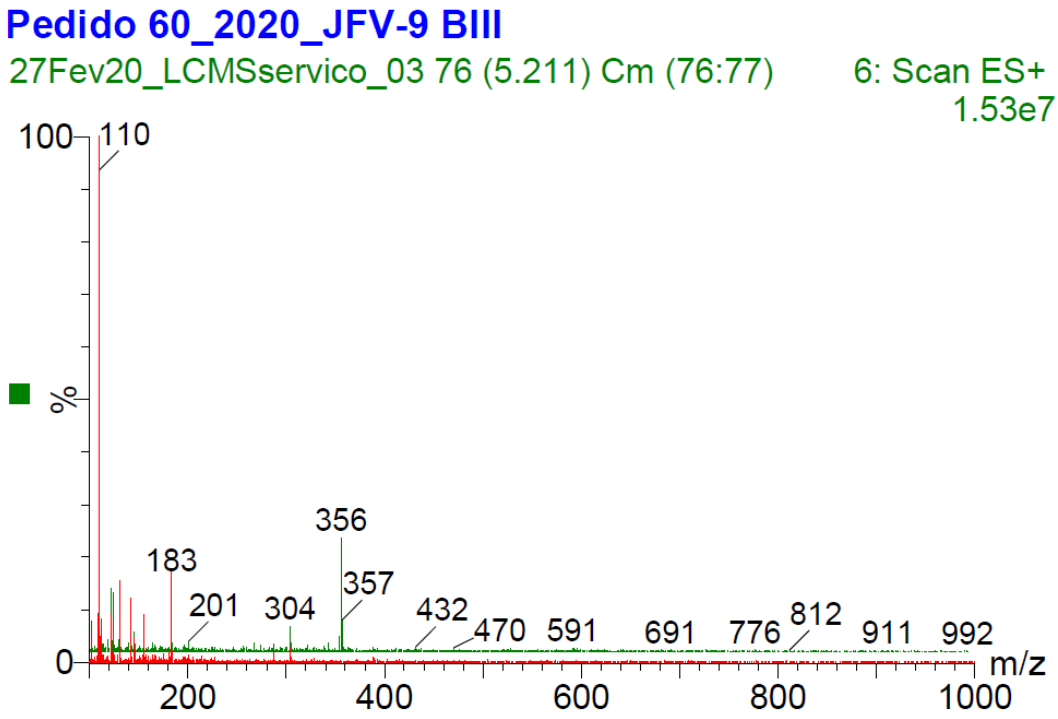

Annex 26 - ESI+ Mass spectrum of the upper band of the prep TLC (JFV-2 Synthesis) - 5.21 min

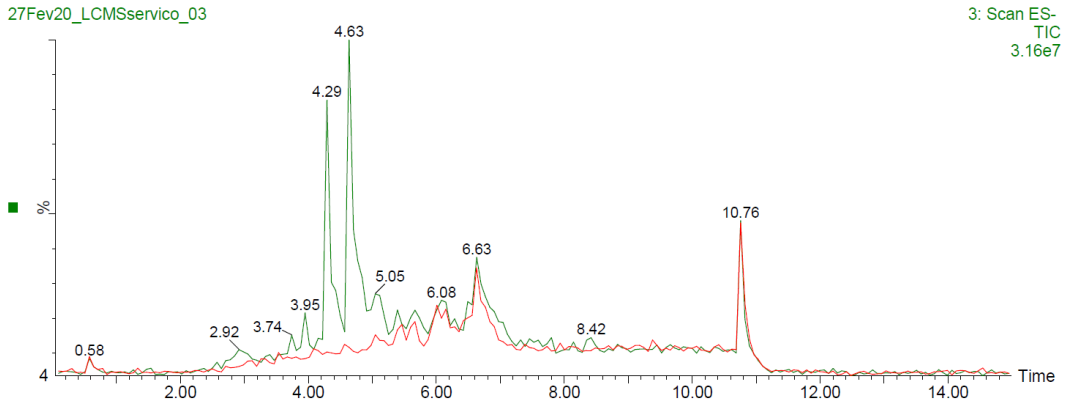

Annex 27 - Chromatogram of the upper band of the prep TLC (JFV-2 Synthesis) - ESI-

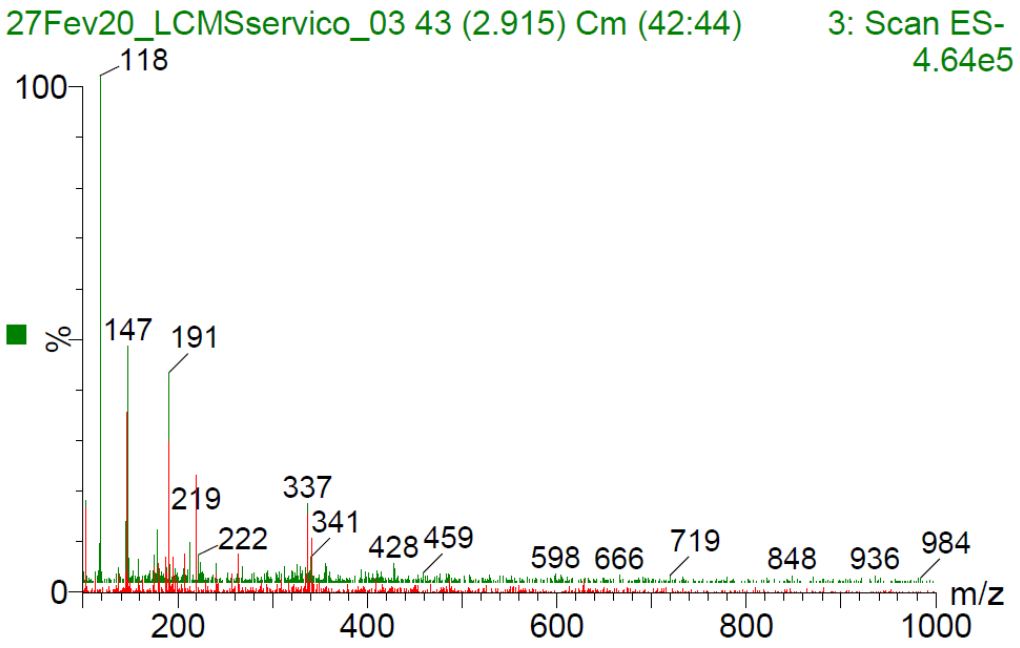

Annex 28 - ESI- Mass spectrum of the upper band of the prep TLC (JFV-2 Synthesis) - 2.92 min

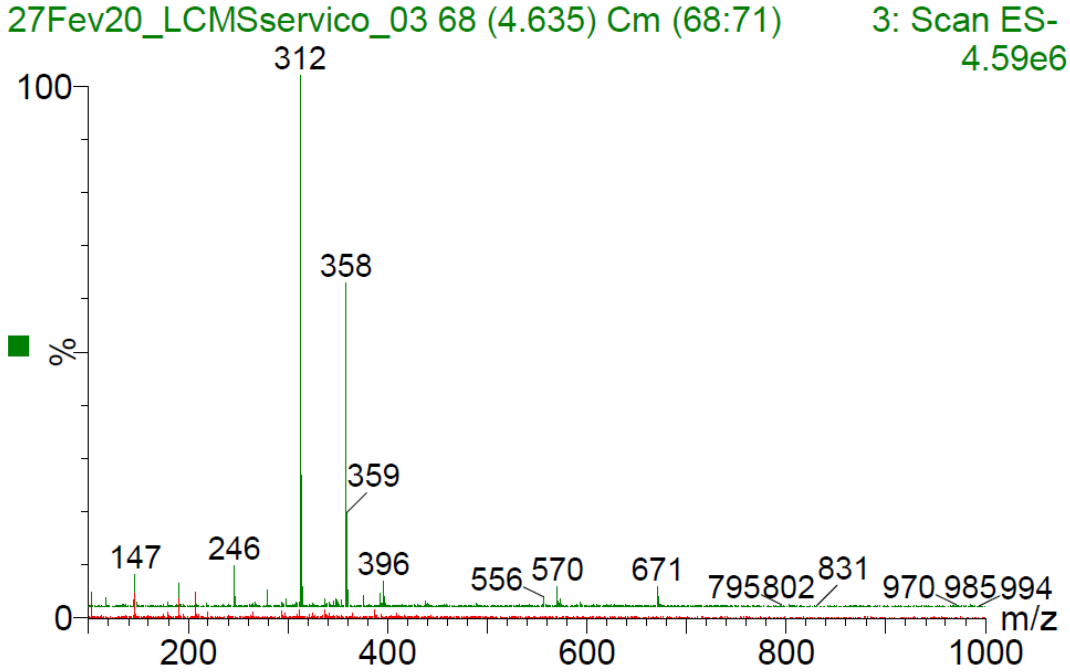

Annex 29 - ESI- Mass spectrum of the upper band of the prep TLC (JFV-2 Synthesis) - 4.63 min

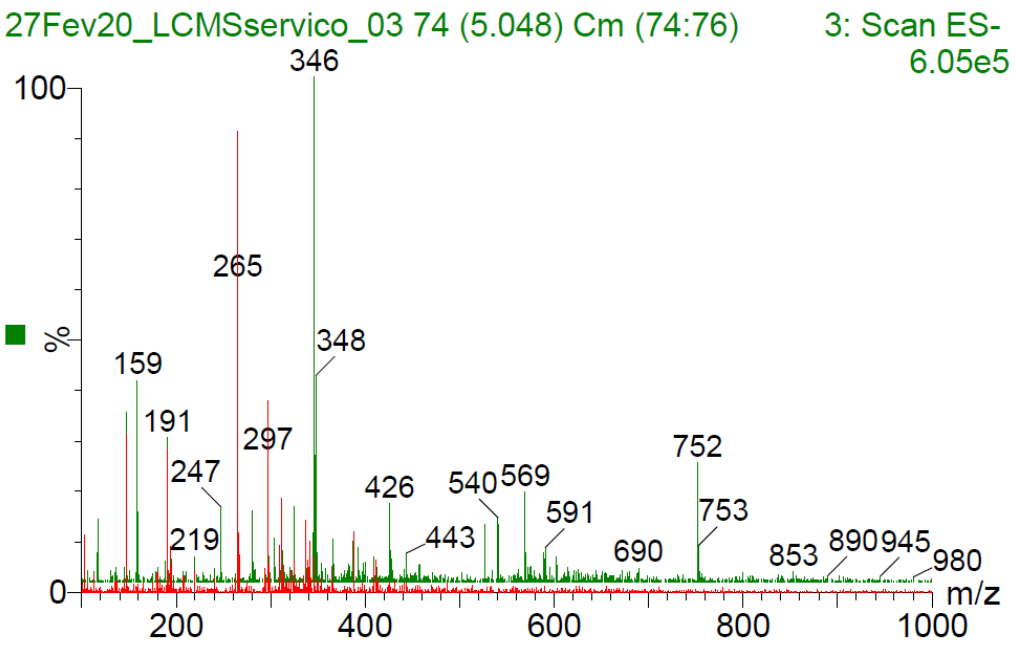

Annex 30 - ESI- Mass spectrum of the upper band of the prep TLC (JFV-2 Synthesis) - 5.05 min

CN-MMT

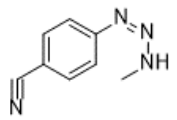

m/z: 160.07 (100.0%), 161.08 (8.7%), 161.07 (1.5%)

JFV-2

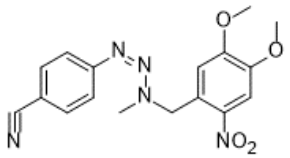

m/z: 355.13 (100.0%), 356.13 (20.6%), 357.13 (2.8%)

CN-Aniline

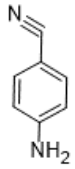

m/z: 118.05 (100.0%), 119.06 (7.6%)

DMNBA

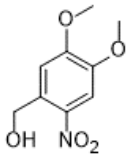

m/z: 213.06 (100.0%), 214.07 (10.1%), 215.07 (1.5%)

JFV-1

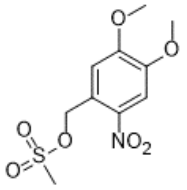

m/z: 291.04 (100.0%), 292.04 (12.0%), 293.04 (4.7%), 293.05 (2.0%)

Demethylated CN-MMT

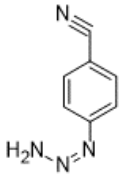

m/z: 146.06 (100.0%), 147.06 (9.0%)

JFV-2-Ani

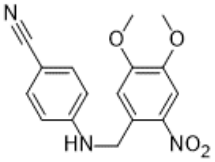

m/z: 313.11 (100.0%), 314.11 (17.6%), 315.11 (2.4%), 314.10 (1.1%)

Diazonium Compound

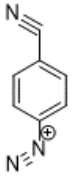

m/z: 130.04 (100.0%), 131.04 (8.7%)

JFV-1-Cl

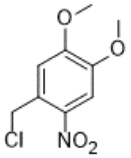

m/z: 231.03 (100.0%), 233.03 (32.8%), 232.03 (10.3%), 234.03 (3.2%)

Annex 31 - Compounds of interest when analysing the mass spectra of the upper band of the prep TLC (Synthesis of JFV-2)

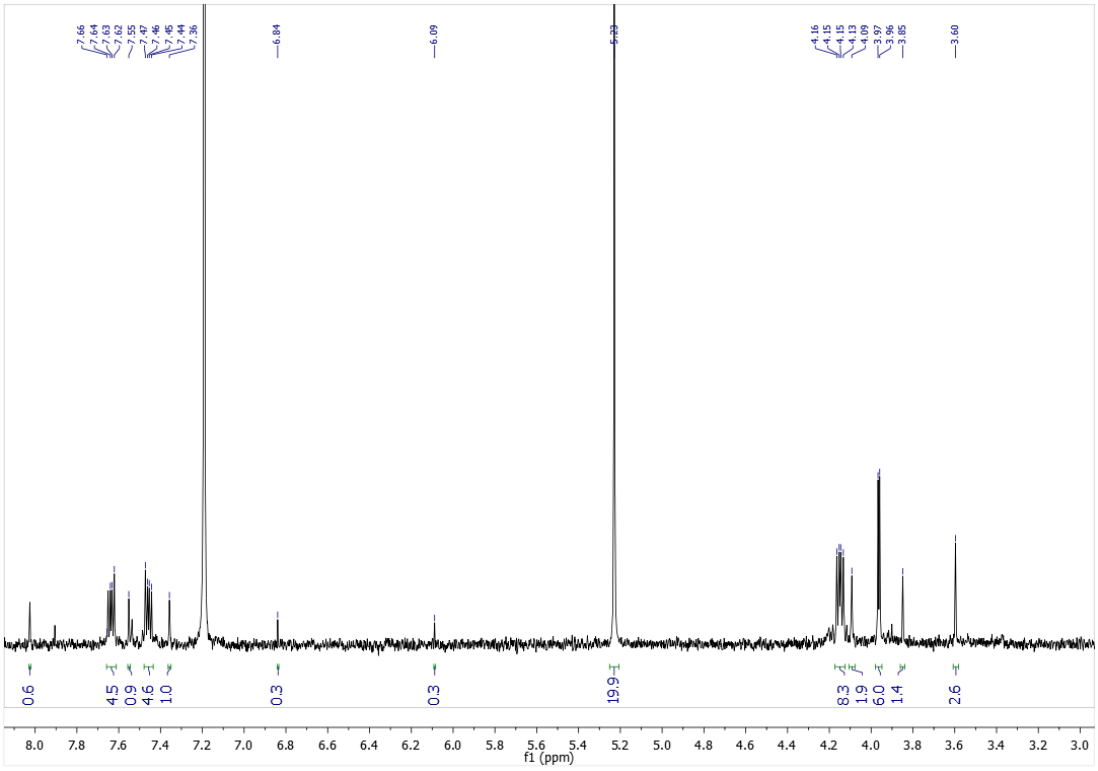

Annex 32 - ^{1}H NMR spectrum of the upper band of the second prep TLC (JFV-2 Synthesis Attempt 2)

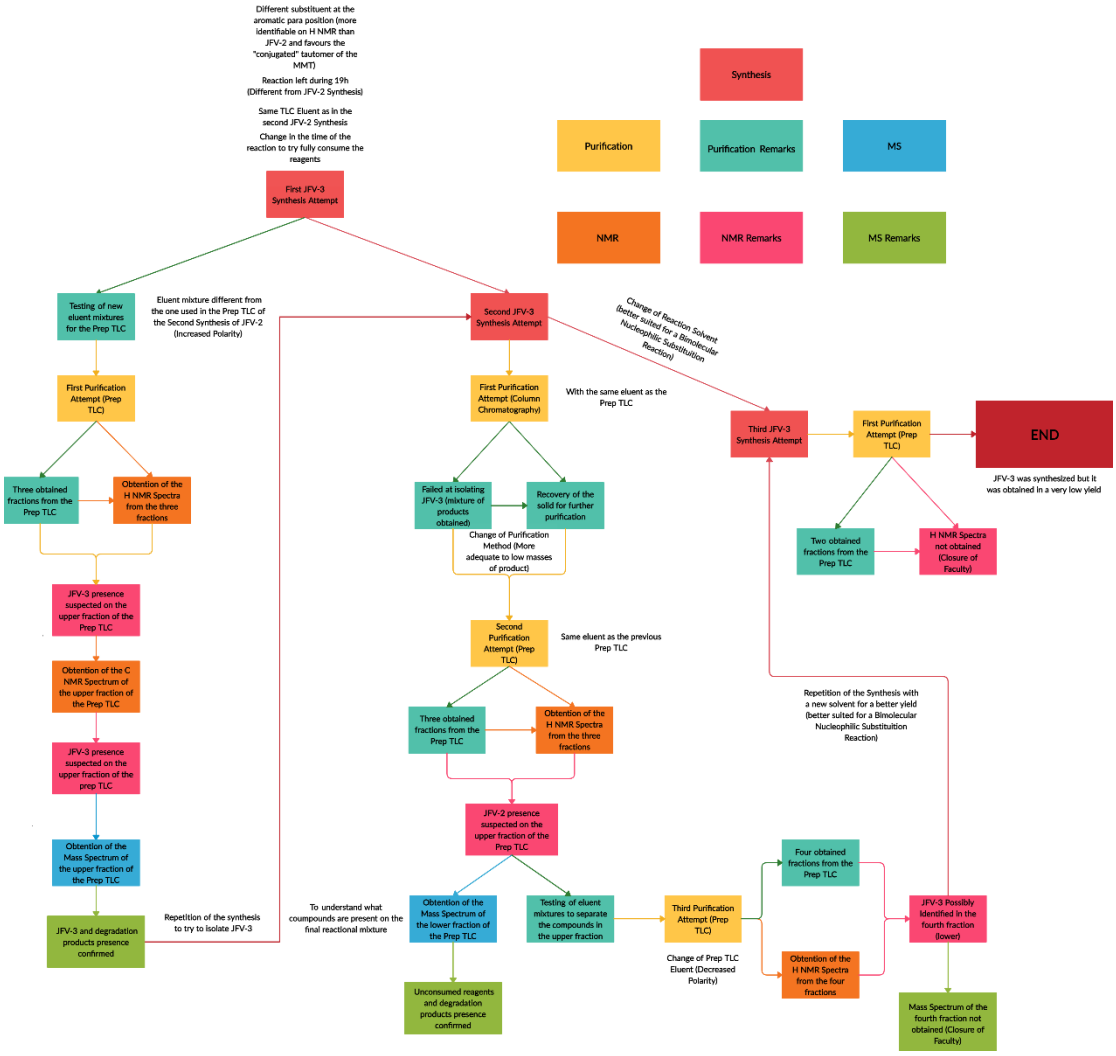

Annex 33 - Flowchart of the work executed for synthesizing JFV-3

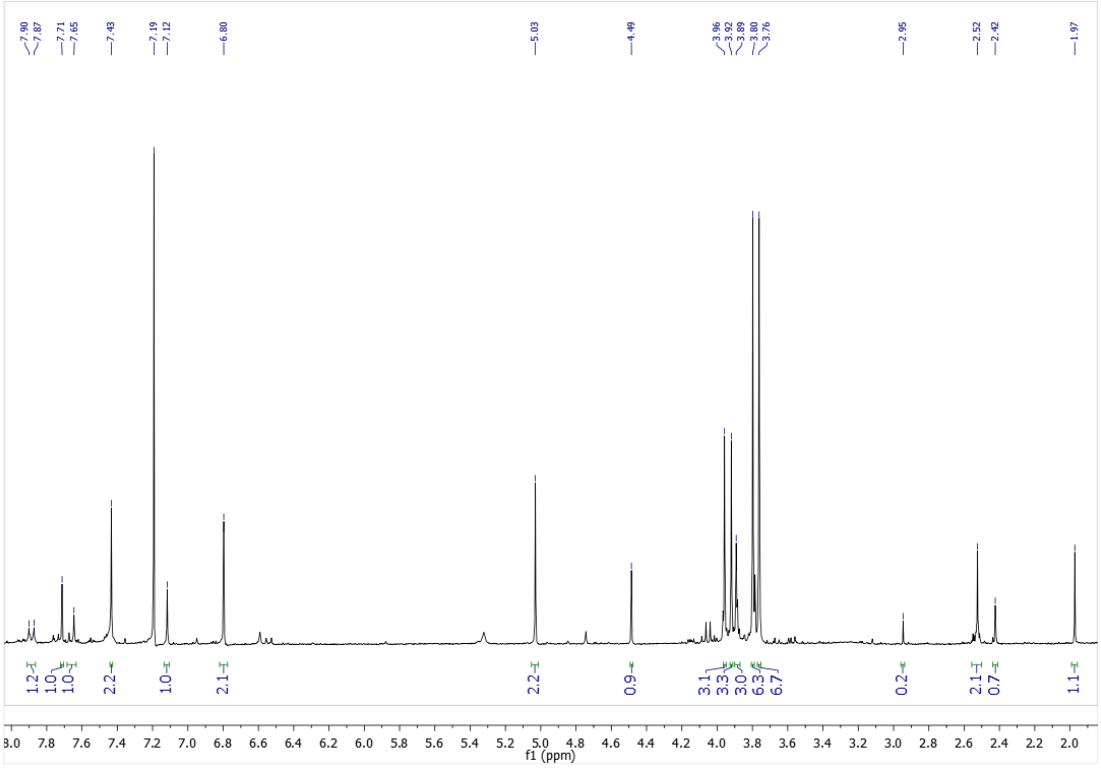

Annex 34 - ^{1}H NMR spectrum of the top band of the prep TLC (JFV-3 Synthesis Attempt 1)

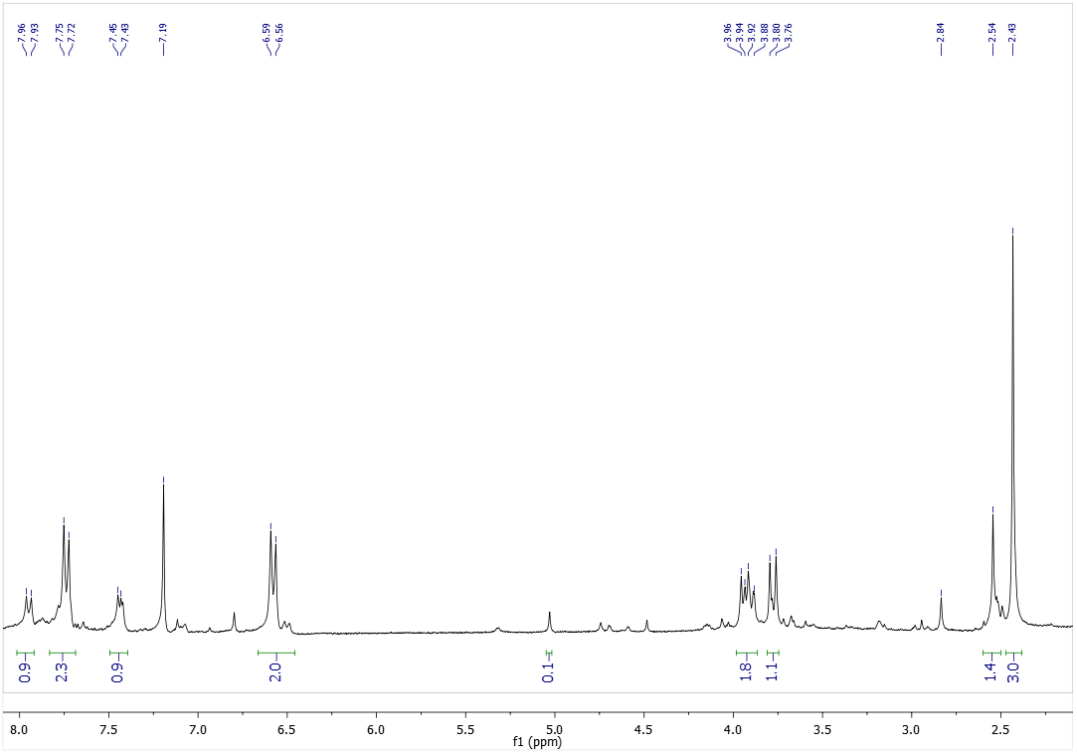

Annex 35 - ^{1}H-NMR spectrum of the middle band of the prep TLC (JFV-3 Synthesis Attempt 1)

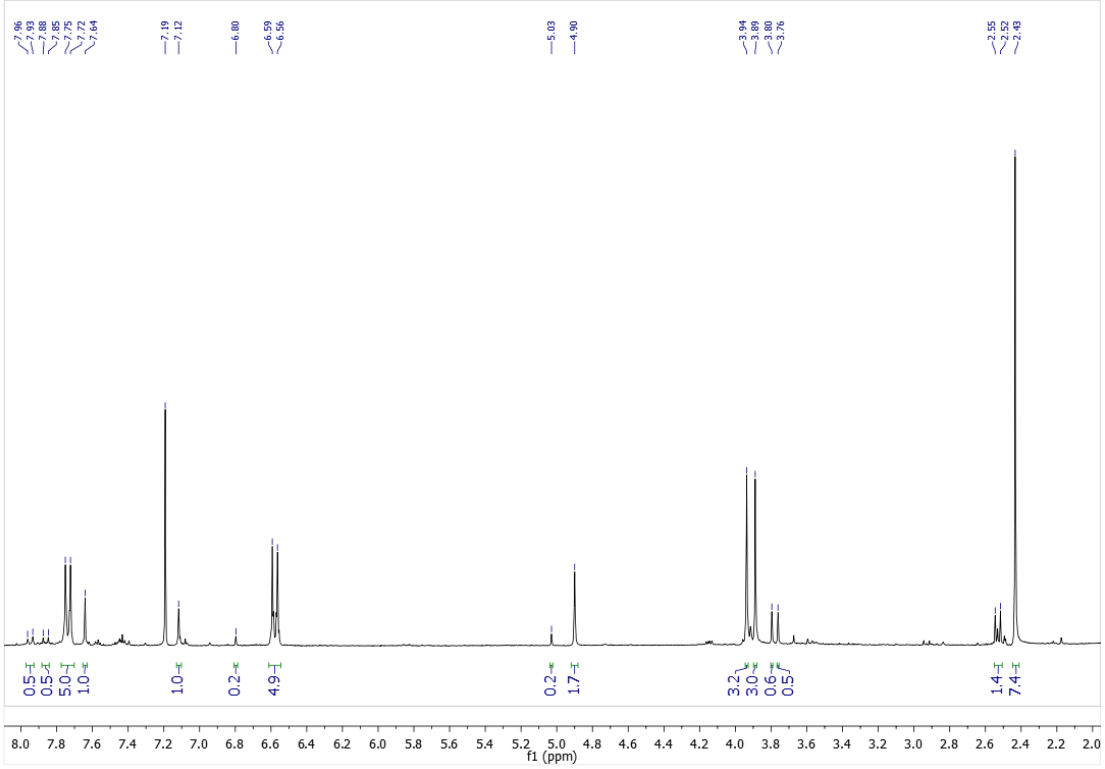

Annex 36 - ^{1}H-NMR spectrum of the lower band of the prep TLC (JFV-3 Synthesis Attempt 1)

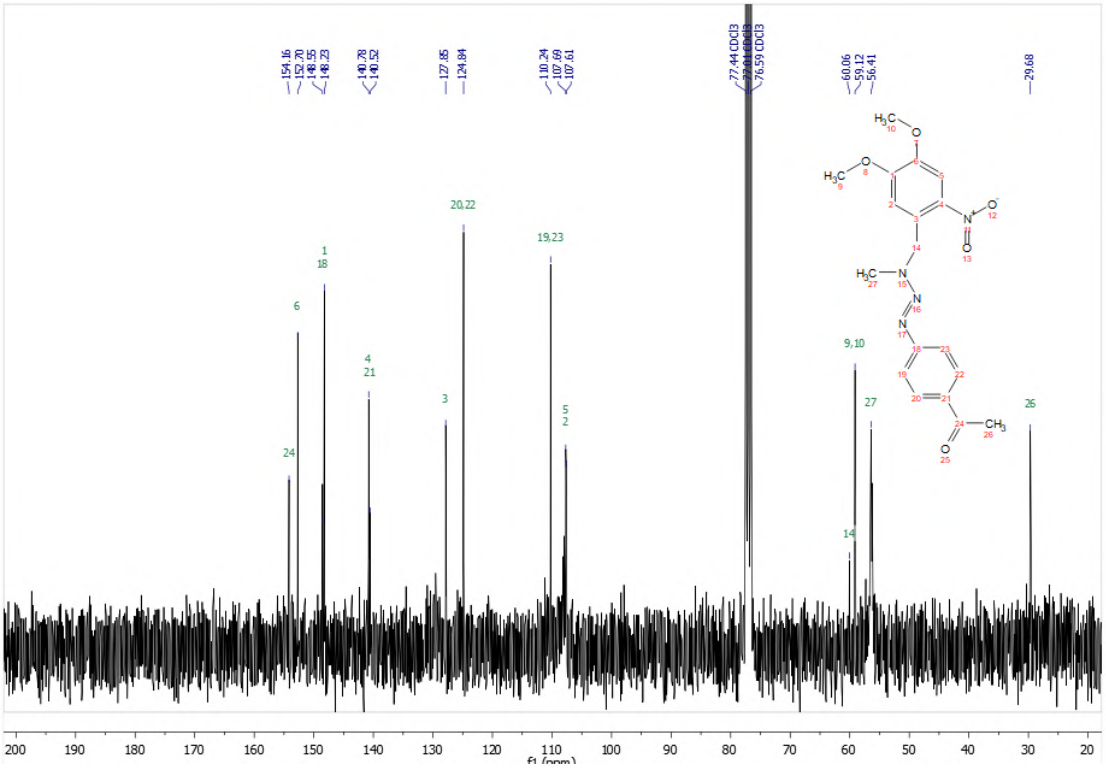

Annex 37 - ^{13}C-NMR spectrum of the top band of the prep TLC (JFV-3 Synthesis Attempt 1)

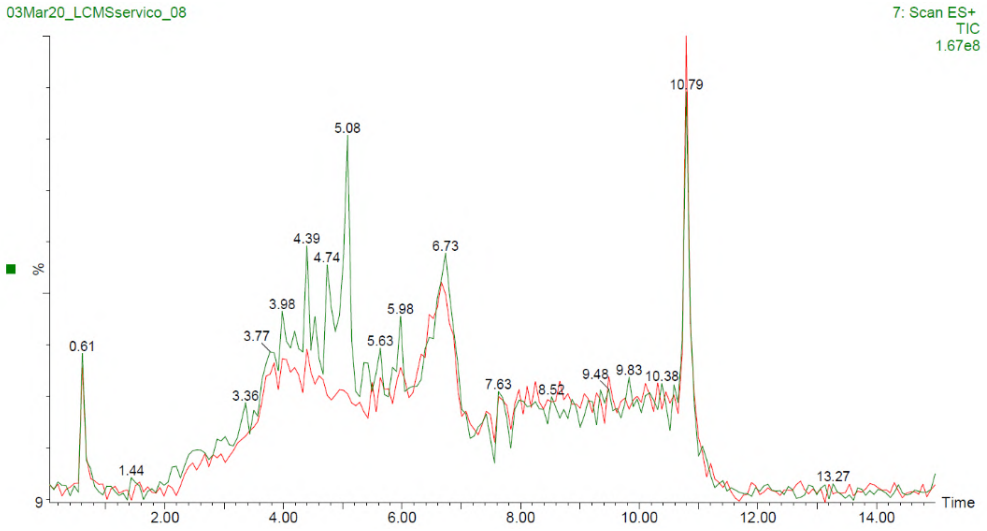

Annex 38 - Chromatogram of the top band of the prep TLC (JFV-3 Synthesis, Attempt 1) - ESI+

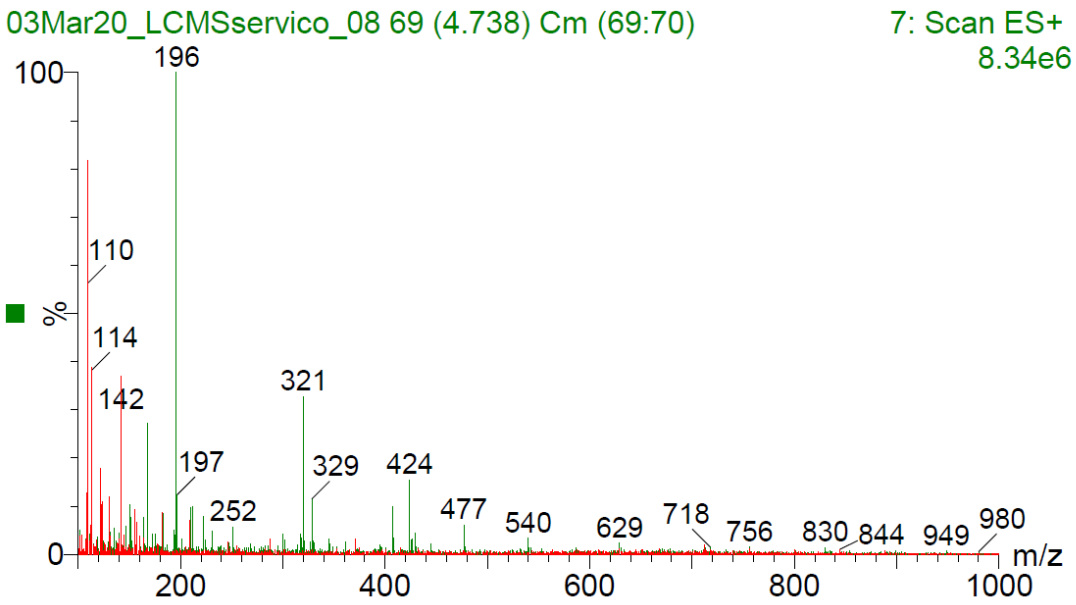

Annex 39 - Mass spectra of the upper band of the prep TLC (JFV-3 Synthesis, Attempt 1) - ESI+ (4.39 min)

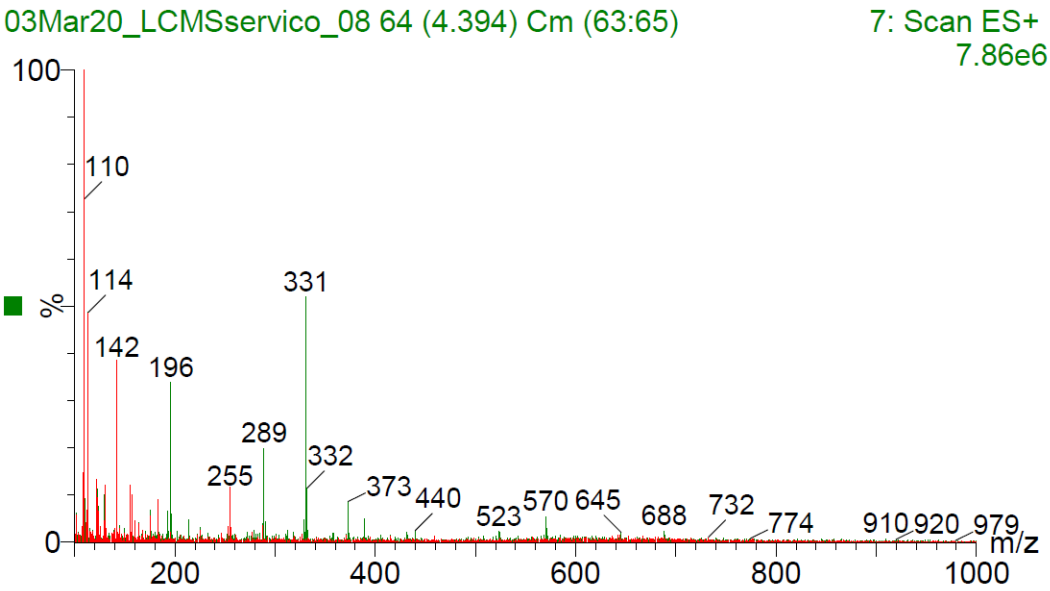

Annex 40 - Mass spectra of the upper band of the prep TLC (JFV-3 Synthesis, Attempt 1) - ESI+ (4.74 min)

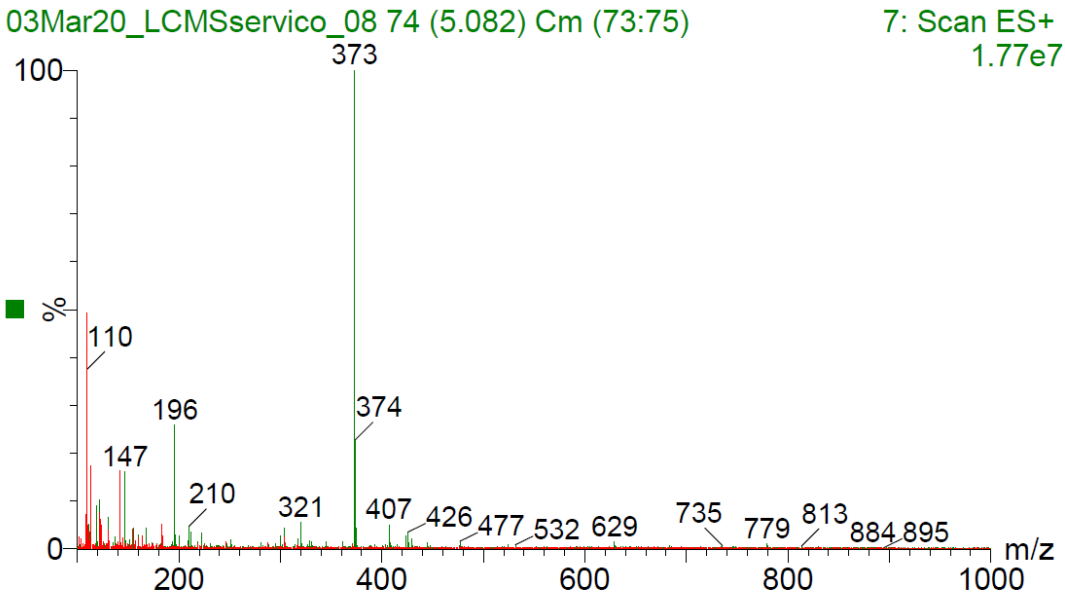

Annex 41 - Mass spectra of the upper band of the prep TLC (JFV-3 Synthesis Attempt 1) - ESI + (5.08 min)

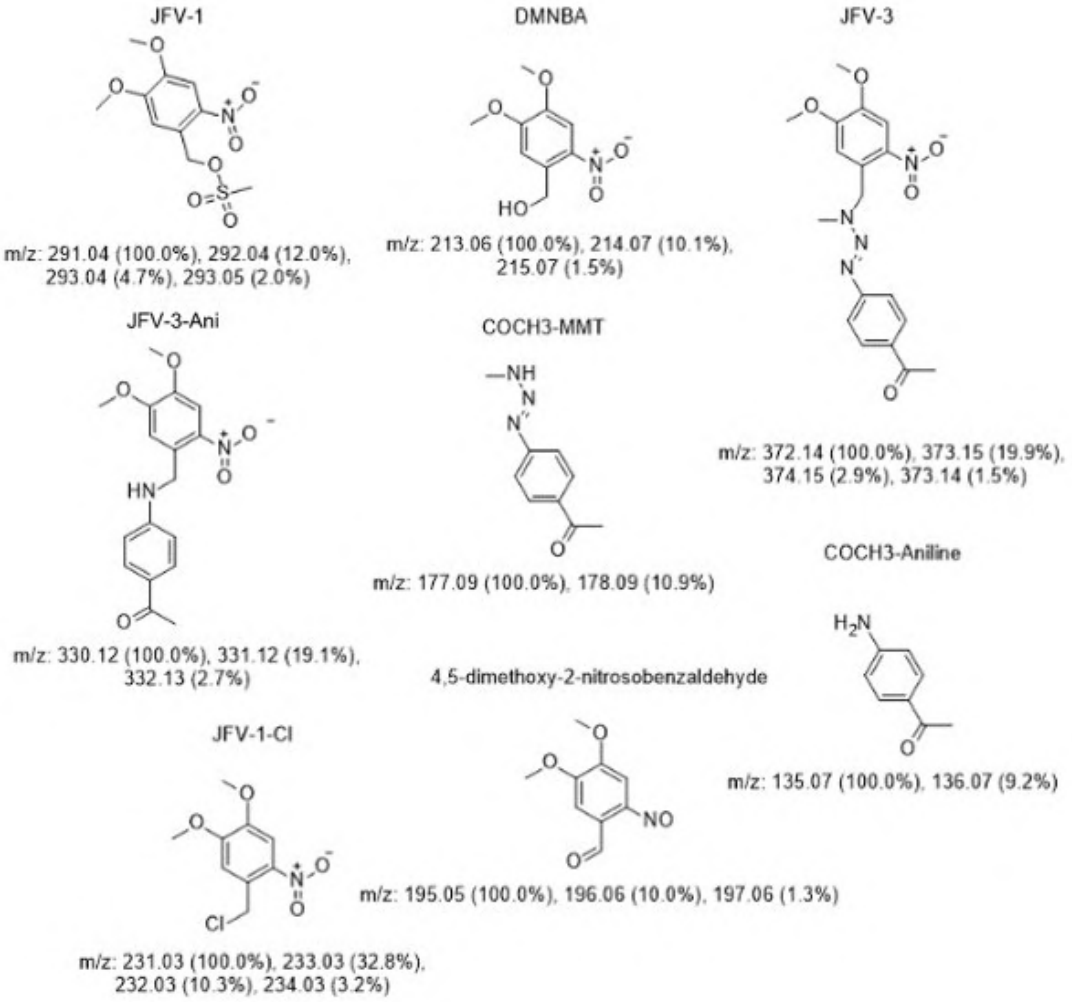

Annex 42 - Compounds of interest when analysing the mass spectra of the prep TLCs (JFV-3 Syntheses)

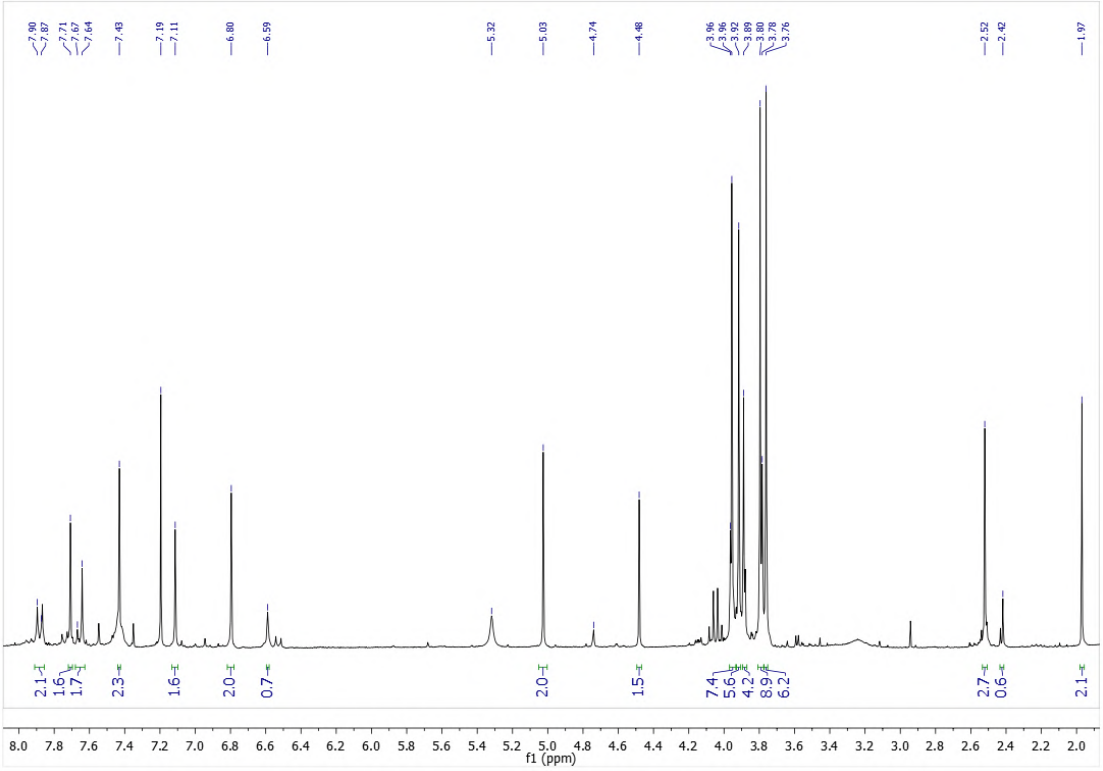

Annex 43 - ^{1}H-NMR spectrum of the top band of the prep TLC (JFV-3 Synthesis Attempt 2)

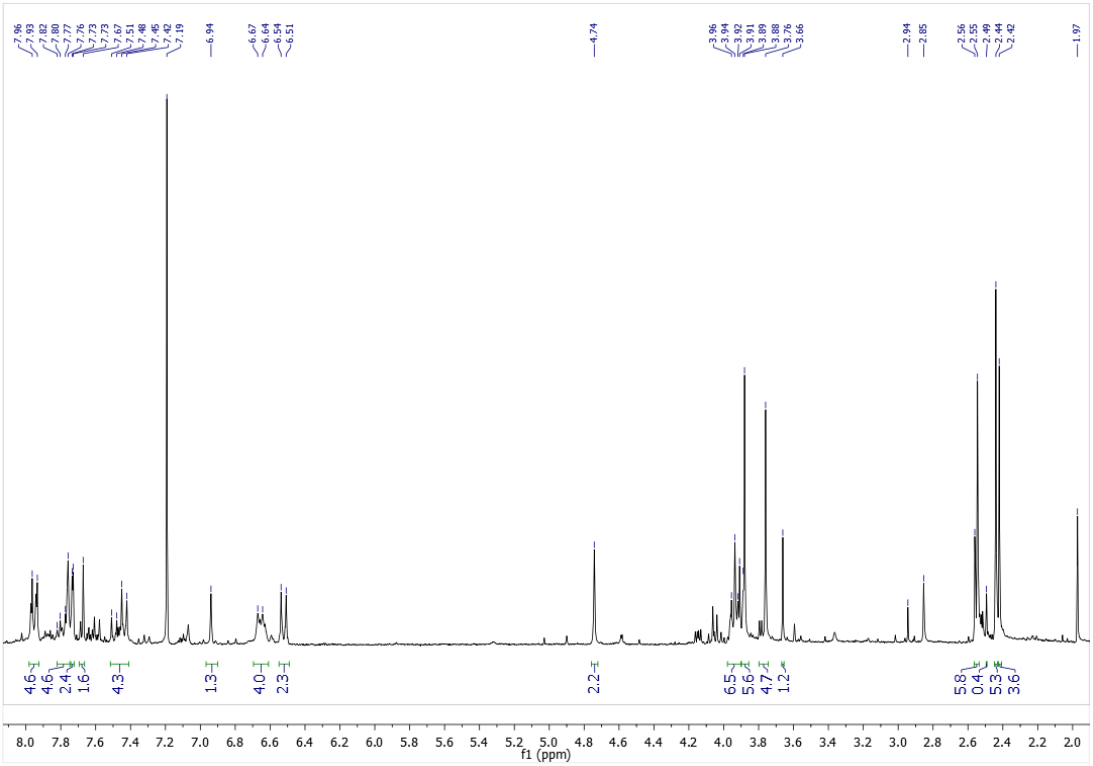

Annex 44 - ^{1}H-NMR spectrum of the middle band of the prep TLC (JFV-3 Synthesis Attempt 2)

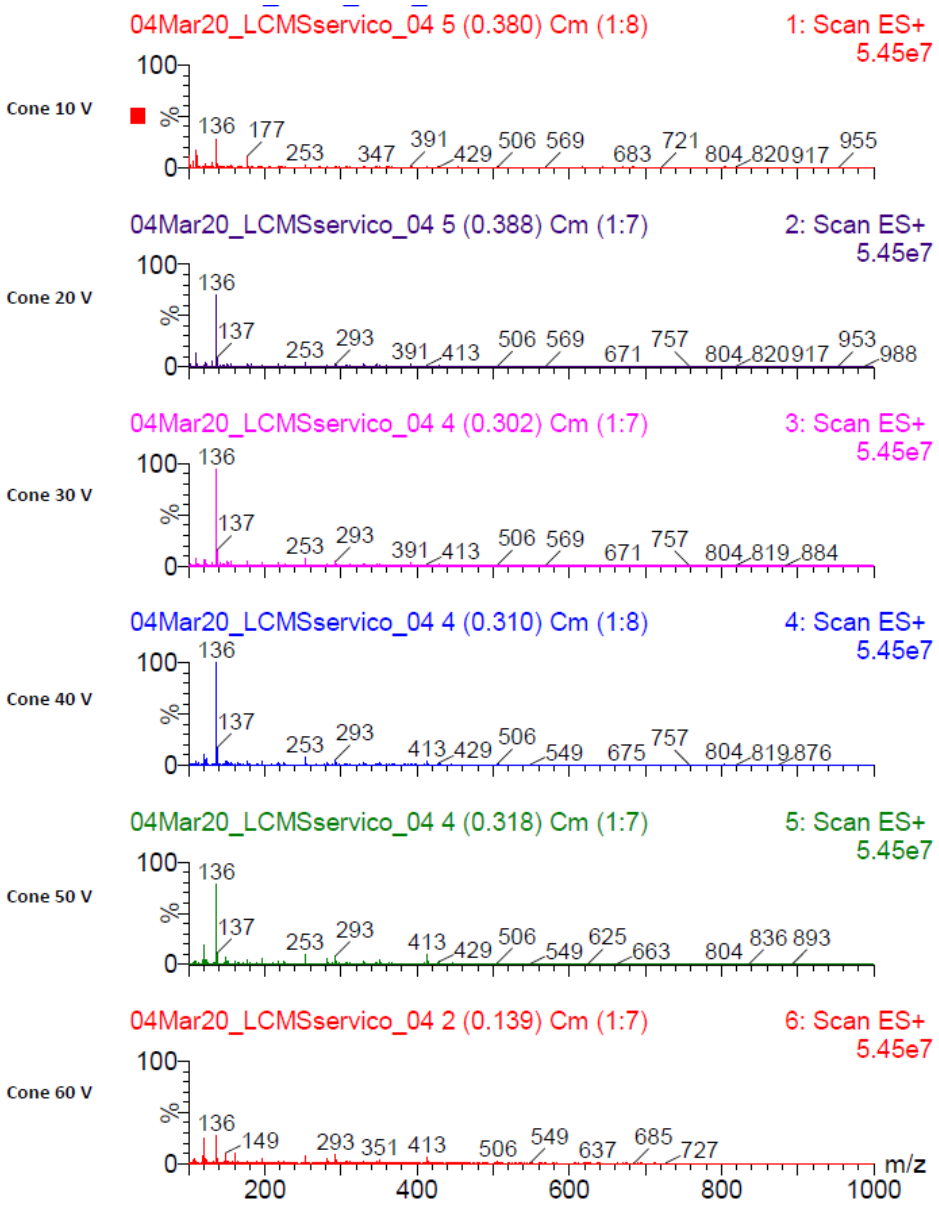

Annex 45 - Mass spectra of the lower band of the prep TLC (Synthesis of JFV-3, Attempt 2) - ESI+

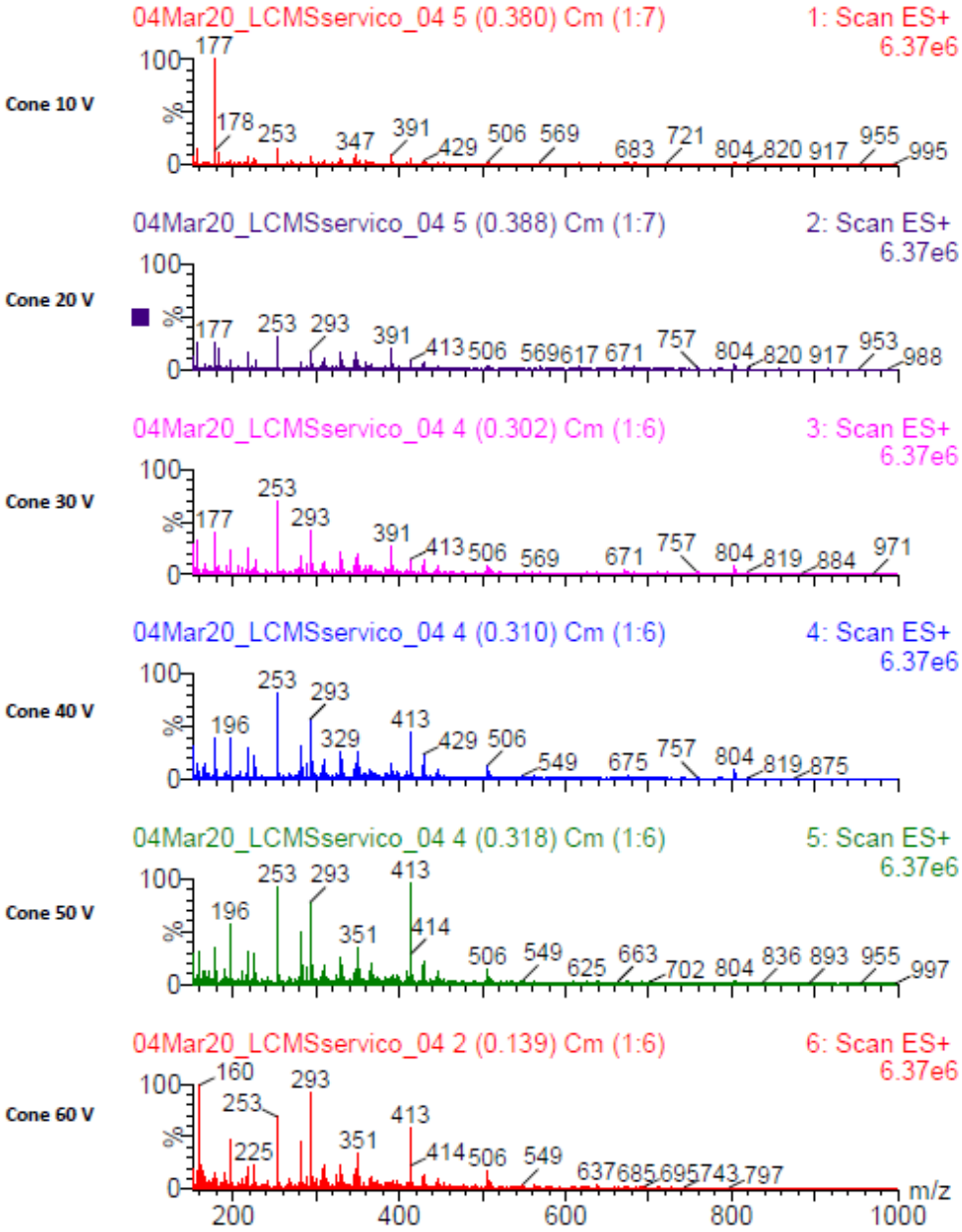

Annex 46 - Mass spectra of the lower band of the prep TLC (Synthesis of JFV-3, Attempt 2) - ESI+ (with zoom)

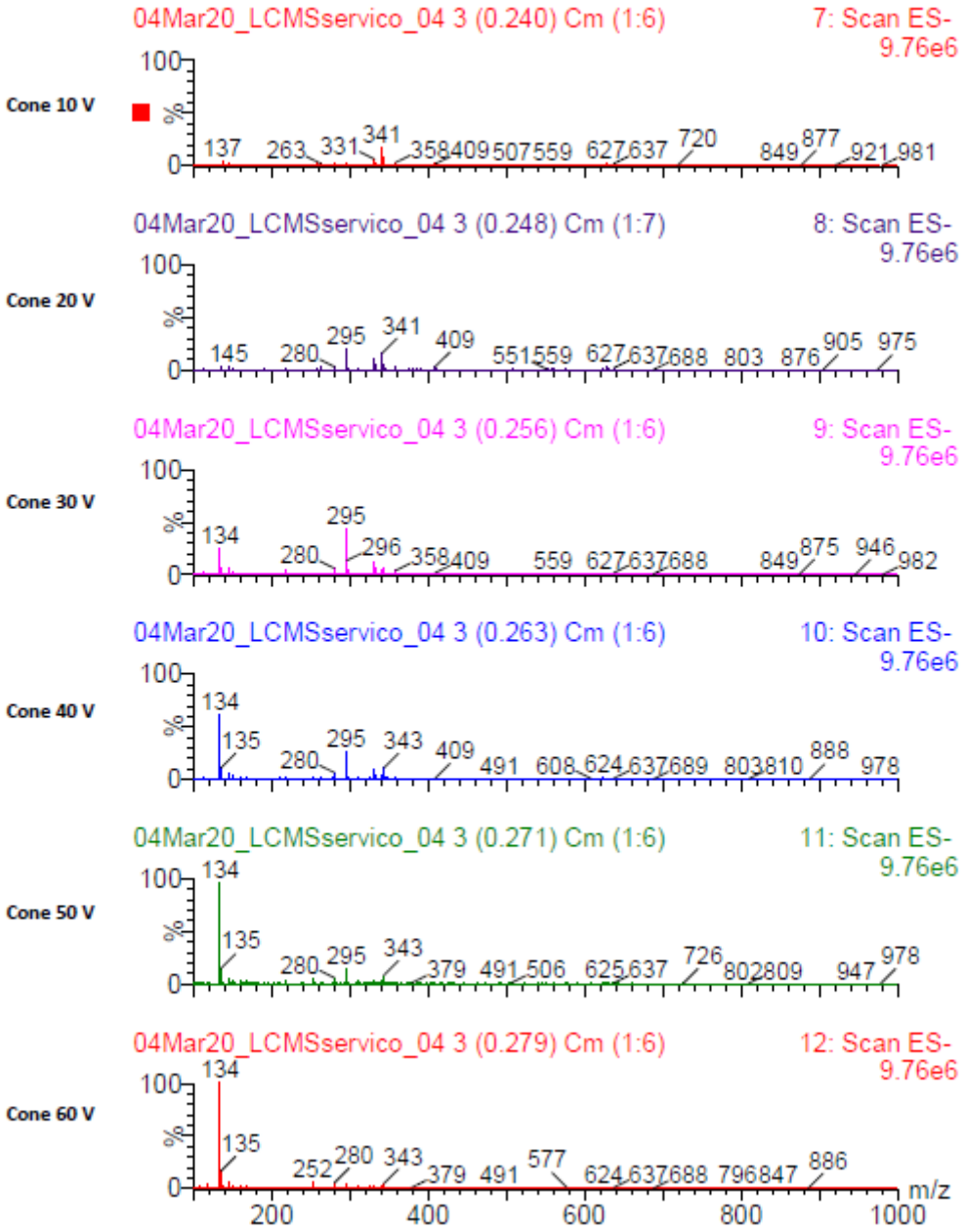

Annex 47 - Mass spectra of the lower band of the prep TLC (Synthesis of JFV-3, Attempt 2) - ESI-

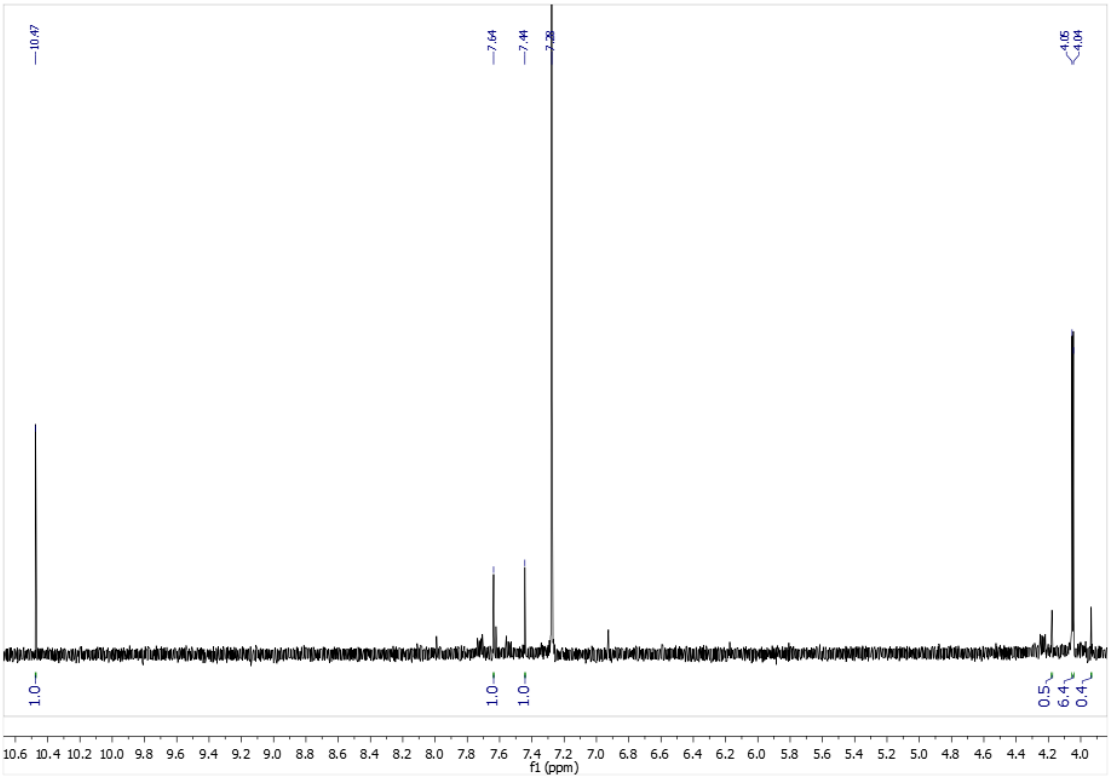

Annex 48 - ^{1}H-NMR spectrum of the first band of the second prep TLC (JFV-3 Synthesis Attempt 2)

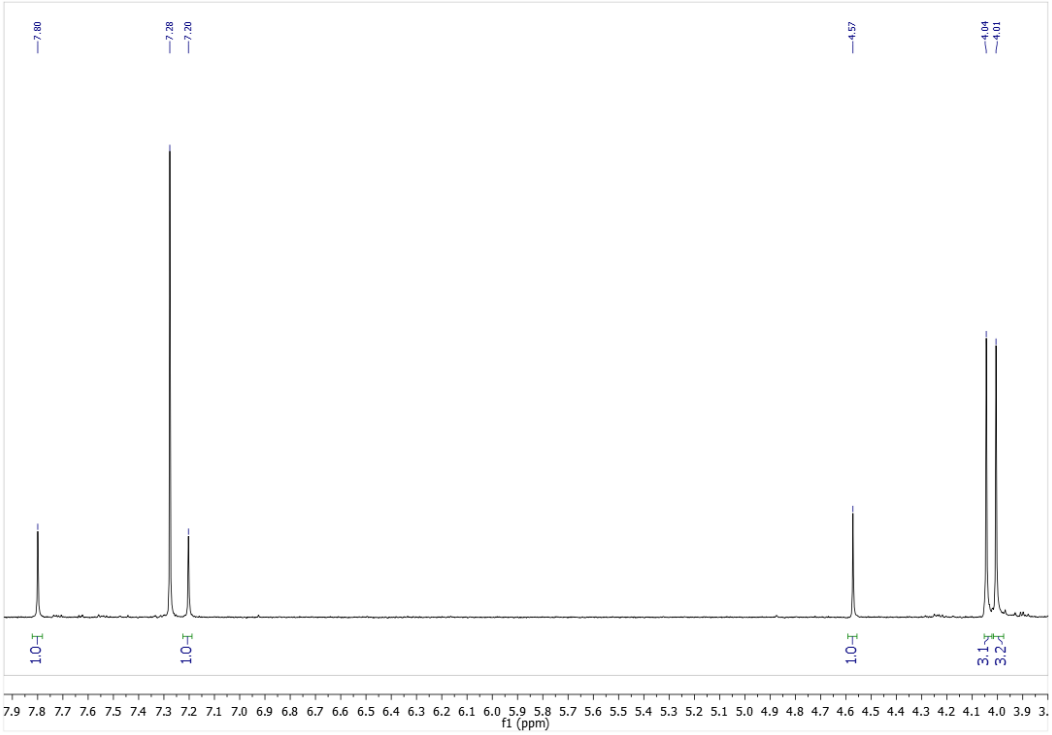

Annex 49 - ^{1}H-NMR spectrum of the second band of the second prep TLC (JFV-3 Synthesis Attempt 2)

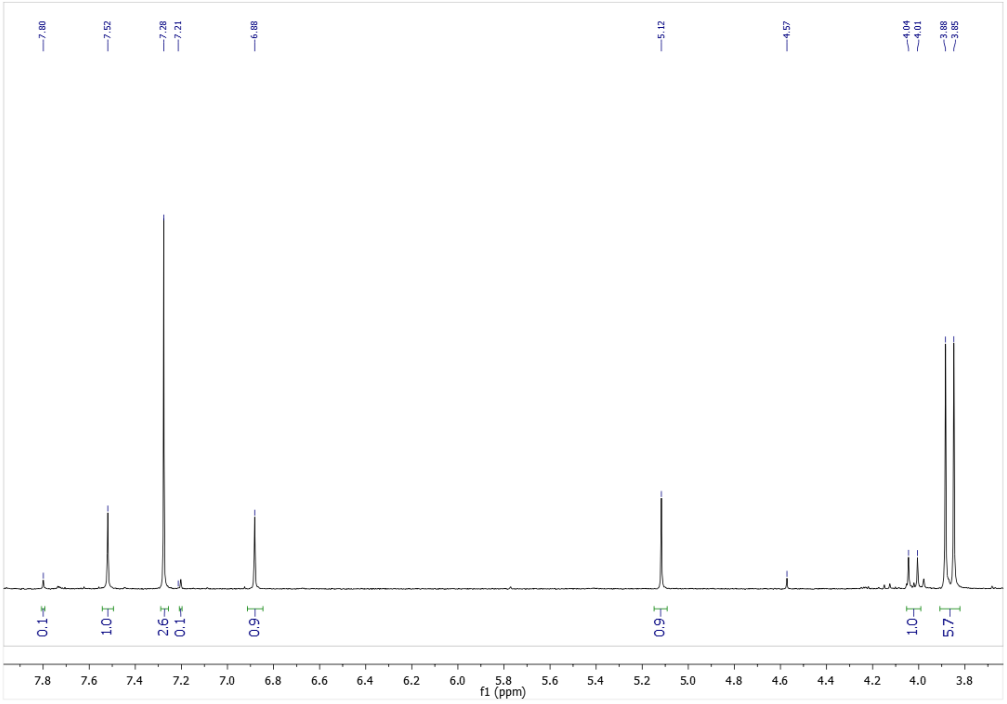

Annex 50 - ^{1}H-NMR spectrum of the third band of the second prep TLC (JFV-3 Synthesis Attempt 2)

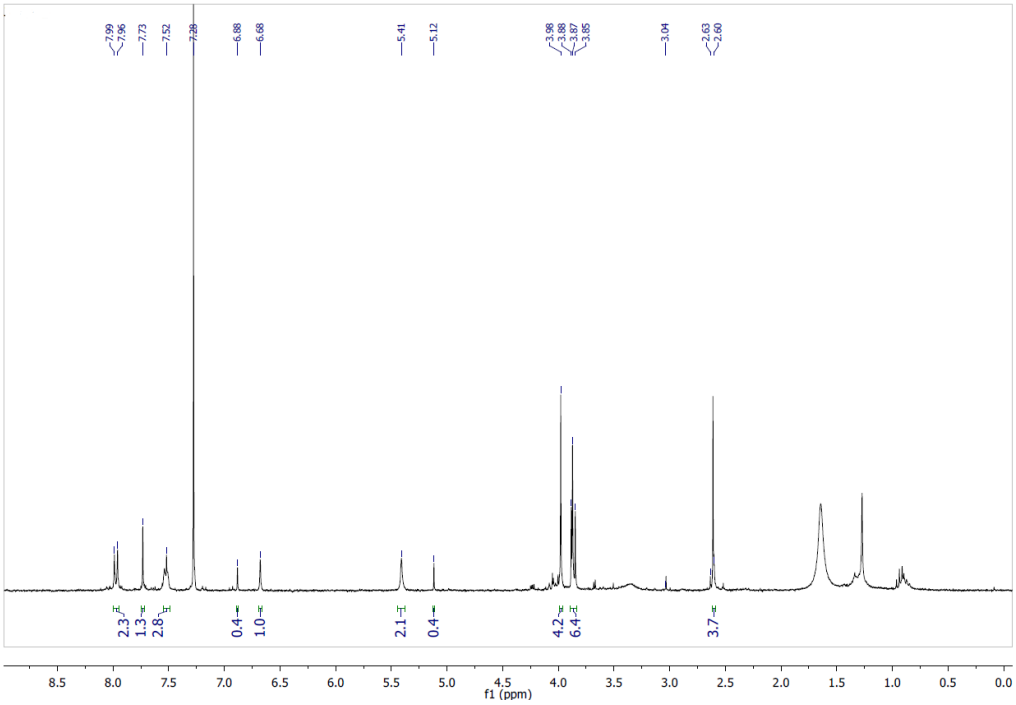

Annex 51 - ^{1}H-NMR spectrum of the fourth band of the second prep TLC (JFV-3 Synthesis Attempt 2)

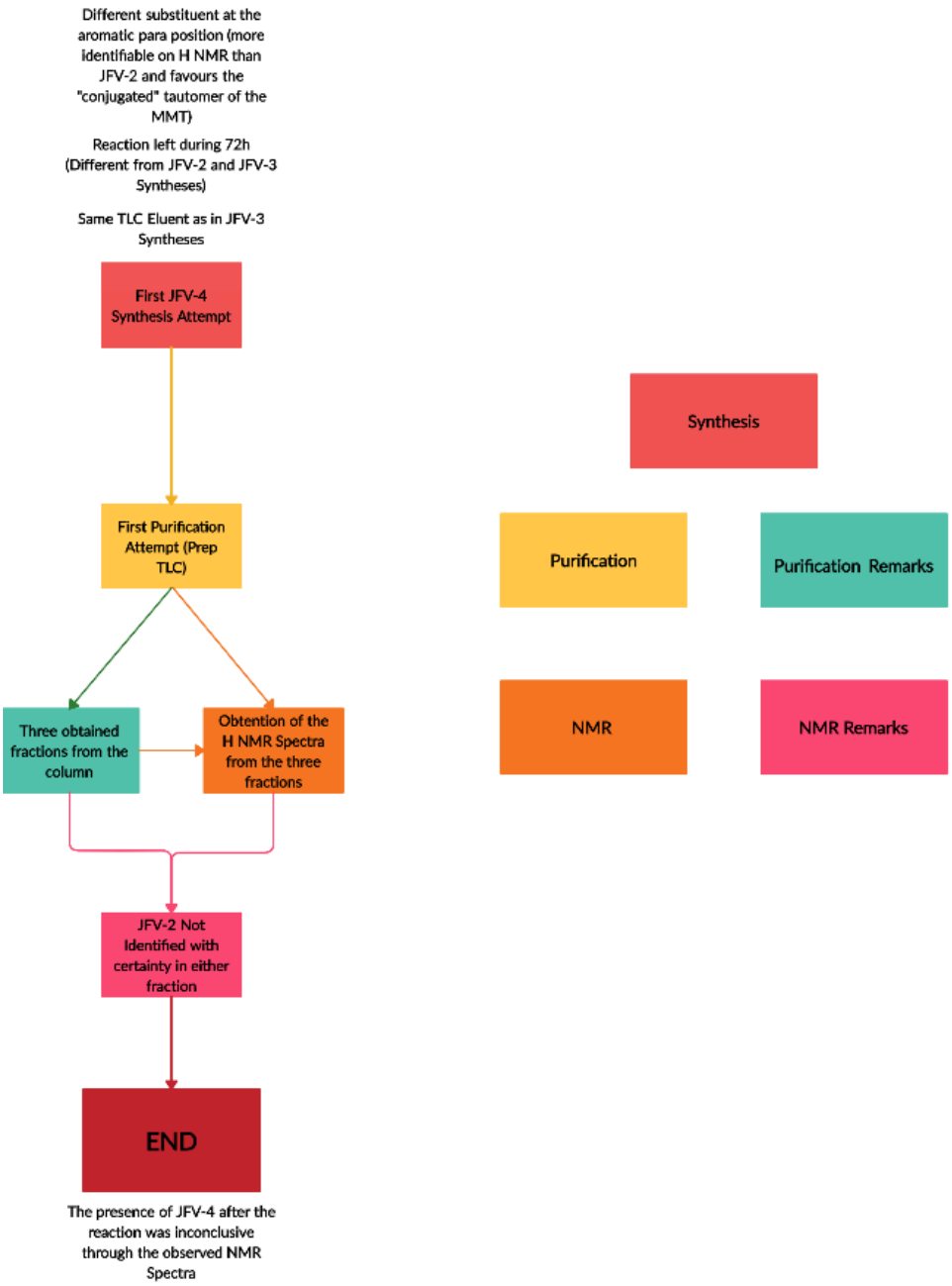

Annex 52 - Flowchart of the work executed for synthesizing JFV-4

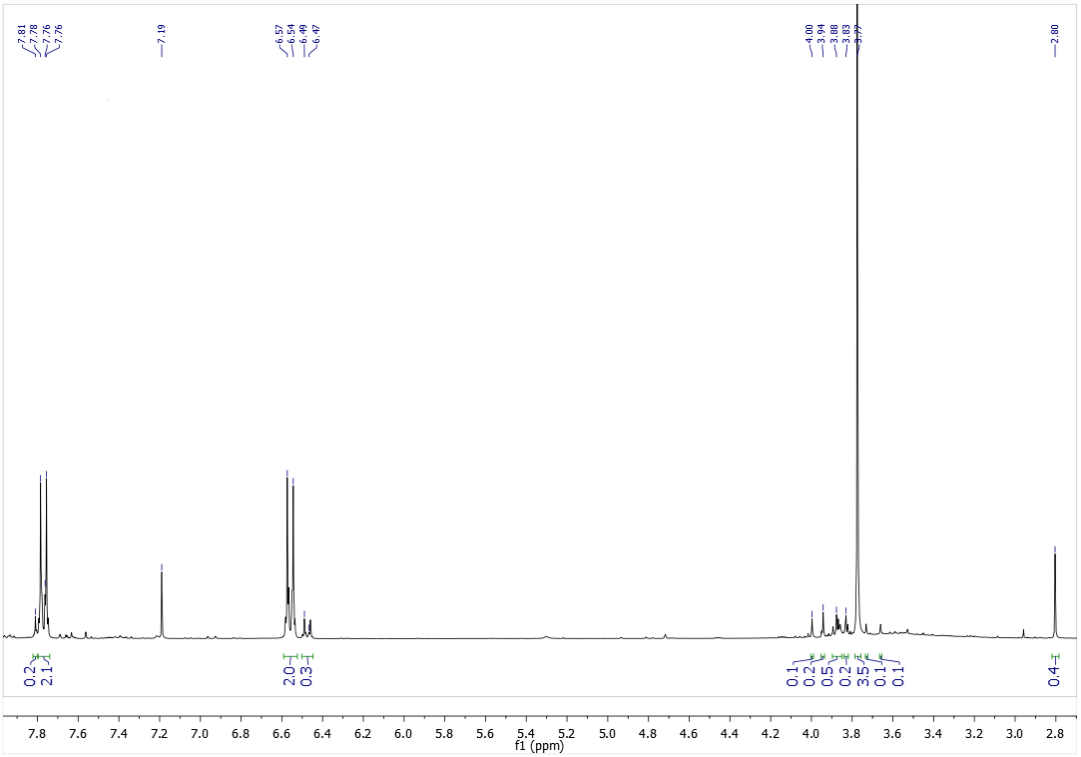

Annex 53 - ^{1}H NMR spectrum of the upper band (JFV-4 Synthesis)

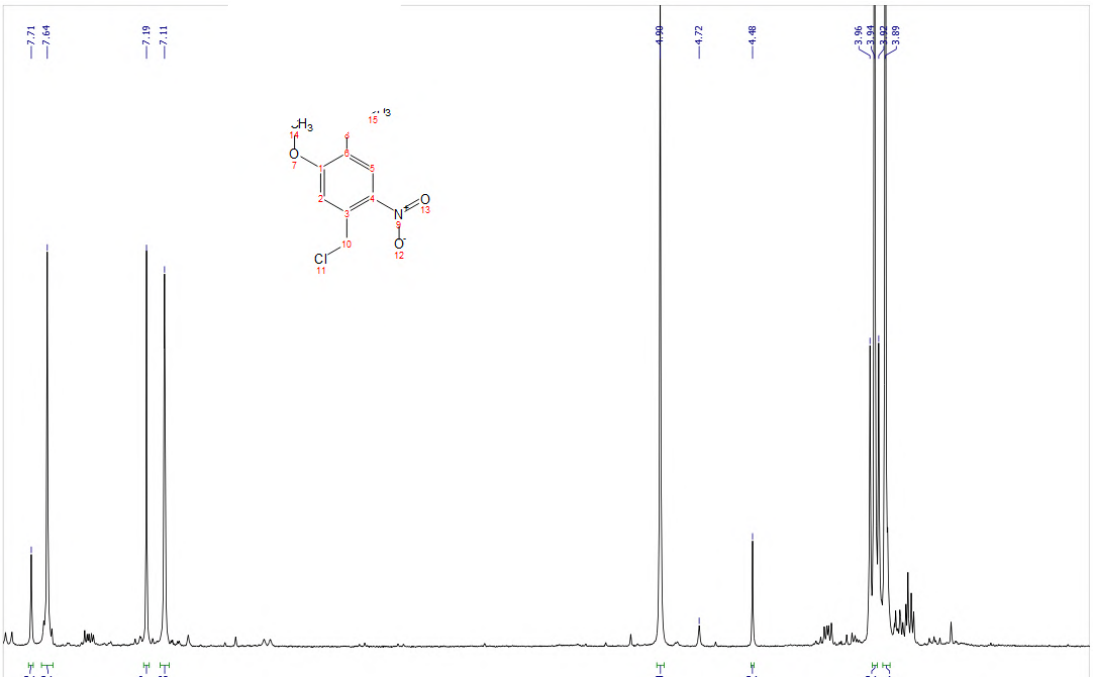

Annex 54 - ^{1}H NMR spectrum of the middle band (JFV-4 Synthesis)

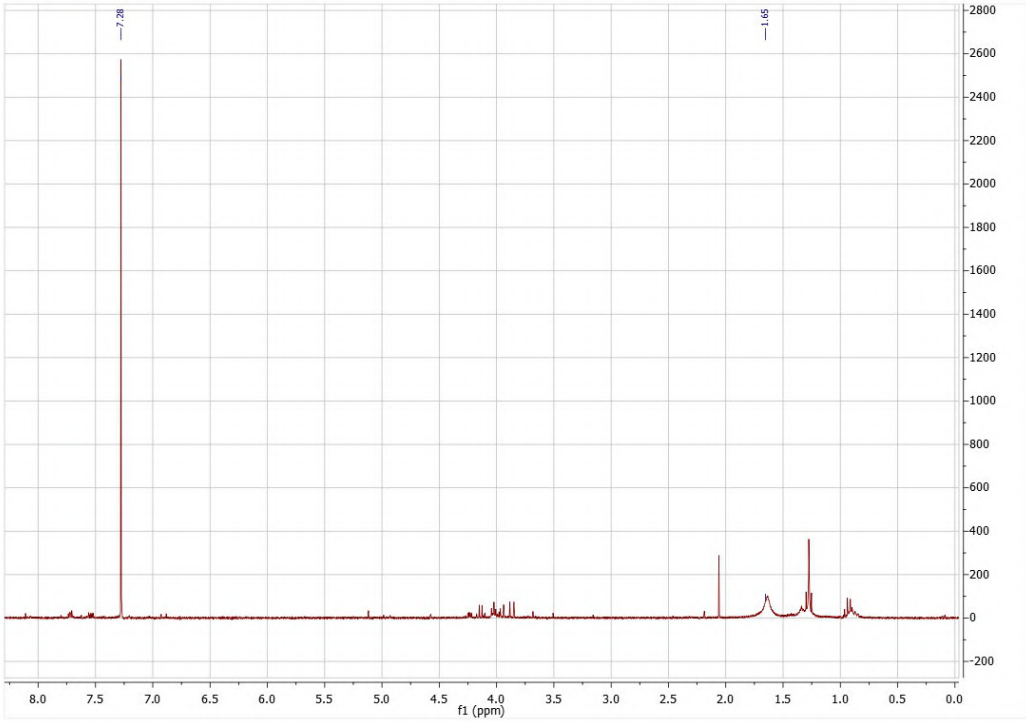

Annex 55 - ^{1}H NMR spectrum of the lower band (JFV-4 Synthesis)